Technische Universität München
TUM School of Engineering and Design

A holistic, model-predictive process control

for plastic-metal direct joining

Stefan Peter Meyer

Vollständiger Abdruck der von der TUM School of Engineering and Design der Technischen Universität München zur Erlangung eines

Doktors der Ingenieurwissenschaften (Dr.-Ing.)

genehmigten Dissertation.

Vorsitz:	Prof. Dr.-Ing. Rüdiger Daub
Prüfer*innen der Dissertation:	1. Prof. Dr.-Ing. Michael F. Zäh 2. Prof. Frank E. Pfefferkorn, Ph.D.

Die Dissertation wurde am 07.04.2022 bei der Technischen Universität München eingereicht und durch die TUM School of Engineering and Design am 19.07.2022 angenommen.

Stefan Peter Meyer, M.Sc.:
A holistic, model-predictive process control
for plastic-metal direct joining
154 pages with 26 figures and 14 tables
Technical University of Munich (TUM)
TUM School of Engineering and Design
Institute for Machine Tools and Industrial Management (*iwb*)

Editors' Preface

In times of global challenges, such as climate change, the transformation of mobility, and an ongoing demographic change, production engineering is crucial for the sustainable advancement of our industrial society. The impact of manufacturing companies on the environment and society is highly dependent on the equipment and resources employed, the production processes applied, and the established manufacturing organization. The company's full potential for corporate success can only be taken advantage of by optimizing the interaction between humans, operational structures, and technologies. The greatest attention must be paid to becoming as resource-saving, efficient, and resilient as possible to operate flexibly in the volatile production environment.

Remaining competitive while balancing the varying and often conflicting priorities of sustainability, complexity, cost, time, and quality requires constant thought, adaptation, and the development of new manufacturing structures. Thus, there is an essential need to reduce the complexity of products, manufacturing processes, and systems. Yet, at the same time, it is also vital to gain a better understanding and command of these aspects.

The research activities at the Institute for Machine Tools and Industrial Management (*iwb*) aim to continuously improve product development and manufacturing planning systems, manufacturing processes, and production facilities. A company's organizational, manufacturing, and work structures, as well as the underlying systems for order processing, are developed under strict consideration of employee-related requirements and sustainability issues. However, the use of computer-aided and artificial intelligence-based methods and the necessary increasing degree of automation must not lead to inflexible and rigid work organization structures. Thus, questions concerning the optimal

integration of ecological and social aspects in all planning and development processes are of utmost importance.

The volumes published in this book series reflect and report the results from the research conducted at *iwb*. Research areas covered span from the design and development of manufacturing systems to the application of technologies in manufacturing and assembly. The management and operation of manufacturing systems, quality assurance, availability, and autonomy are overarching topics affecting all areas of our research. In this series, the latest results and insights from our application-oriented research are published, and it is intended to improve knowledge transfer between academia and a wide industrial sector.

Rüdiger Daub Gunther Reinhart Michael Zäh

Acknowledgments

"The universe consists of seven regions:
North, South, West, East,
Before, After, and Home."

(Walter Moers in *The 13½ Lives of Captain Bluebear*, 2000)

I wrote this thesis as a Research Associate at the Institute for Machine Tools and Industrial Management (*iwb*) at the Technical University of Munich, funded by the German Federal Ministry of Education and Research (BMBF) and the Deutsche Forschungsgemeinschaft (DFG, German Research Foundation).

I would like to thank Prof. Dr.-Ing. Michael F. Zaeh, Head of the Chair of Machine Tools and Manufacturing Technology at *iwb*, for making it possible for me to graduate from this unique institute. I would also like to thank my second supervisor, Prof. Frank E. Pfefferkorn, Ph.D., from the University of Wisconsin-Madison. In 2016/2017, I was able to spend my most enjoyable time in my studies at this university (right next to the Camp Randall Stadium), completing my master's thesis and experiencing unforgettable moments in and around the Badger State. I also thank Prof. Dr.-Ing. Rüdiger Daub for taking over the chairmanship.

Special thanks go to my colleagues, Christian Schieber, Maximilian Busch, Matthias Wimmer, and Sepp Wimmer, all of whom contributed to the successful completion of this thesis with their critical remarks and helpful comments. Furthermore, I would like to thank all of my colleagues in the machine tools research team and the entire *iwb* for the numerous professional and amusing discussions on, and adjacent to, my topic. I also thank Philipp Rinck and Xiao Fan Zhao for all of the enjoyable times together in our office – it was always a

great pleasure to talk to you about science and all other topics beyond research. Another thank you goes to the *iwb* sports group. Whether freeletics, running, skiing, or triathlon, every day offered a rewarding challenge. A special thank you also belongs to Maren Herold, who contributed significantly to the success of this work through her active support as a student assistant.

I thank my family immensely – my father, Hermann Meyer, for encouraging me through his enthusiasm for technology, and supporting me, no matter what; and my aunt Lisa Euringer for the numerous dinner invitations, but especially for her passion for enjoying the nature and discovering foreign places. Also, special thanks to my grandma, Elsa – without you, I wouldn't be the person I am now. And last but not least, Anja. Thank you for your love, your time, your patience, and your support during the last years.

Weißbach a. d. A., March 18, 2022 *Stefan P. Meyer*

Contents

List of abbreviations

0D	zero-dimensional
1D	one-dimensional
2D	two-dimensional
3D	three-dimensional
ABS	Acrylonitrile butadiene styrene
approx.	approximately
ARC	Adaptive robust control
AWGN	Additive white Gaussian noise
C	Carbon (chemical element)
C x	Conclusion; x represents a natural number
CF	Carbon fiber
CFRP	Carbon-fiber-reinforced plastic(s)
CNC	Computerized numerical control
CORSIA	Carbon Offsetting and Reduction Scheme for International Aviation
COVID-19	Coronavirus disease 2019
Cr	Chromium (chemical element)
CW	Continuous-wave
E modulus	Elastic modulus or Young's modulus
e.g.	exempli gratia (English: for example)
EGD	European Green Deal

EN AW	European norm aluminum wrought
et al.	et alii (English: and others)
EU	European Union
EU ETS	European Union Emissions Trading System
F	Field of action
FDM	Finite difference method
FEM	Finite element method
Fig.	Figure(s)
FLW	Friction lap welding
FPJ	Friction press joining
FSpJ	Friction spot joining
FSW	Friction stir welding
FVM	Finite volume method
GF	Glass fiber
GFRP	Glass-fiber-reinforced plastic
H	Hydrogen (chemical element)
HBM	Hottinger Baldwin Messtechnik (company)
I controller	Integral controller
IPO	Interpolation frequency
i.e.	id est (English: that is)
iwb	Institut für Werkzeugmaschinen und Betriebswissenschaften (English: Institute for Machine Tools and Industrial Management) of TU Munich (TUM)
Laser	Light amplification by stimulated emission of radiation (acronym)
LQR	Linear-quadratic regulator

MCH	Machining center Heller
MIMO	Multi-input multi-output
Mo	Molybdenum (chemical element)
MPC	Model-predictive control
N	Nitrogen (chemical element)
n. No.	no number
NC	Numerical control
No	Numero sign
O	Oxygen (chemical element)
OOA	Out-of-autoclave
P controller	Proportional controller
p.	Page
PA	Polyamide
PA6	Polyamide 6
PA12	Polyamide 12
PA66	Polyamid 6.6
PBT	Polybutylene terephthalate
PC	Polycarbonate
PE	Polyethylene
PE-HD	Polyethylene with high density
PE-LD	Polyethylene with low density
PE-LLD	Polyethylene with linear chains and low density
PEI	Polyetherimide
PEO	Plasma-electrolytic-oxidation
PET	Polyethylene terephthalate
Ph.D.	Doctor of Philosophy
PI controller	Proportional-integral controller

PID controller	Proportional-integral-differential controller
PLC	Programmable logic controller
PMMA	Polymethyl methacrylate
PO	Polyolefin
POM	Polyoxymethylene
PP	Polypropylene
pp.	Pages
PPS	Polyphenylene sulfide
PS	Polystyrene
PSU	Polysulfone
PVC	Polyvinyl chloride
PW	Pulsed-wave
RAC	Remote ablation cutting
RLS	Recursive least-squares algorithm
SAN	Styrene-acrylonitrile resin
SG	Sub-goal
SISO	Single-input single-output
SK	Steilkegel (English: steep taper)
SM	Solution module
SP	Scientific progress
Tab.	Table(s)
TC	Thermocouple(s)
TPE	Thermoplastic elastomer
TUM	Technical University of Munich
TWI	The Welding Institute
TWT	Tool-workpiece thermocouple
V	Vanadium (chemical element)

WLAN	Wireless local area network
wt%	Percentage by weight
XWB	Extra-wide body

Symbols, units, and definitions

Variable	Unit	Definition
Greek symbols		
α	°	Tilt angle of the FPJ tool
α_{th}	$^1/_{\mathrm{K}}$	Coefficient of linear thermal expansion
β	–	Correction factor
Δ	–	Difference
ϵ	–	Emissivity
λ	nm	Wavelength
λ_{th}	$^{\mathrm{W}}/_{\mathrm{m\,K}}$	Thermal conductivity
ρ	$^{\mathrm{kg}}/_{\mathrm{m}^3}$	Density
σ	–	Standard deviation
Latin symbols		
a_0, a_1	–	unknown coefficients
A	–	Matrix A
A^T	–	Transpose of matrix A
$A_{50\,\mathrm{mm}}$	%	Elongation at fracture
A_B or A_F	$^{€}/_{\mathrm{a}}$	Total annual costs for the adhesive bonding system using an autoclave or for an FPJ-based system
A_{Th}	m^2	Area
b_0, b_1	–	unknown coefficients

Variable	Unit	Definition
C_B or C_F	€	Investment costs for the adhesive bonding system using an autoclave or for an FPJ-based system
d_{fiber}	mm	Cross section of the reinforcing fiber
d_{foc}	µm	Spot diameter of the laser beam at the focus
d_w	mm	Working distance (distance between the optics and the surface of the component)
dT	K	Infinitesimal temperature difference
dx	mm	Infinitesimal thickness
D_B or D_F	€/a	Imputed depreciation per year for the adhesive bonding system using an autoclave or for an FPJ-based system
e	–	Euler's number (mathematical constant)
$e(t)$	–	Control error
E	MPa	Elastic modulus or Young's modulus
E_t	mm	Plunge depth
F_a	N	Axial force along the tool axis
F_x	N	Axial force along the x-axis
F_y	N	Axial force along the y-axis
F_z	N	Axial force along the z-axis
h	W/m² K	Heat transfer coefficient
I_B or I_F	€	Imputed interests per year for the adhesive bonding system using an autoclave or for an FPJ-based system
J_{n_P}	–	Cost function along the prediction horizon n_P
k	–	Floating sampling time
k_B	W/m² K⁴	Stefan-Boltzmann constant
K_z	–	Gain
$l(x, y)$	–	Cost term of the MPC
l_{fiber}	mm	Length of the reinforcing fiber

Variable	Unit	Definition
M_a	N m	Tool axis torque
M_B or M_F	€/a	Maintenance and service costs per year for the adhesive bonding system using an autoclave or for an FPJ-based system
n	1/min	Rotational speed of the tool (RPM rate)
n_C	1/min	Control horizon
n_P	–	Prediction horizon
$\boldsymbol{P}_{cost}$	–	Symmetric cost weighting matrix
q	W/m²	Heat flux
$\boldsymbol{Q}_{cost}$	–	Symmetric cost weighting matrix
$r(t)$	–	Feedback variable
$\mathbb{R}$	–	Set of real numbers
$\boldsymbol{R}_{cost}$	–	Symmetric cost weighting matrix
R	%	Imputed interest rate
R_m	N	Tensile strength
$R_{p0.2}$	N	Yield strength
s	–	Variable of the Laplace transformation
t_D	s	Dwell time
t_k	s	Sampling time of the MPC at time k
t_t	s	Dead time
T	°C	Temperature
T_C	°C	Crystallization temperature (range)
T_F	°C	Temperature at the friction surface
T_J	°C	Temperature in the plastic part
T_m	°C	Melting temperature
v	mm/min	Feed velocity
$V(x)$	–	Total cost weighting of the MPC
$w(t)$	–	Nominal value

Variable	Unit	Definition
x	mm	x-coordinate
$\boldsymbol{x}(t)$	–	Control variable (vector or scalar)
$\boldsymbol{x}_{im}$	–	Controlled variable(s) in the idle mode (vector)
$\boldsymbol{x}_k$	–	Controlled variable at time k (vector)
$\dot{\boldsymbol{x}}(t)$	–	Derivation of the controlled variable(s) (vector or scalar)
$\overline{\boldsymbol{x}}(0)$	–	Internal variable of the MPC at time $t = 0$ (vector)
$\overline{\boldsymbol{x}}(n_P)$	–	Internal variable of the MPC at the time n_P (vector)
$\overline{\boldsymbol{x}}(t_k)$	–	Internal variable of the MPC at the time t_k (vector)
$y(t)$	–	Control signal or manipulated variable
$\boldsymbol{y}(t)$	–	Manipulated variable (vector)
$\boldsymbol{y}_{im}$	–	Manipulated variable(s) in the idle mode (vector)
$\overline{\boldsymbol{y}}(t_k)$	–	Internal variable of the MPC at the time t_k (vector)
Y	–	Permissible manipulated variable range of the MPC
$z(t)$	–	Disturbances

1 Introduction

"I just want to say one word to you. Just one word. [...]
Are you listening? [...]
Plastics. [...]
There's a great future in plastics." [1]

(Mr. McGuire (Walter Brooke) in *The Graduate*, 1967)

At the beginning of the 21st century, humankind faces significant environmental challenges (United Nations 2015). In response to these issues, climate protection is one of the political priorities of the European Union (EU). Therefore, the EU Commission launched the European Green Deal (EGD) as a global growth strategy for a climate-neutral and resource-saving economy. The EGD of the EU Commission includes a proposal to reduce the amount of free emission allowances available to airlines as part of the EU Emissions Trading System (EU ETS) (European Commission 2019, p. 13). Since 2020, the global Carbon Offsetting and Reduction Scheme for International Aviation (CORSIA) has forced international air traffic only to grow CO_2-neutrally (ICAO 2016). For these reasons, the German government, in the Statement of Leipzig, has highlighted lightweight design as a key technology to reduce fuel consumption and realize the goal of CO_2-neutral aviation (Altmaier et al. 2019). One approach being pursued is the use of innovative materials, such as fiber-reinforced plastics or high-strength aluminum alloys. These

[1] This conversation, between Mr. McGuire (Walter Brooke), and Benjamin Braddock (Dustin Hoffman), from the movie *The Graduate* (1967), highlights the relevance of this novel type of material.

materials have experienced a rapid growth in the aircraft industry in recent years (Figure 1.1) (Marsh 2010).

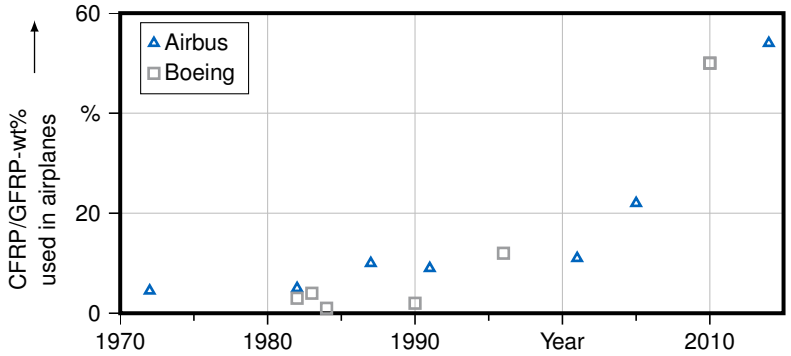

Figure 1.1: Percentage by weight (wt%) of carbon-fiber-reinforced plastic (CFRP) and glass-fiber-reinforced plastic (GFRP) parts used in civil aviation (based on Edelmann (2012))

The Airbus A350 XWB[2] family consists of pure CFRP side shells, reinforced with metallic stringers and frames (Figure 1.2) (Edelmann 2012; Premium AEROTEC GmbH 2014). These stringers and frames are adhesively bonded onto the side shells. Since thermoplastics can be processed faster than thermoset plastics, the latter are increasingly being replaced by thermoplastic components (Barile et al. 2020; Edelmann 2012). From a chemical perspective, adhesive bonds between thermoplastics and metals are difficult to realize. To deal with this, new joining technologies must be developed for bonding metallic and thermoplastic semi-finished products. The study leading to this cumulative thesis aimed at contributing to a better understanding of the novel friction press joining (FPJ) technology, which is suitable for joining thermoplastic materials and aluminum alloys without additional materials or additives. In this context, the intention was to achieve a consistently high quality of the bond without an inefficient, time-consuming parametrization of the controller to regulate the process. The primary scope of consideration was to identify the cause-and-effect correlations, and to model the relevant process

[2] XWB: Extra-wide body

input and output parameters, for FPJ. In terms of the required criteria, this process is an emerging alternative to well-established technologies.

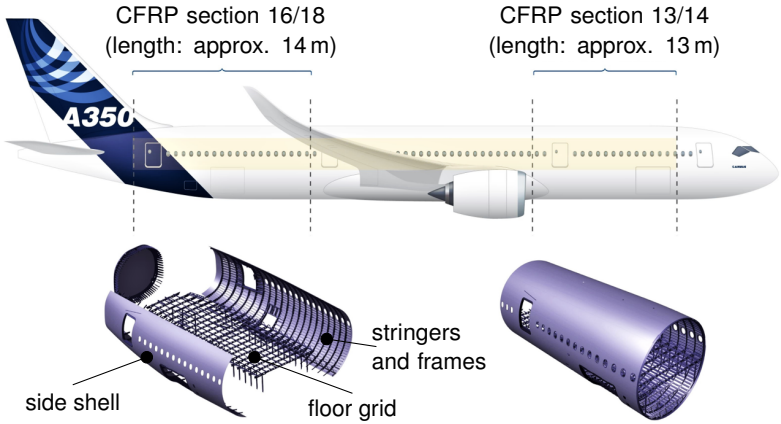

Figure 1.2: Airbus A350-900 with marked shell elements reinforced by stringers and frames (based on PREMIUM AEROTEC GMBH (2011))

One approach to realizing this aim was to examine the closed-loop control of the forces and temperatures occurring during the joining process. These parameters are significant in every plastics engineering process and have a considerable influence on the bond strength (SCHUCK 2009, pp. 59–64). This study focused on commercial aviation and, in particular, its structural components. In this sector, weight-reducing approaches are a key factor in fulfilling the legal regulations (ICAO 2016). Moreover, the cycle-time-optimized and large-volume production of composites is attracting the interest of current research (AIRBUS SE 2019; DIAZ et al. 2017; QUILTER 2001). Therefore, this publication-based study addressed civil aviation as an exemplary case in various contexts. Chapter 2 provides the fundamental technical principles required for understanding this work. In addition, Chapter 3 deals with the state of the art concerning plastic-metal bonds and control engineering concepts. Based on this state of the art, the need for action was determined, and the approach to achieving the aim is specified (Chapter 4). After describing the experimental setup (Chapter 5), the main contents of the scientific publications that stemmed from this work are summarized (Chapter 6). Finally, in Chapter 7, the results

of the study are outlined, the economic aspects of the researched outcome are evaluated, and the benefits are discussed, based on the state of the art.

2 Fundamentals

2.1 Chapter overview

This chapter deals with the fundamentals of FPJ and introduces the required technical terminology. The first part includes the material-technical principles of polymer science and the related basics of aluminum alloys. Based on these insights, the relevant adhesion theories for plastic-metal bonds are presented. According to this theoretical framework, the process of FPJ, the fundamentals of heat transfer modeling, and related aspects of control engineering are discussed.

2.2 Plastic-metal bonds

2.2.1 Overview

In the following, essential aspects of plastic-metal bonds, and the terminology necessary for understanding the following chapters, are presented. In the first part, the fundamentals of materials science for plastics and aluminum are explained. Additionally, fibers are introduced as a reinforcing additive in plastic components. Based on the fundamentals of materials science, adhesion theories are explained regarding plastic-metal bonding. Based on these, the aspects of surface treatments are discussed.

2.2.2 Principles of polymer engineering

Terminology and classification

Although the terms *plastic* and *polymer* are often used synonymously, in this thesis, a differentiation is drawn between *polymer*, *plastic*, and *additive*:

Polymer: A polymer is an organic or semi-organic macromolecule. It consists of repeating structural units (monomers) and is characterized by a high molecular mass. (Osswald & Menges 2012, p. 3)

Plastics: Plastics are synthetic-organic materials that contain macromolecules as their primary components (Osswald & Menges 2012, p. 3).

Additive: An additive is a component of a plastic that modifies its polymer properties, enabling its use as a material (e.g., processing auxiliaries, stabilizers, pigments, fillers, and reinforcing materials) (Osswald & Menges 2012, p. 3).

Based on the macrochemical structure, the thermomechanical behavior, and the molecular dynamics (also known as Brownian motion[3]), plastics can be classified into four groups (Figure 2.1): *thermosets*, *elastomers*, *thermoplastics*, and *thermoplastic elastomers* (TPEs) (Baur et al. 2013, p. 42).

Thermosets: Thermosets are close-meshed, three-dimensionally cross-linked macromolecules. These plastics are neither meltable, swellable, nor deformable. (Osswald & Menges 2012, p. 72)

Elastomers: In contrast to thermosets, elastomers are wide-meshed, three-dimensionally cross-linked macromolecules. The operating temperature is above the glass transition temperature (T_G)[4]. Due to the wide-meshed cross-linking, they are swellable when exposed to chemicals. Their chain flexibility at room temperature allows the elastomers to deform reversibly. (Osswald & Menges 2012, p. 72)

[3] Brownian motion denotes the irregular and abrupt thermal motion of small particles in liquids and gases.

[4] The so-called glass transition divides the brittle energy-elastic temperature range (glass range) from the soft entropy-elastic temperature range (rubber-elastic range).

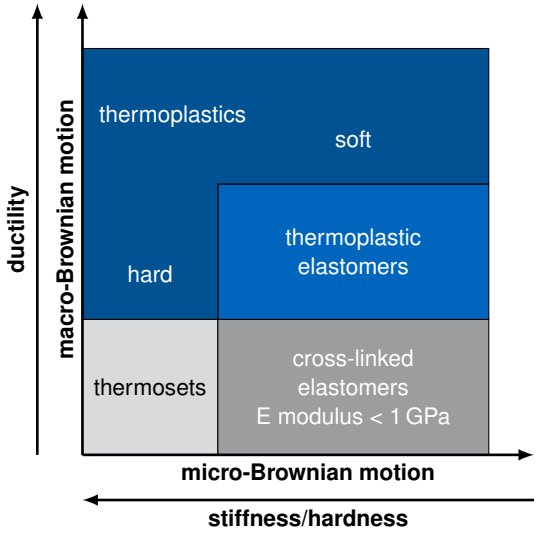

Figure 2.1: Classification of plastics according to their molecular mobility at room temperature (based on BAUR et al. (2013, p. 42))

Thermoplastics: Thermoplastics consist of non-cross-linked chain structures. Because of this setup, these materials can be reversibly melted and reprocessed. (KAISER 2016, pp. 112–115)

Thermoplastic elastomers: TPEs have similar deformation properties at room temperature as elastomers, but can be reshaped by applying thermal energy (KAISER 2016, p. 115).

Due to their macrochemical structure, only thermoplastics (and TPEs) can be reversibly melted, and thus welded. Since TPEs have no relevance in aviation structural engineering, only thermoplastics are considered hereafter.

Thermoplastics: An overview

The formational behavior and mechanical properties of thermoplastics depend on the molecular structure and can be modified by additives. Warming these

materials reduces the inner van der Waals interactions between the macromolecules, accelerating their natural movement[5]. Consequently, a reshaping of the plasticized plastic is possible. (Fahrenwaldt 2009, p. 129)

Based on their internal structure, these plastics can be classified into *amorphous* and *semi-crystalline* plastics, as well as into *mass plastics*, *engineering plastics*, and *high-performance plastics*, in terms of their heat-deflection temperatures[6] (Figure 2.2). This categorization is accompanied by their material price and the quantity of their application. (Kaiser 2016, pp. 28–31)

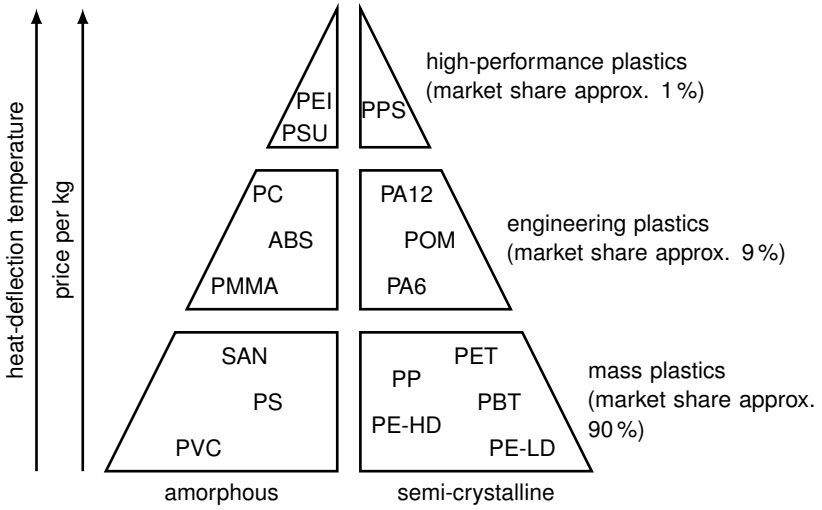

Figure 2.2: Classification of typical thermoplastics according to their heat-deflection temperatures, production volumes, and price; the market shares refer only to thermoplastics (based on Kaiser (2016, p. 31))

Amorphous thermoplastics are translucent, hard, and chemically non-resistant. In contrast, semi-crystalline thermoplastics are characterized by properties such as opacity, toughness, and chemical resistance. (Osswald & Menges

[5] van der Waals forces refer to weak, non-covalent interactions between atoms or molecules.
[6] Heat-deflection temperature refers to the resistance of the plastic to deformation under a given load at a raised temperature.

2012, pp. 60–63) In the following, three types of semi-crystalline thermoplastics, relevant to this study, are presented in more detail.

Polyethylene Polyethylene (PE) is a frequently used plastic in the field of polyolefins (POs). It is a semi-crystalline, non-polar plastic, obtained by radical or catalytic chain polymerization[7], comprising aliphatic hydrocarbons $(C_2H_4)_n$. As initial monomers, propene and ethene are used to form high-molecular-chain structures. (KAISER 2016, pp. 249–251; BAUR et al. 2013, pp. 431–432)

Depending on the form of polymerization, different chemical structures are obtained. Based on these structures, PEs can be categorized into three groups (Figure 2.3):

- Polyethylene with high density (PE-HD)
- Polyethylene with linear chains and low density (PE-LLD)
- Polyethylene with low density (PE-LD)

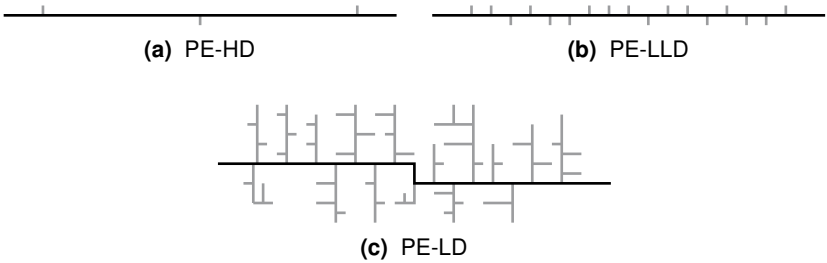

Figure 2.3: Simplified molecular structure of different types of PE, with a black main chain and gray side chains (based on BAUR et al. (2013, p. 27))

Compared to other polymers, all PE types have a low density. In addition, these materials are characterized by their toughness, combined with high

[7] Polymerization is a universal umbrella term for synthesis processes that produce polymers from monomers of the same or different reactants.

elongation at breakage, low moisture absorption, and high chemical resistance. (Kaiser 2016, pp. 256–258)

The chemical structures of the PE derivatives influence the proportion of crystallinity in the plastic component. Linear molecules with short side chains (such as PE-HD and PE-LLD) have a higher share of crystallinity than molecules with long side chains (i.e., PE-LD). This high crystallinity leads to higher stiffness, but also a high shrinkage while cooling down. Because PE-HD has an excellent chemical resistance, due to its high crystalline content, such plastics are often used for large containers and petrol tanks. While PE-LLD is mainly used to produce thin films (up to 5 µm), PE-LD is utilized to cover electrical cables. (Kaiser 2016, pp. 251–258)

Polyamide Polyamides (PAs) are among the most relevant technical semi-crystalline plastics. A distinctive feature of all PA types is their carbon-amide (CONH) group and their high polarity. (Domininghaus et al. 2008, pp. 643–646)

This carbon-amide group enables a hydrogen bond to form between adjacent molecules, resulting in a high toughness, a high deflection temperature, and a high Young's modulus. Furthermore, an excellent friction, abrasion resistance, and resilience against solvents and lubricants characterize this group of materials. One disadvantage is their sensitivity to hydrolysis and their ability to absorb water, which affects their flexibility and tensile strength. This group of materials is often reinforced with glass fibers (GFs), aramid fibers, or carbon fibers (CFs). (Domininghaus et al. 2008, pp. 638–641; Illing et al. 2017)

Polyphenylene sulfide Polyphenylene sulfide (PPS) is a semi-crystalline, high-performance thermoplastic polymer with aromatic monomer units linked by sulfur atoms.

Due to their linear, barely branched structures, these materials are highly crystalline. In combination with their chemical configuration (aromatic ring and sulfur atom), this results in high chemical resistance, high strength, and high heat-deflection temperatures. This group of plastics is usually combined

with reinforcing agents to counteract the brittleness of the material. (Baur et al. 2013, pp. 495–497)

Based on this spectrum of properties, fiber-reinforced PPS is mainly used for components in the aircraft industry (Küll 2002).

Fiber reinforcement

According to Lomov & Verpoest (2005, p. 1), a fiber is defined as a fine, flexible object with a large length-to-thickness ratio (greater than 100) with a circular cross-section.

As a reinforcing material in plastics, fibers are classified according to their length (l_{fiber}) and material. The standard terms used in the literature are (Schürmann 2007, p. 138):

Short fiber: $l_{fiber} = 0.1\,\text{mm} - 1\,\text{mm}$

Long fiber: $l_{fiber} = 1\,\text{mm} - 50\,\text{mm}$

Endless fiber: $l_{fiber} > 50\,\text{mm}$, respectively: $l_{fiber}/d_{fiber} \longrightarrow \infty$

The lengths of short and long fibers are determined in the initial state (short fiber granules or rod-shaped granules) at the beginning of their manufacturing (extrusion or injection molding). Since these fibers break as a result of mechanical and thermal stress in the melting process of the granules, their lengths in the plastic component being produced are up to 88 % shorter than in the starting material (Turkovich & Erwin 1983; Albrecht et al. 2018). Therefore, for this study, short and long fibers were grouped together.

Continuous fibers are only available in sheet or fabric form. The fibers of these sheets are impregnated with the matrix material (thermoplastic or thermosetting plastic) and, as a semi-finished product, adapted to the final contours and consolidated in a later process step.

Another distinction is the fiber material. *Natural fibers*, such as flax, jute, and hemp, are renewable raw materials characterized by low impact resistance (Albrecht et al. 2018). Due to their uncontrollable properties, these fibers are only rarely used in plastics engineering (Ehrenstein 2006, p. 42). *Organic*

fibers are known for their high level of inner orientation, resulting in direction-dependent mechanical properties. Typical examples are carbon, aramid, and polyester fibers. Finally, *inorganic fibers*, such as glass or metal fibers, excel due to their amorphous structures and low production costs (SCHÜRMANN 2007, p. 26).

Each fiber material offers individual advantages and disadvantages. In plastics engineering, aramid, glass, and carbon fibers are of particular relevance (SCHÜRMANN 2007, p. 26). Combined with a matrix material, these fibers form reinforced composite materials.

2.2.3 Principles of aluminum alloys

Due to their high specific strength and low density, aluminum alloys are increasingly replacing steel as an engineering material (OSTERMANN 2014, pp. 9–10). These light metals are classified into hardenable and self-hardening (naturally hard) alloys, as well as into wrought and cast alloys. While the rheological properties are of primary importance for casting alloys, the main focus of wrought alloys is on their mechanical forming properties. In this study, experimental investigations were exclusively conducted on wrought alloys. Thus, casting alloys are not considered further.

Wrought alloys are named according to the standard DIN EN 573-1, and have the abbreviation EN AW (European norm aluminum wrought) and a four-digit number. This number defines the alloy designation and the chemical composition, and divides the wrought aluminum alloys into eight groups (Table 2.1) (DIN EN 573-3). The first digit denotes the main alloying element or elements. The additional digits group the material according to its chemical composition.

Naturally hard alloys owe their mechanical properties mainly to solid solution hardening. During this process, the alloying elements are deposited as interstitial or substitution atoms in the crystal lattice, causing local distortion. This distortion has a slip-impeding effect, meaning that displacements can no longer occur in one plane. This effect leads to higher required energy for deformation, macroscopically indicated as an increase in strength. Moreover, cold work

Table 2.1: Classification of wrought aluminum alloys according to the main groups with their main alloying elements (based on OSTERMANN (2014, p. 191) and DIN EN 573-3)

Group	Main alloying element	Hardenability
1xxx	99 % aluminum	self-hardening
2xxx	Copper	hardenable
3xxx	Manganese	self-hardening
4xxx	Silicon	self-hardening
5xxx	Magnesium	self-hardening
6xxx	Magnesium and Silicon	hardenable
7xxx	Zinc	hardenable
8xxx	Other	self-hardening

hardening, such as rolling, can further improve the strength of naturally hard wrought alloys. With additional heating, their maximum strength usually decreases again. (OSTERMANN 2014, pp. 74–80, 154–155)

The aerospace industry primarily uses hardenable, high-strength, heat-treated alloys of the series 2 and 7 (HUDA et al. 2009; BODILY et al. 2012). According to BARGEL et al. (2000, p. 276), this heat treatment – also known as hardening – comprises three steps:

Solution heat treatment: In this step, the material is heated to dissolve the alloying elements in the aluminum (Al) solid solution[8] (BARGEL et al. 2000, p. 276).

Quench hardening: The heated material is then quenched to room temperature, resulting in a supersaturation in the solid solution (BARGEL et al. 2000, p. 276).

Hardening: After the quenching, the material is artificially aged (cold or hot). This involves storage (artificial aging) at room temperature for a defined time or being slightly heated, depending on the alloying element.

[8] A synonym for solid solution is mixed crystal.

> This process causes the foreign atoms to precipitate into the alloy and distribute homogeneously in the microstructure. (Bargel et al. 2000, p. 276)

With this process of heat treatment, the material properties can be set in a defined way. Thus, the aluminum alloy's mechanical properties depend not only on the individual alloying elements, but also on the thermal and mechanical posttreatment. According to DIN EN 515, a letter (F, O, H, W, or T) and a possible suffixed number define the material condition (temper designation) that indicates the treatment (Table 2.2).

Table 2.2: Selected temper designations for wrought aluminum alloys (based on DIN EN 515)

Condition	Treatment
F	as fabricated
O	annealed
H	strain hardened
W	solution heat treated
T	thermally treated
T3	solution heat treated, cold worked, and naturally aged
T6	solution heat treated and artificially aged

2.2.4 Theories of adhesion

Overview and terminology

This section provides an insight into the fundamentals of adhesion bonding mechanisms and the possibilities for their systematic modifications.

In many respects, direct bonding (direct joining) of thermoplastic components with metals is comparable to adhesive joining, except that the plastic serves simultaneously as a joining partner and as an adhesive. According to Habenicht (2016, p. 315), a model of an adhesive bond consists of two joining partners and an adhesive (Figure 2.4a). This model can be simplified for a

direct bond, as is the case with FPJ (Figure 2.4b). The mechanical strength of such joints is determined by two phenomena – cohesion and adhesion.

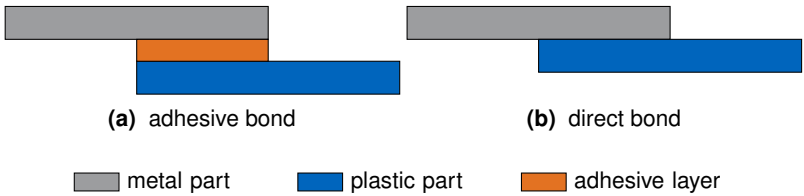

Figure 2.4: Simplified illustration of (a) an adhesive joint with an adhesive boundary layer indicated (based on HABENICHT (2009, p. 315)) and (b) a direct bond between a metal and a plastic component

Cohesion – from the Latin *cohaerere* (English: to connect) – describes the internal strength (i.e., the binding forces) between the atoms and molecules in a substance. Cohesive failure refers to the breakage of a joining partner. Usually, the weak point in a bond is caused by the low bonding forces in the interface layer between the plastic component and the metal part – the adhesion forces.

From the Latin *adherere* (English: to adhere), *adhesion* refers to the bonding between two interfaces. The adhesive forces act within a boundary layer and are responsible for the adhesion between the metal component and the plastic part. In the case of the adhesive failure of a composite, the cohesive forces exceed the sum of all forces in the boundary layer. The adhesion is usually the limiting factor of a bond. According to HABENICHT (2009, p. 324) and SCHONHORN (1985), there is no theory that describes adhesion holistically. Thus, several individual theories have been elaborated (Figure 2.5). In most cases, a combination of different mechanisms is important for bonding in a given system. The extent to which various theories can be applied to a compound depends on multiple factors, such as the surface roughness or the material of the component. Relevant theories for plastic-metal bonds are addressed in the following sections.

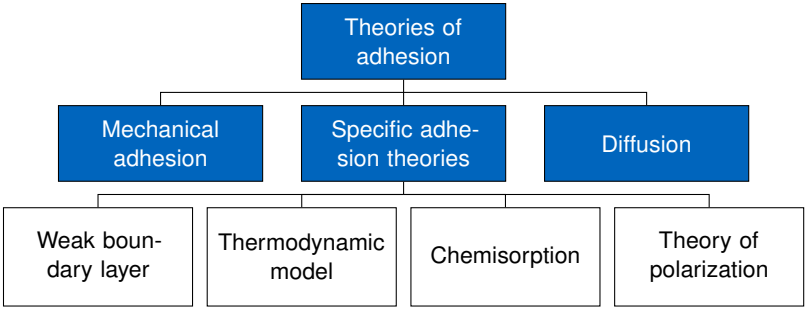

Figure 2.5: Overview of the major adhesion theories relating to plastic-metal bonds (based on ACHEREINER (2009, p. 6))

Mechanical adhesion

The term *mechanical adhesion* defines the form-fit connection of two materials. For plastic-metal direct bonds, the molten plastic penetrates cavities, capillaries, or undercuts on the surface of the adherent (metal), filling these spaces to create a form-fit when solidified (MITTAL & PIZZI 1999). The bond strength of such joints can be improved by a systematic roughening of the metal's surface. A result of this pretreatment is the occurrence of physical and chemical changes, causing further adhesion mechanisms (HABENICHT 2016, pp. 81–82).

Diffusion

VOYUTSKII & VAKULA (1963) presented a molecular physical theory of diffusion. Due to micro-Brownian molecular motion, macromolecules diffuse into the respective joining partner interfaces. During this diffusion, physical bonds form between the two contacting joining surfaces, resulting in an intertwined interface. This phenomenon requires macromolecules with a high degree of mobility and two (in chemical terms) very similar materials. Due to these prerequisites, this form of adhesion occurs almost exclusively when two identical elastomer materials are in contact (HABENICHT 2009, pp. 189, 325). For plastic-metal bonds, this theory is only relevant if a primer is used in which

the diffusion processes can occur. Thus, this phenomenon can be ignored for plastic-metal direct joining.

Specific adhesion theories

The term *specific adhesion* encompasses all adhesion theories based on physical, chemical, or thermodynamic principles acting in the region of 0.2 nm to 1 nm. These theories are used individually or in combination. The four most crucial theoretical concepts are outlined in more detail below. (Flock 2012, p. 13)

Weak boundary layer The theory of the weak boundary layer, presented by Bikerman (1961), describes a fragile interlayer at the interface between a plastic and a metal. According to the author, three possible factors can explain the formation of such a layer: (1) air inclusions (bubbles) at the interface can lead to an insufficient wetting of the metal; (2) residues of chemical reactions can appear as a coating that inhibits joining partner bonding; and (3) a superficial contamination of the adherent by low-molecular substances, which weaken the bond strength by introducing predetermined breaking points.

Such layers can be removed either by cleaning with solvents or by using a material-removing pretreatment to avoid their formation and their negative effect on the bond strength. Due to the simplistic nature of the model – neglecting the crystallinity of the plastic, the chain lengths, the orientation of the polymers, and the cross-linking of the molecules – this theory cannot explain the adhesion in its entirety. However, it is very suitable for explaining a change in the bond strength based on a surface pretreatment. (Achereiner 2009, p. 7)

Thermodynamic model Sharpe & Schonhorn (1964) investigated the correlation between (free) surface energy[9] and bond strength. They postulated that van der Waals forces are the leading cause of the resulting bond strength.

[9] Free surface energy refers to the amount of work required to increase the surface area of a solid phase.

Other intermolecular forces, such as London forces[10], were found to be subordinate in their magnitude. Also, the authors interpreted the van der Waals forces as being a prerequisite for chemisorption (see next subsection). They showed that an increasing (free) surface energy leads to a higher bond strength. According to the study, this is caused by the roughness of the metal joining partner's surface, combined with the increased real surface.

Chemisorption The chemisorption theory, also called chemical adsorption, describes the formation of covalent bonds at the interfaces of the contact partners. While other theories primarily consider intermolecular forces, this model explains irreversible changes in the joining zone (Mittal & Pizzi 1999). This effect was discovered by Schröer (1994), using the example of copper and polar plastics.

Theory of polarization The theory of polarization described by de Bruyne (1939) is based on the interaction between the joining parts resulting from the electrical polarity of their atoms and molecules. This theory presupposes polar groups, such as amide or sulfide units, in the materials, whereby spatial charges shift in the molecules (electric dipoles). This causes an electric dipole moment, where two oppositely charged molecules attract each other. In this context, an increased electronegativity is a criterion for polarity. This theory explains the adhesion of PAs to metals. It does not explain the low adhesion of non-polar materials, such as PE, to metals. (de Bruyne 1939)

In addition to the dipole interactions, hydrogen bridge bonds can arise between joining partners in contact. These are a dominant bond type for amide groups. (Domininghaus et al. 2008, p. 645)

[10] London forces are weak attractive forces between polar or non-polar molecules and atoms caused by the spontaneous polarization of a particle, thereby inducing dipoles in adjacent particles.

2.2.5 Surface treatment

Terminology

As discussed in the previous section, the boundary layer between individual joining partners is a decisive feature for the resulting bond strength. For this reason, the surfaces of the workpieces to be joined are processed before bonding. According to HABENICHT (2009, pp. 542–558), this process – called surface treatment – consists of three main steps:

Preparation: The joining partners' surfaces are deburred, cleaned, and degreased in this preliminary step in order to reduce the influence of the weak boundary layer (HABENICHT 2009, pp. 543–547).

Pretreatment: The surfaces are processed by various methods (based on physical, chemical, mechanical, or their combined effects), resulting in a change of the surface topography and its chemical structure (HABENICHT 2009, pp. 547–548).

Posttreatment: Surface posttreatment includes coating with adhesion promoters and the storage of the materials to avoid unwanted contact of the surface with the environment (HABENICHT 2009, p. 555).

The focus of this study was on the pretreatment only. In this context, the pretreatment of metallic surfaces using laser (light amplification by stimulated emission of radiation) radiation allows a systematic modification of their surface topography. Other benefits of this method include rapid and contact-free processing and that no chemicals are needed. Due to this, laser-based surface pretreatment is advantageous compared to other methods, and is introduced in more detail in the following. (HABENICHT 2009, pp. 552–553; WIRTH et al. 2011)

Laser-based surface modification

A laser is a system that emits monochromatic light with a high intensity and a long coherence length. When this light is focused and collimated onto a surface, the material and the laser radiation interact. Such interactions depend on the

wavelength, the intensity, the polarization, and the tilt angle of the laser beam. Furthermore, the material's temperature, its reflection characteristics, surface structure, and the material itself affect these physical interactions. (Ganeev 2014, pp. 1–8)

Depending on the amount of energy emitted by the laser system, the surface of the material is heated, melted, or vaporized (Thyagarajan & Ghatak 2011, pp. 473–479). With a low energy input, the heating processes can be used to form metallic materials (Merklein 2001) or for local hardening (Bergweiler 2013). Melting and remelting processes occur at a medium level of energy input, causing the material's plastification. This effect can be used either for laser beam welding, laser beam cutting, or the additive build-up of structures (Earl et al. 2012).

To obtain a surface texture, laser beam cutting processes, such as modified remote ablation cutting (RAC) processes, are used. These are characterized by the fact that a high-intensity laser beam is guided along the material's surface at a velocity of several meters per second. During this process, the vaporized material causes a recoil pressure that ejects the molten material out of the process zone. As a result, cutting kerfs are created, whose depth can be adjusted from a few micrometers up to millimeters by multiple exposures. Various authors have used this effect to create parallel grooves, cross patterns, and cycloidal structures. In this work, the structures created using the RAC process are referred to as *microstructures*. (Musiol et al. 2011; Rodríguez-Vidal et al. 2016; Fuchs et al. 2014; Schwab et al. 2018)

In contrast to RAC, the additive build-up for *macroscopic* surface structuring uses the humping effect. This procedure, studied at The Welding Institute (TWI), is known as Surfi-Sculpt® (Dance & Kellar 2004). In this process, the molten metal is accelerated in the direction opposite to the welding direction due to a high vapor pressure, resulting in an accumulation of material residues at the weld seam (Earl et al. 2012). Based on this process, different structures, such as pins and honeycombs, can be produced, with heights of up to 10 mm.

The two aforementioned methods use continuous-wave (CW) laser radiation for the structuring of the surfaces. An alternative way of structuring surfaces involves the use of pulsed-wave (PW) laser radiation with a high pulse frequency.

During the respective processes, a temporary heating occurs on the material surface, resulting in evaporation of the top layer (ablation). At the same time, the rest of the component is not affected. This local ablation cleans the surface of low-molecular residues, such as oils and greases, and modifies the surface topography, making this process suitable for surface preparation and surface pretreatment. The fine and highly-porous oxide structures generated by this process at the surface of the metal are defined as *nanostructures*. (Heckert & Zaeh 2014a)

2.3 Principles of friction press joining

2.3.1 Friction stir welding and friction press joining

Based on friction stir welding (FSW) (DIN EN ISO 25239-1), FPJ has been developed as an innovative joining process for bonding plastic components with metal sheets in an overlap configuration. A fundamental distinction between these two processes is the tool used and the surface pretreatment of the metallic joining partner. The joining process itself is analogous to FSW. (Wirth et al. 2011) Therefore, this technology is referred to in certain paragraphs.

Another term for FPJ that is used in literature is friction lap welding (FLW); both terms can be considered equivalent. The term FPJ was mentioned during a German conference in 2011 (Weddeling et al. 2011), while the term FLW can be found in several international publications. Since this study mainly refers to the results of FPJ publications, this term is used in the following. Furthermore, due to their analogy, all such technologies can be summarized under the umbrella term *friction stir welding processes* (FSW processes).

2.3.2 Process Sequence

FPJ is a five-step process. The first step – surface pretreatment – is a preliminary process (step 0) that affects the bond strength between the joining partners significantly. The actual joining consists of a sequence of four consecutive actions (Figure 2.6) (Meyer et al. 2021b):

0. Surface modification: In this upstream process step, the joining zone of the metallic joining partner is pretreated to increase the bond's adhesive forces.

1. Touch-down: In the first phase of the joining process, the tool rotates at a constant rotational speed (n) around its longitudinal axis. By applying an axial force (F_a) in the negative z-direction, the tool is pressed onto the metallic surface. This phase ends when the tool has reached a certain z-position or a specified axial force is applied.

2. Dwelling: The tool remains at the plunge spot for a defined duration (dwell time (t_D)). This procedure causes the heating by friction and a subsequent deformation of the material, resulting in the release of dissipative energy and further heating of the process zone.

3. Joining: Following the dwell time, the tool is guided at a constant feed velocity (v) over surface of the metallic joining partner. Thereby, the plastic melts in the joining zone and bonds to the pretreated surface of the metallic joining partner (after cooling).

4. Retreat: The joining process ends with the retraction of the tool in the positive z-direction.

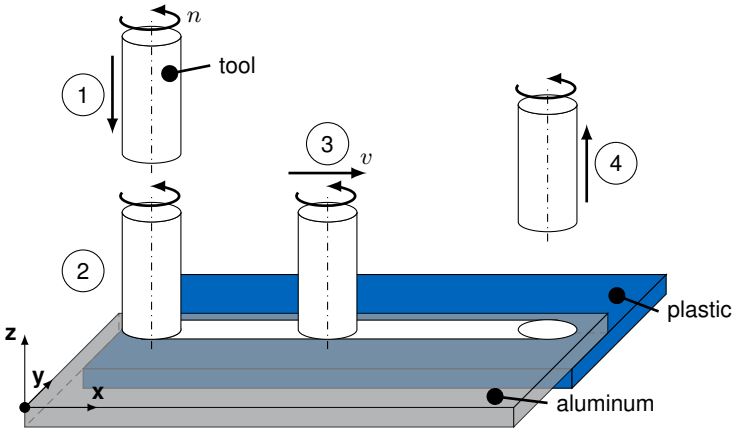

Figure 2.6: Schematic process sequence (steps 1 – 4) of FPJ (based on MEYER et al. (2019b))

2.3.3 Characterization of the FPJ process

The FPJ process is influenced by various input variables that affect the system's dynamics and, thus, the bonding process. These inputs include offline adjustable variables, inline adjustable variables, and non-adjustable and non-controllable variables (disturbances). The process responses are named outputs. These outputs include inline measurable variables and offline measurable variables. (Roth 2016, pp. 12–24; Ruhstorfer 2012, pp. 5, 13)

A precise classification of the individual parameters is not possible, as a classification depends on the control strategy. In this work, the experiments were performed with four different control strategies: rotational-speed-control, temperature-control, position-control, and force-control. In this context, it has to be noted that either the rotational-speed-control or the temperature-control can be used excluding the other mode. The same applies to the position-controlled process or the force-controlled process, which are mutually exclusive. Some combinations of these different control strategies (rotational-speed-control and position-control; rotational-speed-control and force-control; temperature-control and position-control; temperature-control and force-control), however, are, in any case, possible (Table 2.3).

Table 2.3: Overview of the four control methods used in this work with information about the respective input and output parameters

Control mode	**Input**	**Output**
Rotational-speed-control	Rotational speed (n)	Temperature (T)
Temperature-control	Temperature (T)	Rotational speed (n)
Position-control	Plunge depth (E_t)	Force (F_z)
Force-control	Force (F_z)	Plunge depth (E_t)

The following Figures 2.7 and 2.8 illustrating the input and output variables refer to a position-control in combination with a rotational-speed-control, as mainly used according to the state of the art.

Inputs

As previously mentioned, the input variables for FSW, and thus for FPJ, are classified into offline adjustable variables, inline adjustable variables, and non-adjustable variables (disturbances) (Figure 2.7). The offline adjustable variables include the *workpiece*, the *welding and clamping system*, and the *tool*. The inline adjustable variables, however, are understood as *input process parameters*. The last group, the non-adjustable variables (disturbances) include all disturbances which affect the process in an undesired manner.

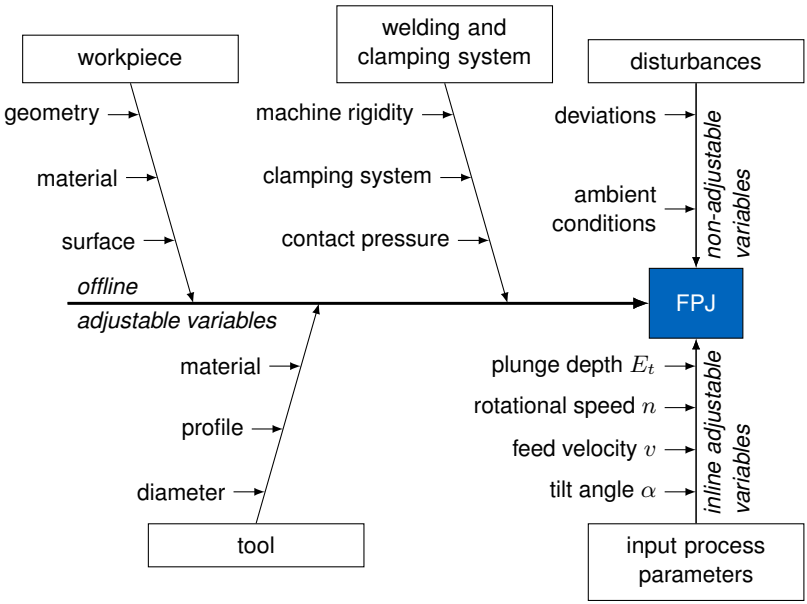

Figure 2.7: Overview of the input variables, divided into offline adjustable variables, inline adjustable variables, and non-adjustable variables (disturbances) for a position- and rotational-speed-controlled FPJ process with selected examples

Workpiece The workpiece is an offline controllable input variable characterized by its geometry, the materials used, and the surface pretreatment. This study was focused on sheet metal geometries with different plate thicknesses, although

the joining of free-form-shaped workpieces is also possible. This joining of free-form-shaped surfaces is accompanied by increased performance requirements for the system used (Ruhstorfer 2012, pp. 131–133). Moreover, complex geometries lead to a varying contact condition along the joining trajectory, affecting the heat input into the workpiece. The materials investigated in the context of this study were limited to two different aluminum alloys and three different thermoplastics. Their thermal and mechanical properties were crucial for the contact conditions (friction) between the workpieces and the tool, and therefore influenced the energy input into the plastic-metal bond.

Welding and clamping system The second offline adjustable input variable is the welding and the clamping system. In addition to FSW machines, (retrofitted) heavy-duty industrial robots and machine tools can be used for FPJ. However, due to the different stiffnesses of the systems relative to each other, the resulting forces in the FPJ process can differ considerably from one another, if a position-control is used (Ruhstorfer 2012, p. 18). To compensate for such differences, appropriate (retrofitted) sensor technology and corresponding control concepts are beneficial. An additional aspect is the influence of the clamping system on the thermal balance. Here, the decisive factors include the different contact conditions caused by the force application points and the contact forces, and the resulting heat transfer coefficients between the workpieces and the clamping. This ultimately influences the resulting temperature in the bond, and therefore the bond strength.

Tool The FPJ tool is cylindrically shaped, and defined by its outer diameter, its front face profile, and the material used. While the tool diameter influences the heat input and pressure distribution in the joining zone, the profiling of the end face affects the optics of the friction track on the metallic joining partner.

Input process parameters The process parameters are variables that are controllable online and adjustable during the process, and can be used to regulate the joining process. Depending on the type of process control – position or force – the manipulated variable is usually the axial force (F_a) or the plunge

depth (E_t) (Soron & Kalaykov 2006). Consequently, the controlled variable is the plunge depth in the position-controlled mode and the axial force in the force-controlled process. For this reason, these two parameters can serve as either input or output parameters. They affect the contact between the tool and the workpiece, and thus the pressure in the interface between the plastic material and the metal. This contact condition influences the resulting temperature (T_J) in the contact zone between the two joining partners.

Similarly, the manipulated variables, such as the rotational speed (n) of the tool or the temperature (T_F) between the tool and the workpiece, can be used as input or output parameters in a rotational-speed-controlled or temperature-controlled process (Fehrenbacher et al. 2014a). While several parameters influence the resulting temperature, the rotational speed is considered the most effective, and is therefore used as a manipulated variable in most temperature-controlled processes (Mishra & Ma 2005).

The feed velocity (v) at which the tool is guided over the surface mainly influences the energy input into the workpiece per section (Lohwasser & Chen 2010, pp. 232–233). To increase this energy input, the feed rate has to be reduced. However, this operation is accompanied by a rise in the resulting process temperatures and a respective decrease in the process forces (X. Zhao et al. 2007, 2009).

The tilt angle (α) is the inclination angle of the tool axis to the normal vector of the workpiece surface. It affects both the plunge depth and the process forces. Typically, the tool is directed towards the part of the seam still to be made, with an angle between 1° to 3° (Figure 2.9).

Disturbances Disturbances are classified as input variables and represent non-controllable influences that affect the process negatively. Such influences include, for example, the ambient temperature, manufacturing deviations, and irregularities in the material itself.

Outputs

The output variables are classified into inline and offline measurable output variables (Figure 2.8). The inline measurable output variables include the *output process variables*. In contrast to that, the *bond properties* are defined as offline measurable output parameters that cannot be identified during the joining process.

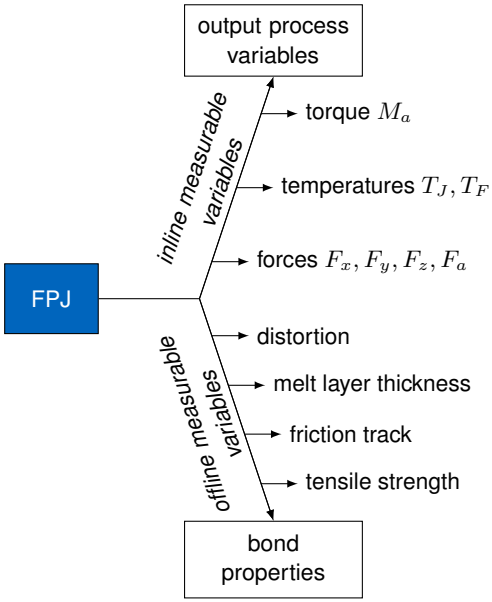

Figure 2.8: Overview of the output variables, divided into offline and inline measurable output variables for a position- and rotational-speed-controlled FPJ process with selected examples

Output process variables As discussed in the section on the *input process parameters*, the categorization of the parameters rotational speed and temperature, respectively, the plunge depth and the axial force depends on the process control strategy (Table 2.3). Thus, the parameters can be classified as input or output parameters (Mahoney & Mishra 2007, p. 2; Bachmann et al. 2017).

The resulting process forces are split into the Cartesian force components F_x, F_y, and F_z. F_x is the force exerted in the direction along the friction track, while F_y is the force perpendicular to the welding direction in the plane of the workpiece surface. The force normal to the workpiece surface, caused by the penetration of the tool into the surface, is labeled F_z. Based on the geometric relationship between F_z and the tilt angle of the tool, it is possible to determine the axial force (F_a) (Figure 2.9):

$$F_a = F_z \cdot \cos(\alpha) \tag{2.1}$$

F_a can be measured using a dynamometer during the process. The torque (M_a) occurs due to the rotation of the tool and the friction between the tool and the workpiece. In the force-controlled mode, the plunge depth (E_t) of the tool into the surface of the part is an output variable that significantly influences the friction track optics. (Mahoney & Mishra 2007, p. 2)

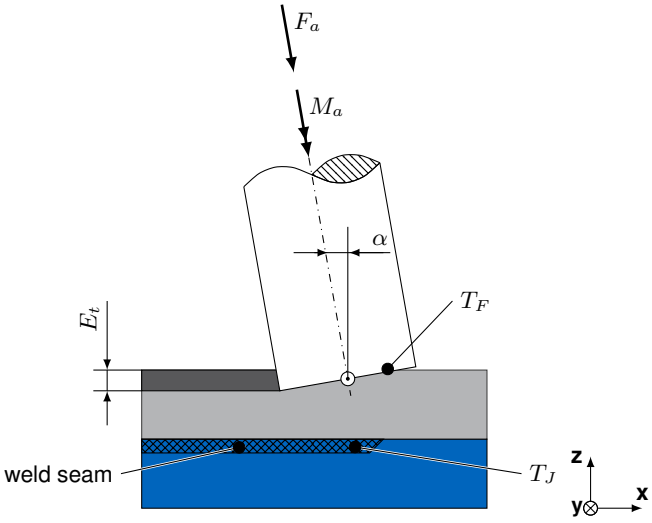

Figure 2.9: Schematic illustration of the FPJ process in a longitudinal cross-section through the weld seam (hatched) and the friction track (dark gray)

The heat introduced into the joining zone results in a temperature field. This temperature field can be measured only at predefined points by thermocouples

placed in the joining zone (temperature T_J) and by thermocouples placed in the front face of the tool (friction zone temperature T_F). The friction zone temperature is an output variable in the rotational-speed-controlled mode and an input variable in the temperature-controlled mode. Similarly, the rotational speed of the tool is an output variable in the temperature-controlled process. (Bachmann et al. 2017)

Bond properties The bond properties that can be measured offline comprise all quantities of the fabricated joint in terms of its quality and characteristics. These quantities can be analyzed with non-destructive methods, such as optical or tactile measurements, to detect the distortion of the workpiece or the resulting friction track on the metallic surface. Destructive methods include the preparation of cross-sections to determine the melt layer thickness, and tensile tests to evaluate the mechanical properties.

2.4 Fundamentals of heat transfer modeling

As mentioned in the previous section, only the temperature T_F can be measured continuously. For this reason, a model has to be developed to determine the interfacial temperature T_J. This section introduces the basics of heat transport modeling, which are required in the further parts of this thesis.

According to thermodynamics, heat is a form of energy exchanged between two systems (i.e., bodies) due to a temperature difference. This energy can be transmitted in three different ways: by conduction, convection, and radiation. Pure conduction can only occur in solids, whereas convection is only possible in fluids. The heat radiation between bodies consists of electromagnetic radiation and depends on the temperature of the bodies and their optical characteristics. Therefore, thermal radiation can also take place in a vacuum, contrary to conduction and convection. In engineering applications, a combination of several forms of heat transfer is commonly considered. (Karwa 2020, pp. 1–4)

Conduction

Thermal conduction refers to the heat transfer between two bodies (or particles and molecules) in direct contact with each other. This form of heat transfer occurs in all solids, liquids, and gases as soon as a temperature difference arises. In pure solids, conduction is the only possible form of heat transfer. The heat flux in homogenous solids is directly proportional to the temperature gradient. Figure 2.10 shows a planar sheet of thickness X. Here, the segment with infinitesimal thickness dx presents a thin section compared to its height. Therefore, this heat conduction can be simplified to a one-dimensional (in direction x only) heat flux problem through the area A_{Th}. Considering a temperature difference caused by the edge temperatures T_1 at the left boundary and T_2 at the right boundary, this results in a heat flux through the body. For the infinitesimally thick section, this results in a temperature difference from its left to its right edge of dT. Thus, for the heat flux q across the area A_{Th}, the following relation occurs (Karwa 2020, pp. 1–2):

$$\frac{q}{A_{Th}} \propto \frac{dT}{dx} \tag{2.2}$$

This proportional correlation can be described by the material-dependent parameter λ_{Th} (thermal conductivity) (Karwa 2020, p. 2):

$$\frac{q}{A_{Th}} = -\lambda_{Th} \cdot \frac{dT}{dx} \tag{2.3}$$

Convection

The term convection refers to the simultaneous heat and mass transfer in fluids induced by fluid flow. This flow can be caused by various forces, including gravity or forces caused by pressure, density, temperature, or concentration gradients. In this context, the terms *forced convection* and *free convection* are distinguished. In the case of forced convection, the heat and mass transport is caused by external forces, including induced forces by pumps or fans. Free convection refers to the transport of heat and material caused exclusively by density and thus gravitational differences. (Karwa 2020, pp. 2–4)

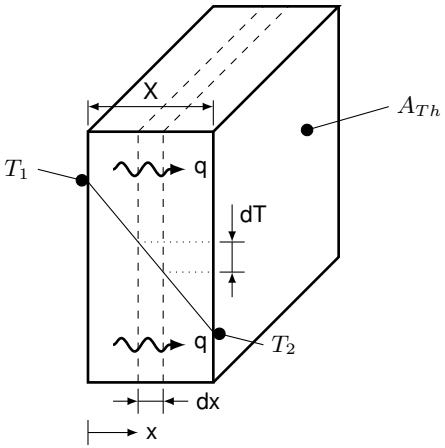

Figure 2.10: Conduction heat flow through a solid body (based on KARWA (2020, p. 2))

Convective heat transfer is always accompanied by heat conduction. For the combined heat transfer occurring between a surface of a solid and a liquid, the following equation applies:

$$q = hA_{Th}\Delta T, \tag{2.4}$$

with ΔT being the temperature difference between the fluid and the surface of the solid, A_{Th} as the area of the solid in contact with the fluid, and h as the heat transfer coefficient. The heat transfer coefficient depends on the thermophysical properties of the fluid and the type of flow (laminar or turbulent flow). (KARWA 2020, p. 3)

Radiation

Thermal radiation refers to the heat transfer by electromagnetic waves caused by the surface temperature of a body. The amount of radiation depends on the temperature of the body and its optical properties, namely the emission coefficient ϵ. Because this heat transport phenomenon is based only on

electromagnetic radiation, it is also present in a perfect vacuum. The radiated thermal energy is directly proportional to the fourth power of the absolute temperature of the body (Karwa 2020, p. 4):

$$q = k_B A_{Th} T^4 \tag{2.5}$$

with k_B as the Stefan-Boltzmann constant, A_{Th} as the surface area of the body, and T as the absolute temperature of the body. The above assumption is based on the idea of a perfect black body. A black body has a surface whose emission and absorption coefficient is 1. This means that the thermal radiation is completely absorbed and no reflection and no transmission occurs. Also, a black body is a perfect radiator. In contrast, real bodies – also called gray radiators – have an emission and absorption coefficient smaller than 1, which means that not all of the thermal radiation can be absorbed. (Karwa 2020, p. 4)

Thermal modeling

In various complex engineering problems, analytical solutions are difficult to identify. For this reason, numerical methods are used to solve such engineering issues (Baskharone 2013, p. 1). Common numerical solution methods are the Finite Element Method (FEM), the Finite Volume Method (FVM), and the Finite Difference Method (FDM). In this thesis and in the context of the state of the art, FEM and FDM were used to simulate the heat conduction in multilayer systems. Therefore, in this section, a brief introduction to the fundamentals of FEM and FDM will be given.

FEM is a numerical method to calculate the approximate solution of partial differential equations. The basic idea of FEM is to divide a domain into a finite number of non-overlapping elements with simple shapes. The solution of the entire domain can be obtained by solving the simple problems from the simple units with a known shape. FEM-models can be solved by the variational method or the weighted-residual method. (Reddy & Gartling 2010, pp. 43–44)

The main steps to solve the problem with FEM are: (1) Discretization of the domain into a series of finite elements with different shapes; (2) assembling the finite elements to obtain the global algebraic equations; (3) defining the boundary conditions and applying these conditions to the equations; and (4) solving the equation to obtain the approximate solution. (Reddy & Gartling 2010, p. 44)

Another numerical method to solve partial differential equations is the FDM. Here, the spatial and the time domain are both divided into a finite number of mesh points (nodes), and the derivative of each point is replaced with a finite difference approximation. The information in between the nodes can be determined by the Taylor series expansions. (Lapidus & Pinder 1982, pp. 4–11)

In the past, the most commonly used numerical method was the FDM. However, FDM has a shortcoming. It only discretizes the domain into regular grids. When the geometric shape is irregular, the divided grids cannot fit perfectly. In this case, FEM has an advantage since the finite element mesh does not have to be uniform, and the simple elements can be of different shapes (i.e., triangles, quadrilaterals). These different shapes allow even complex bodies to be discretized almost perfectly. (Baskharone 2013, pp. 1–3; Lapidus & Pinder 1982, pp. 4–11)

2.5 Relevant principles of control engineering

2.5.1 Terminology

Control engineering deals with the manipulation of a dynamic system in terms of its static and dynamic behavior (Lunze 2016, p. 1; Steffenhagen 2011, p. 15). By doing so, a continuous adjustment of a specified nominal (target) and a measured value is performed (Figure 2.11). The objective of control engineering is to minimize the difference between these two signals due to the systematic influence of the process. According to DIN EN 60027-6, the nominal value is referred to as the *reference variable* ($w(t)$), and the actual detected value as the *feedback variable* ($r(t)$). The difference between these

two variables is termed as the *control error* ($e(t)$). This error is passed on to the *controller*, which determines the *control signal* ($y(t)$) – also known as the *manipulated variable* – based on the given control parameters. This signal is transferred to the *plant* (the dynamic system), where the unpredictable *disturbances* ($z(t)$) occur, and thus the *plant output* ($x(t)$) results. This *plant output* is detected by a measuring unit and fed back to the *reference input*.

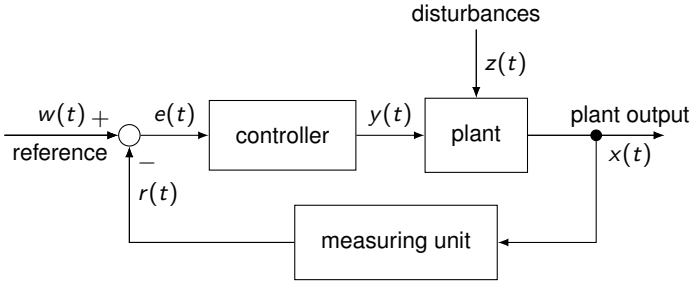

Figure 2.11: Schematic illustration of a control loop with a measuring unit

To affect a process in a targeted manner, a detailed understanding of the dynamic system's (plant) behavior is essential. Based on this knowledge, a suitable control system can be designed. The principles of modeling are discussed in the next section, followed by a description of the model-predictive control (MPC) concept.

2.5.2 Modeling in control engineering

System identification is a method used to identify the correlations between the input and output variables in a dynamic system. In combination with subsequent modeling, it is possible to formulate a mathematical description of all the significant dynamic effects of a system. This model-based definition can be used to design and test different offline-control systems before the entire system is launched. (Lunze 2016, pp. 41–43)

For the modeling of dynamic systems, Bohn & Unbehauen (2016, p. 5) differentiated between theoretical (white-box approach) and experimental (black-box approach) methods. Theoretical modeling is based on the physical

and geometrical description of the temporal behavior of the dynamic system. Thus, pure white-box models can be designed without a real, existing system and are mostly highly accurate. Their disadvantages include the extensive mathematical model required and the uncertainties in identifying internal and external disturbances. (Bohn & Unbehauen 2016, pp. 5, 6, 242)

In contrast to the white-box model, a black-box model uses a real, existing plant for the system identification. Thereby, no preliminary understanding of the system characteristics or the system architecture is necessary, and a time-consuming theoretical analysis can be avoided. By stimulating the system (e.g., by a Dirac pulse or a step function) and simultaneously recording the output variables, predefined model structures can be parametrized in order to optimally describe the plant's behavior. The model's various parameters are determined by an iterative minimization of the deviation between the measured data and the model-predicted data. The advantage of this method is the rapid identification of the dynamic model, even with limited system knowledge. However, the restricted validity of the results, particularly with respect to their transferability to other systems, and the need for a real, existing plant, are unfavorable features. (Bohn & Unbehauen 2016, pp. 6, 242)

A combination of these two methods is the gray-box approach. In this, simple correlations are identified by preliminary theoretical considerations, which reduce the number of tests for the experimental system analysis. Furthermore, generally valid physical parameters can be introduced, and unknown parameters can be determined experimentally. Thereby, this procedure improves the transferability of the developed system models compared to pure black-box models. (Bohn & Unbehauen 2016, pp. 6, 242–243)

2.5.3 Model-predictive control

According to Völz (2016, p. 3), MPC is an innovative approach in control engineering, particularly suitable for nonlinear multivariable systems, whereby boundary conditions of the manipulated variables (output signals) can be considered.

MPC is based on optimization, involving the minimization of the quality criteria of a time-discrete dynamic process model, in order to stabilize the controlled variable(s) ($\boldsymbol{x}(t)$) as a function ($\boldsymbol{f}$) of the input and output variables:

$$\boldsymbol{x}(t) = \text{constant}, \tag{2.6}$$

meaning that

$$\dot{\boldsymbol{x}}(t) = 0 = \boldsymbol{f}(\boldsymbol{x}_{im}, \boldsymbol{y}_{im}), \tag{2.7}$$

where $\dot{\boldsymbol{x}}(t)$ is the derivation of the controlled variable(s) ($\boldsymbol{x}(t)$) of the plant output, $\boldsymbol{x}_{im}$ is equal to the controlled variable(s) in the idle mode, and $\boldsymbol{y}_{im}$ is equal to the manipulated variable(s) in the idle mode. Equations 2.6 and 2.7 specify the purpose of the closed-loop system mathematically. Equation 2.7 illustrates that the derivative, i.e. the change, of the system output remains constant in the steady state (idle mode).

Control engineering applications solve the optimization problem numerically, although this yields only to an approximate solution. For this reason, the optimization is limited to a finite horizon (abort criterion), the so-called prediction horizon (n_P) (Figure 2.12). At the time t_k, the controlled variable ($\boldsymbol{x_k}$, measured output in Figure 2.12) is measured, and the optimum manipulated variable response ($\boldsymbol{y}(t)$, predicted output in Figure 2.12) is calculated. This optimum output characteristic results from minimizing an initially defined cost function (J_{n_P}) along the prediction horizon, where the predicted control input is only considered variable within the control horizon (n_C). By restricting the permissible value range in the cost function, any restrictions on the manipulated variables (y_{min} and y_{max} in Figure 2.12) can be defined and considered. In this context, the following criteria apply to a multi-input/multi-output (MIMO) system[11]:

$$\min_{\overline{\boldsymbol{y}}(\cdot)} \; J_{n_P}(\boldsymbol{x}_k, \overline{\boldsymbol{y}}) = V(\overline{\boldsymbol{x}}(n_P)) + \int_0^{n_P} l[\overline{\boldsymbol{x}}(t_k), \overline{\boldsymbol{y}}(t_k)]dk, \tag{2.8}$$

with

$$\overline{\boldsymbol{x}}(0) = \boldsymbol{x}_k = \boldsymbol{x}(t_k) \tag{2.9}$$

[11] For single-input/single-output systems (SISO system), the matrices and vectors can be replaced by simple variables or functions.

and

$$\overline{\boldsymbol{y}}(t_k) \in Y, \tag{2.10}$$

including the cost term, $l(x, y)$, the (optional) total cost weighting, $V(x)$, the internal variables, $\overline{\boldsymbol{x}}(t_k)$ and $\overline{\boldsymbol{y}}(t_k)$, the prediction time, $k \in [0, n_P]$, and the manipulated variable range, Y. (Völz 2016, p. 4)

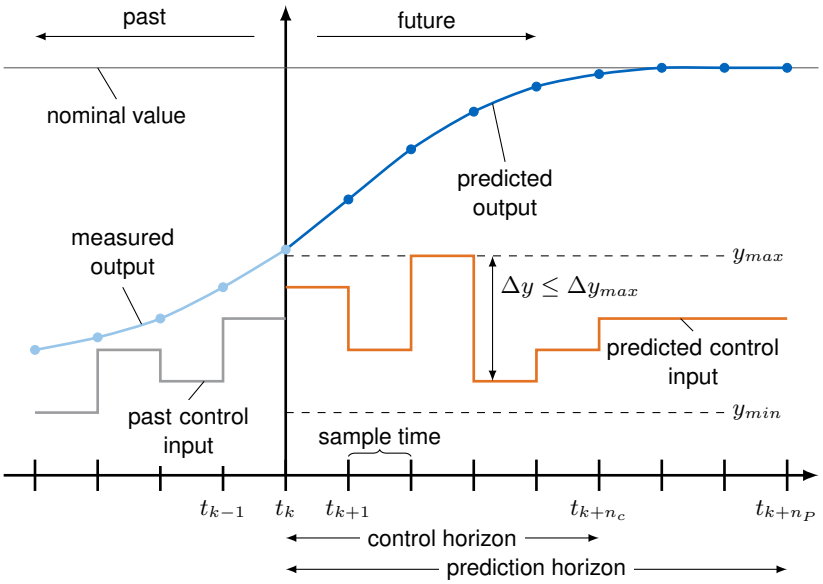

Figure 2.12: Concept of the moving horizon, and a schematic representation of the method of an MPC (based on Dittmar & Pfeiffer (2009))

Based on the approximate solution of the control strategy, the first calculated datapoint of the optimal solution ($y(t_k)$) is applied to the system. Subsequently, according to the moving horizon principle, the system's current condition ($\boldsymbol{x}_{k+1}$) is resampled, and the calculations are repeated based on the new state (Figure 2.13). This new calculation allows the system to detect and compensate for disturbances. (Völz 2016, pp. 4–5)

According to Völz (2016, pp. 5–6), the cost function (J_{n_P}) substantially influences the optimal solution. In the worst case, an optimization problem may not be solvable if the selected cost function is not appropriate. One

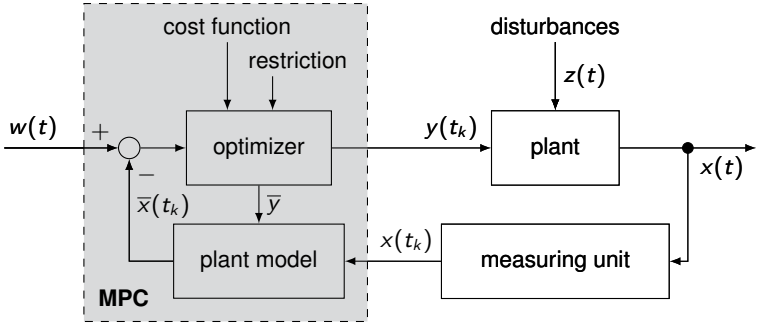

Figure 2.13: Schematic representation of the closed-loop control system of an MPC, including an optimizer and a process model

common approach for J_{n_P} is the quadratic weighting of the conditions and the control variables in the integral cost term ($l(\overline{\boldsymbol{x}}, \overline{\boldsymbol{y}})$) and in the final cost function ($V(\overline{\boldsymbol{x}})$). This results in the cost function for a multivariable system:

$$J_{n_P}(\boldsymbol{x}_k, \overline{\boldsymbol{y}}) = \Delta\overline{\boldsymbol{x}}(n_P)^T \boldsymbol{P}_{cost} \Delta\overline{\boldsymbol{x}}(n_P) + \int_0^{n_P} \left[\Delta\overline{\boldsymbol{x}}(t_k)^T \boldsymbol{Q}_{cost} \Delta\overline{\boldsymbol{x}}(t_k) + \Delta\overline{\boldsymbol{y}}(t_k)^T \boldsymbol{R}_{cost} \Delta\overline{\boldsymbol{y}}(t_k)\right] dk, \tag{2.11}$$

with the symmetric matrices $\boldsymbol{P}_{cost} \in \mathbb{R}^{n\times n}$, $\boldsymbol{Q}_{cost} \in \mathbb{R}^{n\times n}$, and $\boldsymbol{R}_{cost} \in \mathbb{R}^{m\times m}$ allowing the individual weighting of the conditions. The functions

$$\Delta\overline{\boldsymbol{x}} = \overline{\boldsymbol{x}} - \overline{\boldsymbol{x}}_{im} \tag{2.12}$$

and

$$\Delta\overline{\boldsymbol{y}} = \overline{\boldsymbol{y}} - \overline{\boldsymbol{y}}_{im} \tag{2.13}$$

represent the internal states and deviations relative to the aimed steady-state condition (Equation 2.7).

Based on this adjustable cost function, in combination with calculation of the optimized manipulated variable in each time step, a wide range of possibilities arises for controlling highly dynamic complex processes. It should be noted that sufficient computing power must be available to calculate each solution in real-time.

3 State of the art

3.1 Chapter overview

In this chapter, the topic-relevant findings regarding plastic-metal bonds are summarized. The first part deals with FPJ, surface pretreatment, and the associated joining processes essential to the aim of this study. Process control approaches are introduced in the second part, particularly the regulation of the contact force and the process temperatures. The last part deals with the state of the art of heat transfer modeling in FSW processes.

3.2 Plastic-metal direct bonds

FPJ is a complex thermomechanical process, influenced by numerous parameters (Section 2.3). In particular, the axial force (F_a), the rotational speed (n), and the feed velocity (v) have been identified as the most relevant parameters that affect bond strength (Wirth et al. 2014a). The latter two parameters mentioned were evaluated by Liu et al. (2014), and correlated with the resulting melt layer thickness of the plastic part using the term $\sqrt{n/v}$ as a parameter for the energy input. This experimentally identified value consisting of the feed velocity and the tool speed and being a parameter for the energy input was also proposed in a similar form by Arbegast et al. (1999) for FSW. Liu et al. (2014) found a high correlation with the melt layer thickness of PA6, leading the authors to conclude that this value is a reliable parameter for the heat input in FPJ processes. Since the melting process of PA6 does not correlate linearly with the introduced power due to the enthalpy of melting, the

relationship chosen by Liu et al. (2014) for the material combination of PA6 and aluminum is plausible. A generally valid statement for other plastics was not made. Thus, a transfer of the results to other plastic-metal combinations seems questionable.

Besides the study of the energy input during the joining process, the research on FPJ has focused on surface pretreatment in order to increase the bond strength of plastic-metal joints. Fuchs et al. (2014) and Wirth et al. (2014b) investigated the influence of different macro- and micro-structuring methods on the bond strengths of EN AW-6082-T6 with PA6-GF15. These studies showed that the microstructures produced by a CW process lead to a high bond strength and offer economic advantages due to the rapid processing. Also, for non-polar plastics, such as polypropylene (PP), a laser-based surface pretreatment improved the adhesion (Han et al. 2020).

Liu et al. (2015) joined PE and magnesium sheets via FLW using a corona-plasma pretreatment for the plastic part and a plasma-electrolytic-oxidation (PEO) pretreatment for the magnesium alloy sheet. This PEO-pretreated surface formed a fine oxide layer on the surface of the joining partner. This layer allowed the PE to bond with the metal on a microscopic level, penetrating into gaps and undercuts, which resulted in a mechanical adhesion effect, thus increasing the strength of the plastic-metal bond.

Surface pretreatment is not limited to FPJ or FLW. It is also a crucial process step in other plastic-metal direct joining methods. Heckert & Zaeh (2014a,b) compared the laser-based surface pretreatment (macro-, micro-, and nanostructures) and a mechanical pretreatment method (sandblasting) for laser-based heat conduction joining. They showed that micro- and nanostructures are beneficial for different material combinations (EN AW-6082-T6 with PA6-GF15, PA66-GF50, and polybutylene terephthalate [PBT]-GF60). Nanostructuring, in particular, led to high bond strength for the combination of the continuous fiber-reinforced PBT-GF60 and aluminum. It was found that, due to the low surface roughness of the nanostructure compared to the microstructure, the undercuts could be entirely filled. In contrast, the plastic's matrix share was insufficient to fill the undercuts in the microstructure. Thus, no or insufficient form closure (mechanical adhesion) was achieved, and the bond was weakened. Contrary to this, nanostructuring enabled form-fit and further

binding mechanisms, leading to higher bond strength. The fabrication of the macrostructures was considered time-consuming, however. In addition, hot cracks were detected in the obtained pins of the macrostructures, reducing the bond strength. (Heckert & Zaeh 2014b; Heckert 2019)

For direct bonds produced via injection molding, Enami et al. (2020) studied laser micro-drilling, which produces holes with diameters in the range of 40 µm to 80 µm, as a pretreatment method for aluminum surfaces. Tensile strength was found to increase with an increasing number of holes and smaller diameters of the holes. In addition, they showed that the structure of the inner surface of the holes was a decisive factor for the bond strength.

Wunderling et al. (2019) studied a modified RAC process for generating microstructures. They investigated the effects on the distortion of the metallic joining partner, and identified a cycloidal structure as the most suitable method for distortion-minimized structuring. They postulated that this circular structure shows an anisotropic behavior in plastic-metal bonds due to the pattern of the cutting kerfs, and the bond has identical lap shear values regardless of the direction of patterning applied. This approach was verified in a subsequent publication that described the cycloidal structure's effect on the tensile shear strength of steel joined with a thermosetting plastic (Wunderling et al. 2020).

Buffa et al. (2016) investigated an FPJ-like process in which the molten plastic (PP) was pressed through holes drilled into an aluminum sheet leading to a form-fit (quasi-dovetail) joint. The main focus of this work was a simulation-based prediction of a fluid's flowing characteristics. They concluded that the distribution of the pressure in the interface between the plastic and the metal, applied by the FPJ tool, was a decisive criterion for the bond strength.

An additional process variant is friction spot joining (FSpJ), as investigated by Goushegir et al. (2014) and André et al. (2018) for a sandblasted, high-strength aluminum alloy of the 2xxx series in combination with a PPS-CF. Due to the low thermal conductivity, the researchers proved that a thin matrix layer on the fibers was sufficient for a high-strength bond. In comparison, excessive matrix material was found to weaken the bond strength. The authors also postulated that the plastic's low viscosity favored the wetting of the metallic

joining partner. Based on these results, Alessio et al. (2020) focused on simulating the mechanical strength of FSpJ joined aluminum-PPS-CF bonds. By using FEM, the ultimate lap shear force could be determined with a deviation of 8 %, and the displacement at failure with a deviation of 1.6 %. Additionally, the influence of the distance of the tool relative to the aluminum edge (with the same overlap length) could be analyzed. It was found that the maximum force was constant with increasing distance, while the displacement at failure increased. (Alessio et al. 2020; André et al. 2018)

Not only aluminum alloys have been the subject of this area of research; copper has also been successfully tested as a metallic joining partner in the FLW process. Wu et al. (2018) examined air inclusions in the plastic (PA6-CF20) and the feed-velocity-dependent temperature-time profile, finding that, not only did the maximum temperature influence the bond strength and number of air inclusions, but also the time interval during which the maximum temperature occurred.

Interim conclusions

This section on the state of the art shows the feasibility of the process, the importance of the individual process parameters, and the relevance of surface pretreatment to obtain a high bond strength. The contact forces between the plastic component and the metal, and the resulting temperatures have been identified as significant influencing factors (Wirth et al. 2014a; Buffa et al. 2016), although they have not yet been controlled during the process. In addition, the benefits of various surface pretreatment strategies for increasing the bond strength have been presented (Fuchs et al. 2014; Wirth et al. 2014b; Heckert & Zaeh 2014a). In particular, laser-based processes offer advantages in terms of reproducibility, increased strength, and economic efficiency. However, unsolved issues remain concerning the suitability of novel pretreatment structures, such as the cycloidal structures (Wunderling et al. 2019), for FPJ, and whether force- and temperature-controlled processes offer further advantages. For this reason, the following section deals with different control strategies used in FSW processes.

3.3 Control approaches for friction stir welding

3.3.1 Overview

In this section, the state of the art on control strategies for the contact forces and temperatures in FSW processes is reviewed. Each section is concluded with a brief summary.

3.3.2 Force control in friction stir welding

As outlined in the previous section, the axial force of the tool, respectively the contact force between the tool and the metal surface, is among the most significant parameters in the FPJ process, affecting the quality of the plastic-metal bond. To date, there has been no research on force-controlled FPJ. Therefore, this section deals with a related process – FSW.

Gebhard & Zaeh (2008) designed and implemented a force control for FSW on a machining center (Heller MCH 250). Based on the approximately linear relationship between the motor current of the feed drive and the resulting force in the axial direction (z-axis) (Figure 2.6) above 5000 N, a simple proportional controller (P controller) was realized. The motor current was used as a variable in the numerical control program (NC program) and was multiplied by the controller parameter to continuously correct the plunge depth. With force values below 5000 N, this approach had a limited capability of representing the relation between the motor current and the axial force, resulting in a significant difference between the calculated and applied force. (Gebhard 2011) Therefore, this control concept is not suitable for the FPJ process (1000 N to 3000 N). (Buffa et al. 2016; Wirth et al. 2014a)

For the robot-based FSW of complex geometries, Soron & Kalaykov (2006) developed an approach for adjusting the contact force via the plunge depth using a proportional-integral controller (PI controller). Since there was no model for the system's transfer function, the design of the PI controller was determined empirically.

Longhurst et al. (2010) analyzed the influence of the plunge depth, the tool's rotational speed, and the feed velocity as manipulated variables for controlling the axial force. Using the Ziegler–Nichols tuning method (Ziegler & Nichols 1942), a proportional-integral-differential controller (PID controller) was designed for each manipulated variable. It was shown that, by adjusting the tool's rotational speed, the amount of generated thermal energy, and therefore the stiffness in the tool-workpiece contact area, could be varied. Thus, the contact force could be adjusted at a constant plunge depth. The same effect was observed with a control via the feed velocity. At lower feed velocities, more thermal energy is introduced locally into the workpiece. This effect results in an increased softening of the contact area between the tool and the workpiece. It was found that the highest control accuracy was achieved via the rotational speed of the tool, followed by the feed velocity and the plunge depth. However, the authors emphasized that inaccuracies in the process, such as uneven workpiece surfaces, or deflections caused by the machine structure, can only be compensated for by regulating the plunge depth. (Longhurst et al. 2010)

X. Zhao et al. (2007, 2009) used a model-based approach to design a control system. Like Longhurst et al. (2010), these authors investigated different process parameters in order to influence the axial force. They demonstrated that the resulting force was only affected by the tool's rotational speed or feed velocity in a limited way, and that the plunge depth was dominant. Thus, the process model can be simplified in the stationary state to

$$F_z = K_z \cdot E_t^{\beta}, \tag{3.1}$$

with K_z as the gain factor, E_t as the plunge depth, and β as the correction factor. The unknown coefficients were determined by the least-squares method from the experimental and model-based data.

To calculate the dynamic relationship between the plunge depth and the axial force, the authors used a transfer function with two poles and one zero. Additionally, a pure dead time element was implemented to represent the

response time of the input signal processing and the actuators of the system. Thus, the relationship

$$F_z(s) = \frac{b_1 s + b_0}{s^2 + a_1 s + a_0} \cdot e^{t_t} \cdot E_t^{\beta}(s) \tag{3.2}$$

with the unknown coefficients a_0, a_1, b_0, and b_1, Euler's number e, the Laplace variable s, and the dead time t_t was obtained for the dynamic system model. The unknown coefficients were calculated for each experiment separately, using the recursive least-squares algorithm (RLS), before being averaged. The authors used this parametrized system model for the model-based design of the control system. The dynamic approach represents the process with sufficient accuracy, and can thus be used for the control. (X. Zhao et al. 2007, 2009)

A similar approach was chosen by Oakes & Landers (2009). They selected 10 sets of parameters within a predefined process window and used the obtained dataset to parametrize the model. The measured signal was subject to a high level of noise due to the tool's eccentricity and the background noise of the sensor. Therefore, the preprocessing of the measuring signal by a Kalman filter was examined. Due to the designed controller (Smith predictor), in combination with the Kalman filter, it was possible to map a constant nominal force and a sinusoidal variation in the nominal force during the process. (Oakes & Landers 2009)

Davis et al. (2010) used an observer-based adaptive robust control (ARC) approach to regulate the axial force via the feed velocity. In this work, a model was developed to calculate the contact force via the applied power of the spindle motor. The authors showed that this approach considerably reduced the differences between the nominal and real force, even under significant process disturbances. However, it turned out that the model for calculating the force based on the actual motor power had a high degree of uncertainty and required further improvement. Additionally, they highlighted that the feed velocity, as a manipulated variable, could lead to an unacceptably high plunge or insufficient contact between the tool and the workpiece if the workpiece surface differed significantly from the specified welding trajectory. (Davis et al. 2010)

Another model-based approach for designing a force control via the plunge depth has been presented by S. Zhao et al. (2016). Based on X. Zhao et al. (2007, 2009) and Oakes & Landers (2009), the proposed transfer function of the system was used to design a linear-quadratic regulator (LQR), also known as a Riccati controller, and includes a dead time compensation. This concept, similarly to the MPC, is a sub-problem of the optimal control concept. Hence, the manipulated variable is calculated by minimizing a quadratic cost function. The parametrization of the model was based on two times the abrupt changes of the plunge depth during a single weld. Although the general validity was not proven, a reasonable control and disturbance response of the closed-loop system was obtained. (S. Zhao et al. 2016)

Despite the numerous advantages mentioned, controlling the contact force can also be adversarial to the process. As indicated by Gebhard & Zaeh (2008) and Völlner (2010, p. 102), heat accumulation can occur when joining along strongly convex-curved trajectories, which causes the workpiece to soften considerably. This effect resulted in an uncontrolled plunging of the tool into the component during the force-controlled process. (Gebhard & Zaeh 2008)

In response to that, Fehrenbacher et al. (2014a) designed a multivariable system for the simultaneous control of the process force and the temperature for FSW. This approach involved the design of two individual models – for the axial force, controlled by the plunge depth, and for the process temperature, with the rotational speed as the manipulated variable. The authors ignored possible interactions between the two parameters in the control logic. The dynamic relationship between the plunge depth and the axial force was deduced from X. Zhao et al. (2007, 2009), using the system's step responses, caused by an abrupt change in the plunge depth during the welding process. The resulting models were then implemented into a combined MIMO system model, which considered additional coupling terms. Decoupling terms were implemented in the control logic, analogous to the coupling terms in the system model, which respected the interactions between the force and the temperature. This concept avoids the occurrence of undesirable effects on the other process variable. Subsequently, separate integral controllers (I controllers) were designed for the force and the temperature control. This

combined control system can perform nominal trajectories with a defined axial force and a specified temperature. (Fehrenbacher et al. 2014a)

Interim conclusions

In summary, the design of a control system based on a system model, as used by X. Zhao et al. (2007, 2009), Oakes & Landers (2009), and Fehrenbacher et al. (2014a), has advantages in terms of transferability, a reduced experimental workload, and an increase in the system knowledge compared to pure black-box models. In addition, as the presentation of the state of the art has shown, the control of the axial force from adjusting the plunge depth is the only method that compensates for possible irregularities in the material. Furthermore, the approach of S. Zhao et al. (2016) has demonstrated the benefits of optimal control concepts. If one also considers the findings of Gebhard & Zaeh (2008), concerning the uncontrolled plunging of the tool, a multivariable control is advisable, even with simple control strategies, such as those used by Fehrenbacher et al. (2014a). Consequently, the benefits of the optimal control theory, combined with the advantages of a multivariable system that allows the consideration of possible interactions between the variables, should be merged to realize a holistic process control. Therefore, the state of research on controlling the temperature in FSW processes is discussed in more detail below.

3.3.3 Temperature control in friction stir welding

A requirement for controlling the temperature is a possibility for its detection during the process. For this purpose, Fehrenbacher et al. (2008) used a single-channel pyrometer fixed to the FSW spindle to optically measure the temperature of the weld seam surface close to the FSW tool. The temperature signal was regulated by a PID controller, using the feed velocity as a manipulated variable. To regulate the temperature of the shear layer (the aluminum layer around the welding pin) based on the measured surface temperature, a linearized, 0-dimensional heat-conduction model was developed and implemented as a feed-forward control in the closed-loop system. In

additional studies, Fehrenbacher et al. (2011b) showed that, due to the highly temperature-dependent emission coefficients of aluminum materials, temperature measurement using a single-channel pyrometer is not practical. Furthermore, the authors noted that the tool's rotational speed was the most effective control variable for influencing the temperature, since the feed velocity can only be adjusted using low dynamics. Therefore, the rotational speed was used to manipulate the temperature in subsequent investigations (Fehrenbacher et al. 2011a). To compensate for the limitations of pyrometer-based temperature measurement, the temperature was detected using thermocouples (TCs) inserted into the tool, with the tip of the TC positioned on the friction surface. To regulate this variable, an I controller, parametrized by a process model, was used. In these investigations, a high quality of control was achieved, with a temperature deviation of approximately only 10 K. (Fehrenbacher et al. 2011a) Additionally, Fehrenbacher et al. (2014b) proved that the system's transfer function depended on the workpiece's temperature and geometry. This observation was explained by a combination of the different heat-conduction properties of the workpiece, the clamping, and the nonlinear relationship between the energy input into the process zone and the measured welding temperature. These results were merged into a combined temperature and force control for the FSW process (Fehrenbacher et al. 2014a), as mentioned in the previous section. Although the interactions between the two parameters (force and temperature) were taken into account for the model, stability problems were observed in the closed-loop control.

An alternative temperature measurement method for the FSW process was published by de Backer & Bolmsjö (2013). This temperature measurement method is based on the thermoelectric effect (also known as the Seebeck effect) between the tool and the workpiece (tool-workpiece thermocouple, TWT). In a closed electrical circuit, when a heating of one electrical connection occurs, a measurable potential difference results. If the tool and the workpiece are made of two dissimilar materials, both of which are electrically and thermally conductive, this effect can be made use of in FSW. This prerequisite is usually fulfilled for FSW, since the tool and the workpiece usually comprise of two different, thermally and electrically conductive materials. Consequently, the test setup itself acts as a measuring element that can allow the TC inserted into the tool to be omitted (de Backer et al. 2014). One disadvantage of

this method is the need to use the same materials at the measuring point (between the workpiece and the tool) and at the reference point (with a known temperature). Additionally, only the measuring point should be heated. (DE BACKER & BOLMSJÖ 2013) To place the rotating tool in electric contact with the workpiece, the authors used a slip-ring unit (consisting of a slip-ring and a brush) and two copper cables. Due to this design, a measuring chain with three contact points (tool and workpiece, workpiece and copper conductor, slip-ring and brush) and one reference point was obtained. In order to measure the temperature only at the contact point between the tool and the workpiece, and to compensate for the influence of the temperature rise at the other contact points, DE BACKER & BOLMSJÖ (2013) modeled the temperature drift. Using this model, the temperature of the measuring point could be calculated. Thus, the measurement error of the TWT method, compared to the TC approach, could be minimized to 10 K for a 148 s long weld. One disadvantage is that the temperature drift model has to be calibrated for each new workpiece-tool-material combination. Despite this limitation, DE BACKER et al. (2014) used this measurement method to validate a temperature control for the FSW process. For this, a PI controller, with the rotational speed as a manipulated variable, was used to control the temperature. According to the error monitoring, the actual and nominal values remained within a range of ±10 K. In addition to the temperature control system, the authors used the existing force control of the industrial robot, with the plunge depth as the manipulated variable. In contrast to FEHRENBACHER et al. (2014b), the authors did not consider any interactions in the design, and both control systems operated independently of each other.

The two measuring methods – the TC integrated into the tool and the TWT – were compared by SILVA et al. (2017) in terms of their dynamic performance. They found that the method based on the TC in the tool showed a faster response to changes in temperature (MAGALHÃES 2016)[12]. Following DE BACKER et al. (2014), MAGALHÃES (2016) used a slip-ring unit to detect the electrical potential of the TWT measurement system employed in their own investigations. To protect the TWT system from overload, the spindle's

[12] Ana Catarina Ferreira *Magalhães* also published using her maiden name, Ana Catarina Ferreira *Silva*.

maximum rotational speed was limited to 1800 $^{1}/_{\mathrm{min}}$. Despite this limitation, Magalhães (2016, pp. 53–55) postulated that the TWT method could control the FSW plunge and starting phase. They hypothesized that the reliability of this measuring method could be optimized by a further development of the control approaches, and that transferability to other welding processes was possible.

In order to compensate for the temperature-dependent transfer function described by Fehrenbacher et al. (2014b), Bachmann & Zaeh (2016) used a gain-scheduling PI controller. Here, the values of the PI controller variables were selected from an internally stored look-up table based on the process parameters (nominal process temperature and feed velocity), which were used for the welding task. Although the results obtained from this method were promising, its transferability is limited because suitable gain factors have to be identified and stored for each new control task (temperature level, feed velocity, and material) (Bachmann & Zaeh 2016). To compensate for these disadvantages, Bachmann et al. (2017) developed a model-based, adaptive approach to control the temperature in FSW. A semi-analytical process model was developed to map the heat fluxes in the FSW process based on theoretical and experimental system identification. This model uses the rotational speed and process torque of the tool as a quantity for the generated heat energy. The friction between the tool and the workpiece was considered according to the approach of Shaw (1963). Subsequently, this process model was taken to parametrize the $\mathcal{L}1$-adaptive controller. This approach ensures transferability to other tool geometries. Despite this advantage, temperature measurement is still necessary during the process. To counteract this, Bachmann et al. (2018) developed a torque-based approach to determine the welding temperature. The basis for that was a regression analysis (black-box approach) between the measured process torque and the welding temperature, measured by TC. With the control approach developed by Bachmann et al. (2017), this regression model forms the torque-based control. Thereby, a maximum error of $\pm 15\,\mathrm{K}$ was observed between the model's temperature and the temperature measured by TC in the tool. The benefit of this approach is the absence of any separate temperature measurement sensors, while a disadvantage of this black-box approach is its non-transferability to other materials or tool geometries. (Bachmann et al. 2018)

Due to the significant temperature difference between the current and nominal temperature at the start of an FSW process, significant control deviations occur in that phase. PID control systems can only regulate such deviations with limited dynamics. For that reason, Taysom et al. (2016) focused on a model-predictive temperature control for FSW processes. In order to predict the response of the system, a first-order semi-analytical heat conduction model for calculating heat flux in the FSW process was developed and coupled with a numerical heat conduction model for simulation of the heat flux of the tool. This hybrid model, consisting of the semi-analytical and numerical heat conduction model, was calibrated using experimental data. As a result, Taysom et al. (2017) compared the MPC approach to conventional PID control systems. They found that the designed PID controller, configured with a focus on stability, had advantages in nominal temperature changes. In contrast, the MPC has particular advantages in the case of changes of the feed velocity. In summary, it can be noted that the MPC control yields comparable, not necessarily better, results, in terms of control accuracy, compared to PID controllers. Nevertheless, Taysom et al. (2017) postulated that the advantages of MPCs provide an immense benefit for MIMO systems, enhanced models, and more precise data. To improve the latter, Taysom & Sorensen (2019) investigated the effect of various types of filters to reduce the noise of the temperature signal. In this context, a filtering method, using the Bézier curve method, proved to be suitable for noise reduction without delaying the signal.

Interim conclusions

Three major methods have been identified for temperature measurement suitable for temperature control in FSW – a TC in the tool, the Seebeck effect, and the torque-based temperature modeling. The method using TCs has advantages in terms of accuracy and dynamics (Silva et al. 2017), while Fehrenbacher et al. (2014a) demonstrated the advantages of MIMO control systems, and Taysom et al. (2017) emphasized the benefits of the MPC concept. Combining these two approaches by using a MIMO-MPC system could provide the advantages mentioned above resulting in a flexible, precise, and holistic process control.

3.4 Heat transfer modeling in multilayer systems

The transient temperature distribution (temperature field) in multilayer systems (such as in FPJ joints or overlap FSW bonds) during the joining process significantly influences the bond strength of the plastic-metal joints (Liu et al. 2014; Wirth et al. 2014a; Wu et al. 2018). In order to calculate the heat conduction in these multilayer systems, researchers have already developed analytical and numerical methods.

Lu & Viljanen (2006) developed a closed-form approximate analytical solution for the non-stationary heat conduction in a multilayer sphere with time-dependent input temperature changes. In this study, a novel mathematical method for the derivation of an approximate inverse Laplace transform was promoted. A five-layer composite sphere was used as an example. To evaluate the accuracy of the results of the evolved analytical approach, the outcomes of the simulation based on this analytical model were compared with a numerical one based on FVM. The relative error between the two calculation methods (analytical and numerical) was between 4 % and 6 %, depending on the time of observation. Although the results show a high potential of the analytical method for solving the heat conduction equations in multilayer systems, the authors postulated that especially for time steps smaller than 1 h, the accuracy of the numerical solution decreases. This fact has to be considered in particular for FPJ applications. The advantage of the developed method is the low computational complexity, which leads to a low processing time.

Another analytical approach to calculate the transient heat conduction in one-dimensional multilayer systems was published by de Monte (2002). The developed approach extends the method designed by Tittle (1965) for singlelayer systems, based on the separation-of-variables technique, for the calculation of multilayer systems. One of the assumptions of de Monte (2002) was that the thermal properties of the different layers, e.g., thermal conductivity and heat capacity, are temperature-independent and constant in the respective layer throughout the thickness. Carr & Turner (2016) noted that the method of de Monte (2002) provokes instabilities in the calculation, especially when dealing with a large number of layers. These instabilities lead to a significant increase in the computational time. For calculating the heat distribution

in FPJ processes, the assumptions of the temperature-independent material properties and the constant thermal properties within a layer do not represent the actual conditions well enough.

Rodrigo & Worthy (2016) promoted a method for solving the one-dimensional multilayer heat conduction problem based on the Laplace transformation. In this method, the heat conduction problem is initially solved in only one layer. Then, the solution of the multilayer system is expressed as a sequence of time-dependent solutions of the single-layer heat conduction problem with suitable boundary conditions. The solution of the multilayer heat conduction problem is then calculated by using the boundary conditions to determine these time-dependent terms. This method is limited in accuracy for short time constants such as those occurring in FPJ.

Hickson et al. (2011) developed an approach based on FDM to solve the one-dimensional multilayer heat conduction problem. In this approach, the authors used the standard Euler time steps to solve the ordinary differential equations. By using the example of a two-layer system, the exact solution (analytical solution) was compared with the solution of the FDM approach. It was shown that the approaches lead to similar solutions and are therefore comparable. Furthermore, the authors clarified that the analytical solution cannot always be provided, and numerical integration is essential for solving multilayer systems. In contrast, the FDM approach is highly flexible and can be easily applied to different problems.

March (2021) investigated in his Ph.D. thesis a finite volume method for one-dimensional multilayer heat conduction problems, which is applicable to problems with an arbitrary number of layers and is able to deal with general boundary conditions. Particular attention was dedicated to the stability problems. For the time discretization, the forward Euler method, the backward Euler method, and the Crank-Nicolson method were compared. It was shown that especially the backward Euler method and the Crank-Nicolson method provide unconditionally stable results for multilayer systems. In addition, March & Carr (2019) postulated that this method could also be applied to nonlinear heat conduction problems, such as those occurring during the plastic melting process in FPJ.

Nandan et al. (2006) studied the heat distribution in the FSW process using various numerical methods. It was found that the heat flux correlates well with the material flow field. The induced thermal energy was calculated based on the tool geometry, the rotational speed of the tool, and the respective shear stress of the material. The results show that significant plastic flow occurs near the tool. The plastic flow significantly influences the heat transport within the workpiece. The calculated results show an asymmetry of the temperature profiles around the tool due to the superimposed rotational and linear motion of the tool. Consequently, an asymmetry of the heat generated around the surface of the tool probe occurs. Since there is no or only very limited material flow during the FPJ process due to the absence of the probe, the approaches are not applicable.

Buffa et al. (2006) investigated a 3D FEM thermo-mechanical model for FSW. The model was calibrated by experimentally gathered force and temperature data in order to analyze the temperature distribution and the strain of the material in the heat-affected zone and the weld nugget. The authors were able to predict the asymmetric heat distribution on the workpiece surface well. At the same time, they showed that the temperature profile in the weld zone is almost uniform. They attributed this to the fact that in FSW, the tool speed is dominant for heat generation, while the feed velocity has a minor effect on it, smoothing out the asymmetry of the temperature distribution at a certain distance from the tool.

Song & Kovacevic (2003) presented a 3D heat transfer model for FSW. For this model, the induced heat flux was modeled via the tool shoulder and the tool probe. By using a moving coordinate system for the heat source, the calculation of the heat transfer model can be simplified and thus accelerated without affecting the accuracy of the temperature prediction. To validate the model, the results were compared with experimental data. The results showed a high level of accuracy. Based on the validated model, the influence of a preheating of the joining parts was investigated. It was shown that the temperature distribution can be made more homogeneous by a preheating of the joining parts and that the resulting forces in the process are reduced simultaneously.

Since the heat transfer in FSW is usually accompanied by material flow, meshless methods, which can easily calculate these large deformations, have advantages compared to classical mesh-based methods such as FEM or FDM approaches. For this reason, Xiao et al. (2017) investigated an approach to analyze the transient heat transfer in FSW with the meshless particle method. In the approach investigated, a heat source model based on friction is implemented to describe the heat generation in FSW. Similar results could be obtained with FEM models, but the meshless methods require less computational capacity. Since in FPJ processes the material flow has a minor influence on the heat generation, the advantages of the meshless method have no effect in this case.

In order to be able to calculate the temperature in the material in real-time and implement this information in a control system, Fehrenbacher et al. (2008) used a pyrometer to record the surface temperature. This temperature signal was coupled with a 0D heat conduction model to compute the temperature in the material. The authors compared the results with a 3D heat conduction model, which could not be implemented in real-time. They showed that the 0D model yields similar results as the 3D model, but the precision is limited. Nevertheless, all influences (feed velocity and tool speed) can be represented by the 0D model with reasonable precision.

Interim conclusions

The state of the art of thermal modeling shows several approaches to calculate the temperature distribution in multilayer systems, which are suitable to be used for FPJ joints. Analytical methods are highly accurate but have certain disadvantages when applied to the specific problem in FPJ. On the one hand, the methods based on the separation-of-variables cannot be used if the outer boundary conditions are not homogeneous (i.e., constant) (Rodrigo & Worthy 2016), which is inevitably in a heating process. On the other hand, these approaches show considerable errors, especially for very short time steps (Carr & Turner 2016; Lu & Viljanen 2006; de Monte 2002). For this reason, analytical approaches are of limited utility for calculating the temperature in the joining zone during FPJ.

FSW-specific methods mainly use FEM/FDM approaches or meshless-based approaches to calculate the temperature distribution (Buffa et al. 2006; Song & Kovacevic 2003; Xiao et al. 2017). These 3D models have advantages in terms of the predictive accuracy, but they are complex to compute, so they cannot be considered for control applications. Furthermore, FSW simulations focus on material mixing and its role in heat generation. For FPJ, this effect is not decisive due to the absence of the probe. In addition, the investigations of Buffa et al. (2006) show that the asymmetric temperature development is evident on the surface of the part, but in deeper layers, it dissolves, and the temperature profile in the weld zone is almost symmetrical.

A first real-time capable model for the calculation of the temperature near the welding pin during FSW was proposed by Fehrenbacher et al. (2008). Although this 0D model is not very precise, promising results could already be achieved in the experiments.

Following the results of Buffa et al. (2006) and Fehrenbacher et al. (2008), it is evident that simplified models can represent the real temperature distribution at a certain distance from the tool well and, at the same time, can be designed to be real-time capable. For this reason, these approaches can serve as a basis for a targeted modeling of the FPJ process in order to calculate and subsequently control the temperature in the boundary layer between the metal and the plastic. A compromise has to be found between the highly accurate 3D approaches and the real-time analytical methods.

3.5 Recapitulation of the findings

In summary, the state of the art indicates that the mechanical strength of metal-plastic bonds is influenced by the metallic joining partner's pretreated surface and the process parameters, particularly the contact force and joining temperature. A promising approach to ensure a consistent bond quality is given by a systematic modification of the metallic surface and control of the mentioned process parameters. However, some aspects have not been sufficiently considered so far:

- The effect of different laser-based pretreatment methods of the metallic surface on the adhesion mechanisms formed, which has been only sparsely studied in terms of FPJ.
- Control of the forces and temperatures during FPJ, which has been insufficiently analyzed to date.
- Multivariable MPC has been referred to as being a promising approach to control FSW processes, although it has never been implemented or evaluated in the FSW process.
- Real-time capable heat conduction models designed for the use in computing the heat generation in multilayer systems have not yet been researched for FPJ and only limited for FSW.

In the following chapter, these open issues are addressed, and the need for action is outlined in the context of the overall aim of this work.

4 Need for action, objective, and approach

"Would you tell me, please,
which way I ought to go from here?"
"That depends a good deal on where you want to get to",
said the Cat.

(Lewis Carroll in *Alice in Wonderland*, 1865)

4.1 Chapter overview

In this chapter, the overall scientific concept and its respective framework are presented. Based on the state of the art (Chapter 3), the deficiencies of FPJ are deduced, and fields of action are identified. Subsequently, associated sub-goals will be derived, and the corresponding solution modules (SMs) will be presented.

4.2 Need for action

This work's overall objective was to contribute to a generally applicable, holistic process control for the direct joining of thermoplastic components with aluminum sheets. A fundamental approach to the solution is the regulation of the forces and temperatures occurring in the process. Although there were already approaches available to control the process forces and temperatures,

the following three fields of action (F 1 – F 3) were identified as still falling within the scope of this study:

F 1 A proper surface pretreatment of the metallic joining partner significantly improves the bond strength. This modification can positively affect the adhesion mechanisms that occur between the plastic and the metal. The predominant binding mechanisms used in FPJ are influenced by laser-based pretreatments. However, correlations between the pretreatment method, the resulting binding mechanisms, and the bond strength remain unknown.

F 2 In addition to the surface pretreatment, the process parameters significantly influence the bond strength. In order to obtain a high bond strength, the process parameters axial force and joining temperature, in particular, have to be controlled. The common control concepts related to highly dynamic processes are limited in terms of the usability for different material combinations and working points. These limitations lead to a reduced control performance. Novel control algorithms for a predictive and optimized control that compensate for these disadvantages are unavailable for plastic-metal direct joining, and using such an approach as a multivariable control system, which would consider the interactions between various parameters, has not yet been done.

F 3 With the aid of this advanced control method, it is possible to manufacture high-strength plastic-metal direct bonds using FPJ. In order to evaluate the industrial application of FPJ, this new technology must be compared with conventional joining processes. In the aviation industry, plastic-metal bonds are mainly joined using standardized adhesive systems. An advantage of direct joining is the possibility of substituting the adhesive system with the thermoplastic joining partner. Such a replacement would avoid the handling of chemicals and reduce the curing time. However, no studies have been performed yet to compare the bond strength or the economic aspects of direct bonding via FPJ to adhesive joining.

4.3 Objective and approach

To achieve the goal of a generally applicable, holistic process control for the direct bonding of thermoplastic components to aluminum sheets, the following four sub-goals (SG 1 – SG 4) are defined based on the three fields of action:

SG 1 Identify a suitable laser-based surface pretreatment method, applicable to different thermoplastic materials in combination with aluminum alloys, to achieve a high bond strength.

SG 2 Besides the surface pretreatment, the process parameters contact force and joining temperature have to be controlled to increase the bond strength. In a first step, a closed-loop MPC concept and method to control the contact force during FPJ has to be provided. Furthermore, a comparison with conventional control methods is to be carried out regarding the method's transferability to other material combinations. The goal is to avoid time-consuming adjustments of the individual control parameters with a simultaneous increase of the flexibility of the closed-loop control when applying it to different material combinations.

SG 3 The MPC approach elaborated in SG 2 for the control of the contact force will be extended by a temperature control to obtain a multivariable control system for a holistic process control. Interactions between the process force and the corresponding temperature will be considered to increase the performance of the control.

SG 4 After a holistic process control has been established in SG 3, the proof of principle will be given to demonstrate that the maximum achievable bond strength of plastic-metal direct joints produced with FPJ is comparable to that of adhesive joints. In addition, an evaluation of the technological maturity of the FPJ process will be presented, and a discussion of the applicability of FPJ in an industrial environment will be given.

Based on these sub-goals, five solution modules (SMs) are derived in the following. Due to the experimental and explorative scientific approach, these individual steps are presented in chronological order (Figure 4.1):

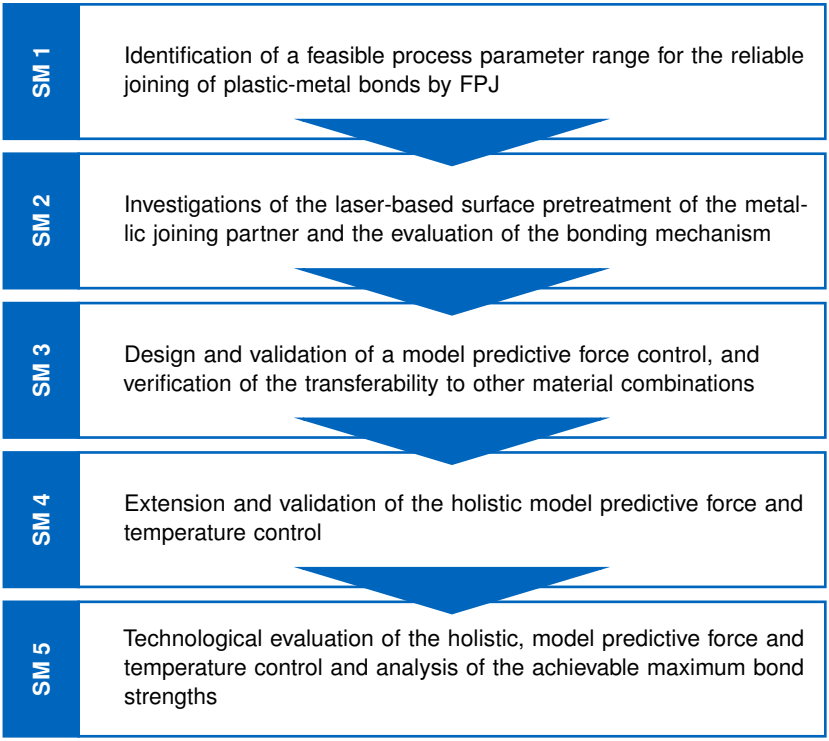

Figure 4.1: Overview of the methodology based on the five defined SMs

SM 1 SM 1 deals with the identification of a suitable parameter range for the reliable joining of plastic-metal bonds by FPJ, using PE-HD and EN AW-6082-T6 as an example. On the basis of that, the process temperatures could be measured and evaluated in terms of the possibility of a closed-loop control.

SM 2 Based on the findings of SM 1, an investigation of the surface pretreatment of the metallic joining partner to increase the bond strength can be conducted. In particular, a comparison of novel structuring concepts with contemporary state of the art approaches, regarding their developing bonding mechanisms and the resulting maximum lap shear strength, can be carried out.

SM 3 After studying the surface pretreatment, in SM 3 an MPC algorithm for controlling the force has to be designed and compared to conventional control concepts. This approach is based on a mathematical model of the relationship between the tool's plunge depth and the resulting axial force. Furthermore, the designed MPC can be analyzed in terms of its transferability to other material combinations, different tools, and process parameters exceeding the initially considered limits.

SM 4 The MPC approach designed in SM 3 has to be extended to a multivariable system for simultaneous force and temperature regulation. For this purpose, a model for calculating the joining zone temperature, between the metal and the plastic component, has to be embedded in the control system. This model-based approach ensures the transferability to other material combinations and guarantees a holistic process control.

SM 5 With the aid of this holistic, multivariable MPC it is possible to analyze the mechanical strength of plastic-metal direct bonds and compare it to standard adhesive joints. In addition, a technology assessment for the FPJ process is conducted, and the possibility of the usage of FPJ in an industrial production environment has to be discussed.

Each of the five SMs has been addressed in an individual publication (P1 – P5) (Figure 4.2). For an elaboration of the results, the following chapter specifies the materials used and the experimental setup. Subsequently, the findings of the individual publications are summarized and briefly recapitulated in Chapter 6.

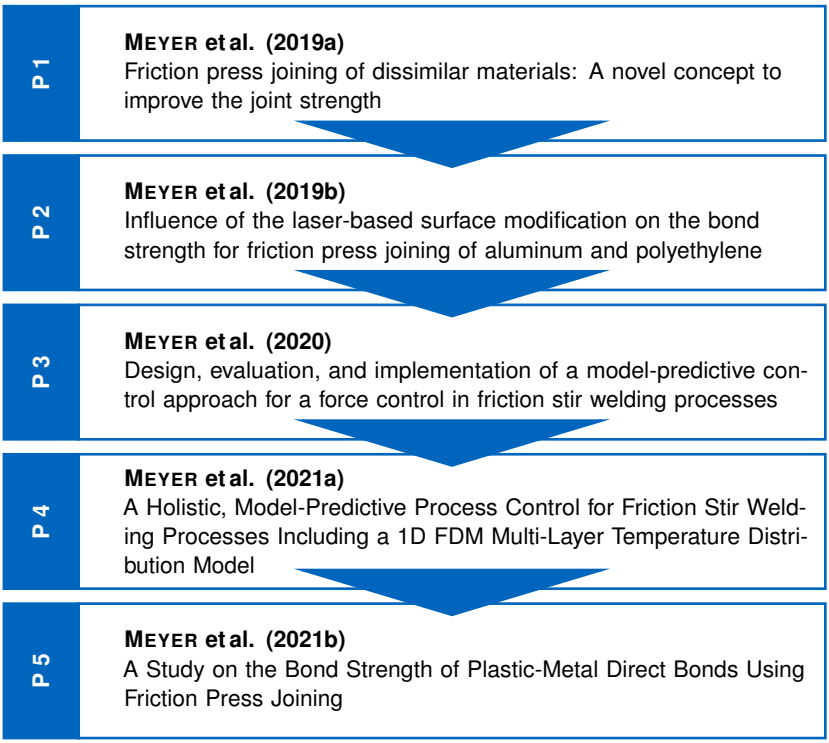

Figure 4.2: Overview of the publications dedicated to the five defined SMs

5 Materials and experimental setup

5.1 Chapter overview

In order to achieve the presented objective (Section 4.3), experiments concerning laser structuring and FPJ were conducted. In this chapter, the materials used and the experimental setup are described, and the analytical methods used to evaluate the results of the experiments are introduced.

5.2 Materials

In the context of this thesis, two different aluminum alloys were joined to three different types of plastics (Table 5.1).

Table 5.1: Overview of the material combinations used in this work, including information on their particular utilization

Material combination		Utilization
Aluminum	**Plastic**	
EN AW-6082-T6	PE-HD	design of the closed-loop control
EN AW-6082-T6	PA6-GF30	evaluation of the transferability of the closed-loop control
EN AW-2024-T3	PPS-CF	evaluation of the transferability of the closed-loop control

A combination of PE-HD and EN AW-6082-T6 served for the system identification of the investigated closed-loop control approaches. The two material

combinations – PA6 with 30 % GF content (PA6-GF30) with aluminum alloy EN AW-6082-T6, and a continuous, endless-CF-reinforced (wt43 %) polyphenylene sulfide (PPS-CF) with aluminum alloy EN AW-2024-T3 – were used to verify the transferability of the closed-loop approach. All test specimens (sheets sized 250 mm × 100 mm, with a thickness of 2 mm to 5 mm) were arranged in an overlap of 35 mm. The trajectory length of the tool moved on the surface of the specimens was set to 200 mm.

The aluminum alloy EN AW-6082-T6 (sheet thickness: 3 mm), supplied by *Hans-Erich Gemmel & Co. GmbH*, Berlin, Germany, is characterized by high corrosion resistance and good formability (DIN EN 573-1; Gemmel Metalle & Co. GmbH 2021). This alloy has been investigated in various studies concerning FPJ (Wirth et al. 2014a,b), and has served as the basis for the design of the control system.

The aluminum alloy EN AW-2024-T3 (sheet thickness: 2 mm), distributed by *Batz + Burgel GmbH & Co. KG*, Friedberg, Germany, is a hardenable, high-strength alloy that is frequently employed in aircraft manufacturing (Kumar et al. 2005). Its disadvantages are its low corrosion resistance and its limited weldability. (Batz + Burgel GmbH & Co. KG 2021)

The two aluminum materials considerably differ in their alloying elements (Section 2.2.3), resulting in different mechanical and thermal properties, covering the wide range of possible values (Table 5.2). This selection allowed an investigation of the transferability of the closed-loop control system to a broad spectrum of aluminum alloys, as it encompasses both a hardenable and a naturally hard alloy.

The PE-HD (sheet thickness: 5 mm), received from *S-Polytec GmbH*, Goch, Germany, was used as a basic material for the design of the control system (S-POLYTEC GmbH 2021).

In order to evaluate the transferability of the obtained results in the individual publications, joining tests were conducted using a PA6-GF30 component (sheet thickness: 5 mm), distributed under the trade name TECAMID 6 GF30 black by *Ensinger GmbH*, Nufringen, Germany, and a PPS-CF with a fiber-mass fraction of 43 %, supplied by *TenCate Advanced Composites BV*, Nijverdal, Netherlands, under the trade name CFRP Cetex TC1100. The fibers in the

Table 5.2: Thermal and mechanical properties of the aluminum alloys EN AW-6082-T6 and EN AW-2024-T3 (GEMMEL METALLE & CO. GMBH 2021; BATZ + BURGEL GMBH & CO. KG 2021)

		EN AW	
Property	**Unit**	**6082**	**2024**
Condition	–	T6	T3
Tensile strength (R_m)	$^{N}/_{mm^2}$	300–350	435
Yield strength ($R_{p0.2}$)	$^{N}/_{mm^2}$	240–320	290
Elongation at fracture ($A_{50\,mm}$)	%	8–14	14
Young's modulus (E)	MPa	70 000	70 000
Density (ρ)	$^{g}/_{cm^3}$	2.70	2.77
Melting temperature (T_m) (range)	°C	585–650	505–640
Thermal conductivity (λ_{th})	$^{W}/_{mK}$	150–185	130–150

PPS-CF laminate were arranged in an atlas configuration (five harness satin weave) (Figure 5.1). Due to the multiple layers of the composite, the total height was 2.17 mm. (ENSINGER LTD 2021; TENCATE ADVANCED COMPOSITES BV 2021)

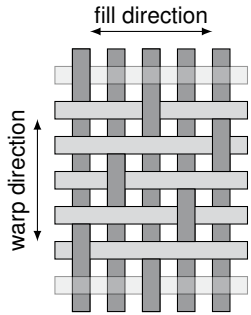

Figure 5.1: Schematic drawing of the five harness satin weave structure, showing the wrap and the fill direction; the non-transparent yarns consist of repetitive unit cells (based on AKKERMAN (2005))

The three thermoplastics are typical representatives of mass, engineering, and high-performance plastics (Figure 2.2). They are, depending on the requirements of the application, utilized in an unreinforced condition (PE-HD), with short GFs (PA6-GF30), and as a continuous fiber-reinforced laminate

(PPS-CF). The selection for this thesis ensured that the obtained findings were tested over a broad spectrum of material combinations (Table 5.3). Hence, the general validity of the results concerning the closed-loop approaches could be confirmed.

Table 5.3: Thermal and mechanical properties of the plastics PE-HD, PA6-GF30, and PPS-CF (S-POLYTEC GMBH 2021; ENSINGER LTD 2021; TENCATE ADVANCED COMPOSITES BV 2021)

Property	Unit	PE-HD	PA6-GF30	PPS-CF
Tensile strength (R_m)	N/mm^2	23	98	752–785
Yield strength ($R_{p0.2}$)	N/mm^2	–	98	608
Young's modulus (E)	MPa	1 100	5 700	56 000–58 000
Density (ρ)	g/cm^3	0.96	1.36	1.55
Crystallization temperature (T_C)	°C	126–130	218	280
Thermal conductivity (λ_{th})	W/mK	0.38	0.41	–
Coefficient of linear thermal expansion (α_{th})	$10^{-4}\,1/K$	1.8	0.6	–

5.3 Experimental setup

5.3.1 Laser systems

Two different laser systems were used for the surface pretreatment. A single-mode fiber laser system, YLR-3000-SM, supplied by *IPG Photonics Corporation*, Oxford, Massachusetts, was selected to generate the microscopic structures (Section 2.2.5). The laser beam was guided via an optical fiber (diameter of 30 µm) to a 3D galvanometer scanning optics (Fiber Elephant 50, produced by *Arges GmbH*, Wackersdorf, Germany). The working distance (d_w) between the optics and the surface of the component was 406 mm. The wavelength (λ) emitted was 1070 nm, with a maximum output power of 3 kW. The focus diameter (d_{foc}) was approximately 50 µm. The laser radiation had a Gaussian intensity distribution.

A pulsed fiber laser system (PowerLine F20, *Rofin-Sinar Technologies Inc.*, Plymouth, Michigan) was applied to generate the nanoscopic structures. With a 2D scanner system, including an F-theta objective with a focal length of 160 mm, the beam was guided over the material surface. The working distance was 183 mm, the wavelength 1064 nm, and the focus diameter approximately 50 µm. (Rofin-Sinar Laser GmbH 2020)

5.3.2 Machine features

All experiments were conducted on a CNC machining center (type MCH 250), produced by *Gebrüder Heller Maschinenfabrik GmbH*, Nürtingen, Germany. This machining center has three translatory axes and one rotational axis (b-axis). This b-axis allows the rotary table on which the clamping and workpiece were mounted to revolve (Figure 5.2). By rotating the b-axis, the tilt angle (α) in the FPJ process could be adjusted. The translatory movable table (translatory table) enabled a maximum axial force (F_a) of 30 kN in the direction of the z-axis. In the x- and y-axis directions, the maximum feed forces were limited to 15 kN. The spindle was positioned horizontally and has a maximum torque of 1340 Nm. It offers two different gears. The maximum spindle RPM rate was 1799 $^1/_{\mathrm{min}}$ in gear one. The spindle has a maximum operating range of 1200 $^1/_{\mathrm{min}}$ to 6000 $^1/_{\mathrm{min}}$ in gear two. The CNC machining center features a Sinumerik 840D controller, with a Simatic S7-300 analog-digital converter and an analog module (SM334, *Siemens AG*, Munich, Germany). The interpolation frequency (IPO frequency) of the controller is 167 Hz. Due to the interfaces provided with the controller, various process data, such as the axis positions and the motor currents, can be monitored.

5.3.3 Clamping system and tools

A clamping system that deforms negligibly compared to the specimens, even under high process forces, was designed to ensure repeatable and reliable securing of the specimens (Appendix C.1). This clamping system was mounted on the clamping plate of the machining center. For each plastic material, the height of the supporting plate was adjusted. This plate had the same height

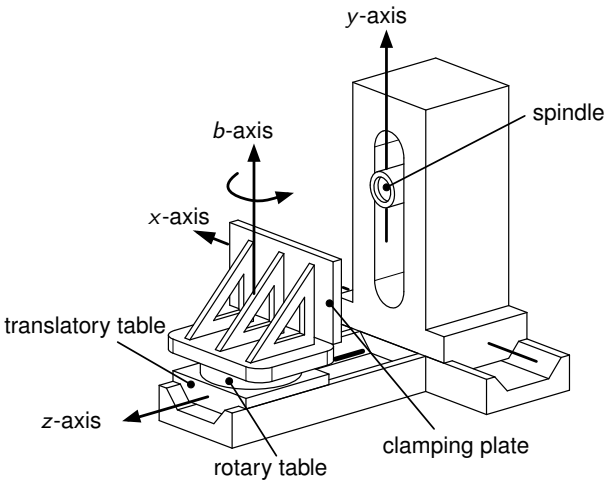

Figure 5.2: Schematic overview of the CNC machining center, MCH 250, with its coordinate system (based on GEBHARD (2011, p. 32))

as the plastic component to avoid gap formation between the aluminum sheet and the plastic component.

For the tests, two cylindrical tools, made of vacuum-hardened XCrMoV5 steel with a diameter of 25 mm, were designed and fabricated (Appendix C.2). For the friction zone temperature measurement, a TC was inserted into the tool in the friction surface (6.25 mm from the center point of the tool) and fixed with a high-temperature adhesive. The tool's front face was either flat or profiled, specified in the corresponding publications.

5.3.4 In-line metrology

Three components are important for implementing a holistic process control – a dynamometer to measure the forces, a temperature sensor unit to detect the temperature at the surface of the aluminum, and a programmable real-time computer to determine the manipulated variables (Figure 5.3).

The axial force (F_a) and corresponding torque (M_a) were measured using a sensor unit called dynamometer (*Hottinger Baldwin Messtechnik (HBM)*,

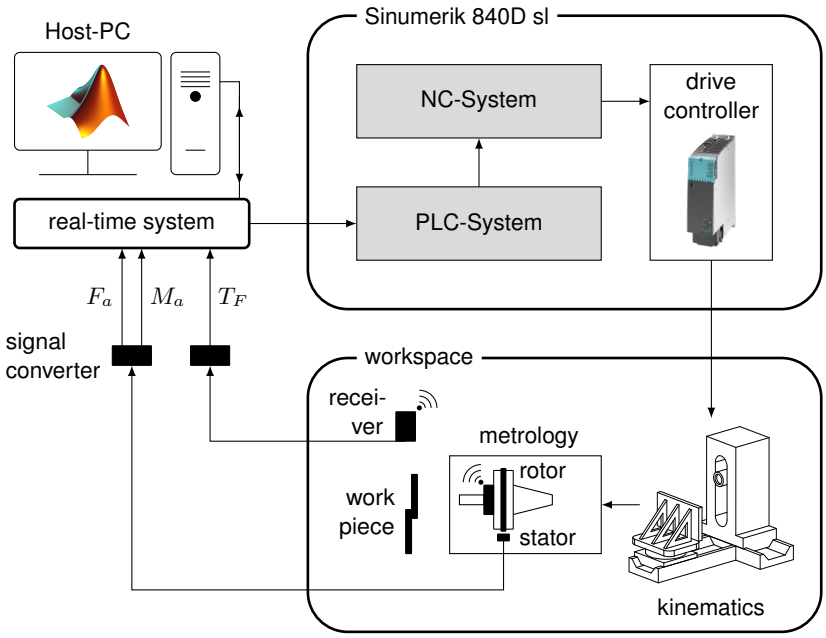

Figure 5.3: Measurement technology used (including the dynamometer and temperature measurement system), and the real-time system, Host-PC, and modified control (Sinumerik 840D sl) of the MCH 250

Darmstadt, Germany). This sensor was integrated between the Weldon adapter for the FPJ tool and the spindle's SK50 adapter. It enabled the detection of an axial force of up to 25 kN and a corresponding torque of up to 200 N m. The sampling frequency of this sensor was 9.6 kHz. (Krutzlinger et al. 2015)

The temperature measurement was realized with the aid of a type-K TC inserted into the tool, combined with a signal-processing unit mounted on the tool holder. This unit converted the measured analog signal into a digital format. Subsequently, the signal was transmitted at 220 Hz via a Wireless Local Area Network (WLAN) to a receiver, from which it was forwarded to a real-time computer. A more detailed overview of the temperature sensor unit's design is given in Costanzi et al. (2017).

The signal processing was implemented on a real-time computer (MicroLab-Box, *dSPACE GmbH*, Paderborn, Germany) with analog and digital input and output interfaces. A Gigabit Ethernet connected the real-time computer to a Host-PC. Via a graphical user interface, developed in ControlDesk (version 7.2) software, the control parameters could be set on the Host-PC. The sample rate of this system was 10 kHz. The signal-processing logic was designed in MATLAB Simulink (R2017a), converted into C code, and transferred to the real-time computer. Through the output interfaces, the control signals could be transmitted to the programmable logic controller (PLC) system of the machining center. With this, an adjustment of the z-position and the spindle's rotational speed was possible.

5.4 Material testing

To analyze the off-line measurable material properties, lap shear tests were conducted to determine the tensile shear strength (R_m). Additionally, thin-sections were used to detect the layer structure of the produced bonds.

For the lap shear tests, performed on a Zwick/Roell Z050, five samples were taken from the specimens, each 25 mm in width. The clamping length was 115 mm. The traverse speed was set to 50 $^{\mathrm{mm}}/_{\mathrm{min}}$ for the combination of PE-HD and aluminum, due to the high elasticity of the PE, and to 5 $^{\mathrm{mm}}/_{\mathrm{min}}$ for the other material combinations.

6 Friction press joining of plastic-metal direct bonds

6.1 Chapter overview

The results reported in the individual publications are presented in the following, in response to the objectives defined in Section 4.3. All publications are referred to in the same way as the defined SMs. The individual papers are briefly summarized to present the associated knowledge gain, including the main conclusions (Cs). This chapter is concluded by an overview of the individual contributions of the author to each article. The corresponding references to the individual papers are listed in the bibliography and in Appendix B.

6.2 Recapitulation of the embedded publications

6.2.1 Publication 1 – "Friction press joining of dissimilar materials: A novel concept to improve the joint strength"

As part of the scope of Publication 1, a parameter range for FPJ of the PE-HD and EN AW-6082-T6 material combination was presented. A partial fractional design of experiments using rotational speed and feed velocity as factors was defined, and test specimens were produced. The surface of the metallic joining partner was pretreated with laser radiation. The maximum tensile shear strengths of the produced test specimens was detected, and these

were correlated with the maximum temperatures (T_J and T_F) in the process zone.

It was found that three characteristic temperature-dependent stress-strain curves could be discerned. Temperatures that were too low, characterized by the fact that the plastic did not melt sufficiently, led to an insufficient bond between the plastic and the aluminum components. Thus, there was a distinct break without any strain hardening or necking. When the temperatures were too high (the plastic degraded), the stress-strain curves showed a small portion of strain hardening and necking. The maximum bond strength was low in the tests with the increased temperatures. For the tests that were within the optimum temperature range, the results showed a high bond strength.

Based on these insights, concepts for improving the joint strength were suggested. In this context, a model-based temperature control for the joining zone temperature (T_J) was presented. In addition, a method for, and the benefits of, a force control were discussed. In order to assess the economic feasibility and the technological maturity of the process, a comparison to adhesive bonding was suggested.

Main conclusions

C 1 The direct bonding of PE-HD with EN AW-6082-T6 using FPJ is possible through a laser-based pretreatment of the metallic joining partner. In addition, a parameter range for reliable bonding was identified and correlated with the measured temperatures.

C 2 An approach for a model-based control of the joining zone temperature (T_J) via the tool's rotational speed (n) was presented and discussed. The temperature in the friction zone (T_F) was suggested as the input parameter for the model.

C 3 A force control via the plunge depth could offer a further advantage regarding the bond strength. For this purpose, a concept for a hybrid position and force control was introduced.

C 4 In order to evaluate the process, in terms of the technological and economic aspects, a benchmark study on adhesive bonding was recommended.

6.2.2 Publication 2 – "Influence of the laser-based surface modification on the bond strength for friction press joining of aluminum and polyethylene"

Based on conclusions C 1 and C 2 in MEYER et al. (2019a), the second publication, MEYER et al. (2019b), addresses the temperature distribution in the bond during joining, and the influence of the surface pretreatment of the metallic joining partner on the bond strength.

To analyze the temperature distribution, a full fractional design of experiments was conducted. The process temperatures in the joining zone and the friction zone were analyzed at different points along the joining path. Thereby, a nearly linear relation between the process parameters – rotational speed and feed velocity – and the respective measured temperatures was demonstrated. In order to assess the influence of the surface pretreatment, three different laser-based structuring methods were selected and validated for the process. Based on the state of the art, four nanostructures and eight microstructures were chosen. The microstructures featured cross (four variants) and circle structure patterns (four variants). The experiments showed that nanostructures led to higher bond strength. As the essential binding mechanism, the van der Waals forces were identified. As a method to characterize the direct bond, a thin-section (approximately 500 µm thick) was examined. From this, four different layers could be distinguished and defined for the first time – *base material 1*, *boundary layer*, *reaction layer*, and *base material 2*.

Based on these results, it was concluded that the reaction layer in the plastic joining partner has to be regarded as a critical interface. To control this layer, and thus the bond strength, a model-based temperature control by adjusting the rotational speed was proposed. Furthermore, due to the high fluctuations observed in the force signal during the position-controlled process, a force control was recommended.

Main conclusions

C 1 The rotational speed (n) and the feed velocity (v) can influence the temperatures at the friction surface (T_F) and at the joining zone (T_J), and the temperature difference (ΔT) between these.

C 2 The joining zone temperature (T_J) has to be controlled to ensure the bond's quality. Thus, the friction surface temperature (T_F) can be applied as an indirectly controlled variable for a model-based control.

C 3 The axial force (F_a) is not constant along the joining trajectory and shows significant fluctuations in a position-controlled process.

C 4 A quasi-chaotic nanostructuring of the metallic surface, generated by a pulsed laser process, leads to a high bond strength for the material combination of PE-HD and aluminum EN AW-6082-T6.

C 5 For direct bonds produced by FPJ, the *boundary layer* between the metallic joining partner and the plastic is the decisive layer in determining the tensile strength. The adhesion mechanisms can be explained by van der Waals forces.

6.2.3 Publication 3 – "Design, evaluation, and implementation of a model-predictive control approach for a force control in friction stir welding processes"

In Meyer et al. (2020), observation C 3 from Meyer et al. (2019b) was studied in more detail. By using a model-based approach, an MPC was designed and analyzed as a means of regulating the axial force (F_a) by adjusting the plunge depth (E_t). In addition, the transferability of the control concept to various material combinations was investigated.

A dynamometer, combined with a high-performance real-time computer, was utilized as a measuring system to determine the axial force. To process the noisy sampled signals with a high frequency, a moving average filter with a window width of 500 points was designed. Subsequently, a system identification for the material combination PE-HD and EN AW-6082-T6 was conducted in

the parameter range based on MEYER et al. (2019a). The plunge depth was abruptly increased twice during the joining phase, and the resulting axial force was detected. Based on these measurements, the dynamic system behavior was modeled using a gray-box method. The model of the transfer function had two poles and one zero. Finally, a parametrization of the system model was performed based on the experimental data.

Several controllers were designed with the aid of the developed system model, and these were compared with each other, simulatively and experimentally, in terms of their stationary and dynamic behaviors. The most promising concepts were examined for their transferability to other material combinations. In particular, the MPC approach proved to be very robust when dealing with model uncertainties, such as changes in the material or the tool geometry, or adapted process parameters beyond the initially considered parameter range. Furthermore, it was found that, with an increasing energy input during the process (increased component temperature), the regulation can compensate for unevenness of a joining partner more effectively. Furthermore, the control becomes more robust with an increased tilt angle of the tool. Additionally, the tool's run-out tolerance was identified as a crucial disturbance factor, and possibilities for its minimization were presented. The publication closed with a generally applicable method for the model-based design of an MPC for pressure welding processes.

It can be summarized that the MPC approach is advantageous for force control during FPJ. In addition, an MPC-based multivariable control for the axial force and the friction surface temperature was suggested. For the multivariable control design, the method for the model-based design of an MPC presented in this paper can be used.

Main conclusions

C 1 A moving average filter is recommended for prefiltering the force signal, if sufficient computing power is available and the disturbance frequencies show an additive white Gaussian noise (AWGN).

C 2 Despite a particular self-regulating effect, force-regulated processes have an advantage in terms of constant process conditions and a defined force set-point.

C 3 The lower the feed velocity (v) of the tool is and the higher the tilt angle (α) is, the more precisely the axial force (F_a) can be controlled. Accordingly, the standard deviation of the force signal can be further reduced.

C 4 The approach of a model-based MPC design is preferable to other methods, particularly when model uncertainties occur, such as material changes, varying process parameters, or modifications in the tool geometry.

6.2.4 Publication 4 – "A Holistic, Model-Predictive Process Control for Friction Stir Welding Processes Including a 1D FDM Multi-Layer Temperature Distribution Model"

In Meyer et al. (2021a), an extension of the model-predictive force-control approach presented in Meyer et al. (2020) – a model-predictive force and temperature control – was presented. Based on a thermal balance equation for FPJ, a torque-dependent system model was designed that considered cross-effects between the axial force and the friction surface temperature. Moreover, a real-time-capable 1D FDM model was implemented, enabling the calculation and indirect control of the joining zone temperature in the plastic component.

Following the thermal FSW model based on Taysom et al. (2016), an equation was presented that considers the specific boundary conditions of FPJ. This torque-dependent differential equation was parametrized experimentally and extended by the state rotational speed. As a result, a second-order state-space model could be designed, incorporating both the rotational speed and the friction temperature as states. Since both the friction temperature and the axial force affect the torque, the corresponding cross-effects of these two variables could be considered via the actual torque specified in the model. Following this mathematical definition of the FPJ process, a multivariable

MPC was parametrized according to the method introduced in Meyer et al. (2020).

This multivariable MPC was validated using the material combination PE-HD and EN AW-6082-T6. Here, an outstanding control performance was found for the friction temperature and the axial force. To determine the performance in terms of model uncertainties, various plastic parts and aluminum alloys were used. Although the results showed an excellent correspondence of the controlled average temperature to the nominal temperatures, a slight oscillation around the nominal temperature was observed, which explains the increased standard deviation. These temperature-control uncertainties were explained by a change in the thermal characteristics of the plastics and the thinner aluminum plate, in particular. The control quality of the axial force was approximately constant compared to the experiments without model uncertainties.

Based on these results, a 1D FDM model[13] was developed to calculate the joining zone temperature (T_J) in the plastic material in real-time, depending on the controlled friction surface temperature. For this purpose, the assembly was abstracted as a layering system consisting of three individual layers (aluminum joining partner, plastic joining partner, and base plate) and modeled as a transient heat conduction problem. Considering the temperature-dependent modeling of the thermal material properties of the aluminum sheet and the plastic component, the temperature distribution could be calculated. To validate these results, the melt layer thicknesses in the joined bond were predicted, and compared with experimental data, since temperature measurement in the plastic component during the bonding process is unfeasible. Thereby, a high correlation was found between the model and the experimental results. Thus, the control system could be extended by a feed-forward control to regulate the temperature T_J via T_F.

In summary, the holistic, model-predictive process control, including the heat conduction model for calculating the joining zone temperature, provided a significant added value for FPJ. Based on this control, it is possible to evaluate

[13] This model can be requested via E-mail from the author.

the economic value of this process. Altogether, the effective implementation of a holistic process control was achieved.

Main conclusions

C 1 The FPJ can be modeled as torque-dependent, based on a thermal balance equation. As a result, it is possible to incorporate the friction temperature and the cross-effects of the contact force based on the torque-dependency of both parameters and linearize them over a broad operating range.

C 2 Based on this system model, an adaptive MIMO-MPC can be designed and implemented in the holistic process control for FPJ.

C 3 By using a 1D FDM multilayered system, the temperature distribution in the bond can be calculated in real-time. Thus, this model can be used as a feed-forward control.

6.2.5 Publication 5 – "A Study on the Bond Strength of Plastic-Metal Direct Bonds Using Friction Press Joining"

In the previous publications, the main focus was placed on process control. The study of Meyer et al. (2021b) deals with a benchmark study between adhesive bonding and process-controlled FPJ. Additionally, a technological and economic analysis of FPJ was performed.

As a first step, the maximum tensile shear strengths of three different material combinations (PE-HD and PA6-GF30 with EN AW-6082-T6, and PPS-CF with EN AW-2024-T3) of plastic-metal direct bonds produced using FPJ were compared to plastic-metal adhesive joints. The results showed that bonds produced by FPJ offered significant advantages, particularly for the combination of PA6-GF30 with EN AW-6082-T6 and PPS-CF with EN AW-2024-T3. For PE-HD and EN AW-6082-T6, there was no fracture in the joining zone because the total adhesive forces exceeded the plastic joining partner's cohesive forces for both the adhesive bond and the FPJ joint.

In addition, a technology evaluation was conducted, based on SCHINDLER (2014). The state of the art and the author's recent research projects were discussed in order to assess the fundamental principles behind, and development of, the technology. In addition, several expert meetings allowed a presentation of the technological maturity profile and the total technological maturity. In this context, it was determined that the technology of FPJ is well advanced and is close to becoming an industrial application. Furthermore, a possible classification as part of the DIN 8580 standard (manufacturing processes) (DIN 8580) was discussed, based on the arising binding mechanisms. Thus, a recommendation for its classification under Item 4.8.1.3 *Activation bonding* was proposed.

Main conclusions

C 1 The maximum tensile shear strengths achieved for the investigated material combinations joined by FPJ are similar to, or greater than, those of comparative samples joined by adhesive bonding.

C 2 The overall technological maturity of FPJ is 61(6) % based on the method of SCHINDLER (2014). Accordingly, this technology is ready to be used in an industrial production environment.

C 3 A classification of FPJ, according to the manufacturing processes standard DIN 8593 under *Activation bonding* (Item 4.8.1.3) is conceivable.

6.3 Individual contributions of the author

The scientific publications which are part of this thesis were elaborated in collaboration with other scientists. In order to fulfill the objectives defined in Section 4.3, the five listed publications were conceptualized, elaborated, and written predominantly by the author. Table 6.1 summarizes the individual contributions of the author of this Ph.D. thesis, in terms of conceptualization, operative work, and writing. The contributions of the other scientists can be found in Table B.1 in Appendix B.

Table 6.1: Overview of the author's contributions to the conceptual and operative work, and to the writing of the publications presented as part of this Ph.D. thesis

Publication	Conceptualization	Elaboration	Writing	Total
1	85 %	90 %	85 %	85 %
2	85 %	90 %	85 %	85 %
3	85 %	40 %	80 %	75 %
4	90 %	80 %	90 %	85 %
5	85 %	90 %	75 %	80 %

7 Conclusion, economic evaluation, discussion, and outlook

7.1 Conclusion

Aircraft manufacturers are being urged to reduce the total mass of their planes to address the growing market for long-distance travel while simultaneously meeting the legal requirements to reduce CO_2 emissions. In this context, fiber-reinforced plastics and high-strength aluminum alloys are increasingly being used in modern aircraft design. Various adhesive systems are available for joining these two dissimilar materials. However, this bonding technology suffers from long curing times, the necessity to handle chemicals, and limited mechanical strength. Due to these aspects, this publication-based thesis focused on the novel technology of FPJ. The prerequisite for an industrial application of FPJ is a reliable and robust process. The influence of disturbances on the bond quality needed to be identified first, and then compensated for by adjusting the process parameters to achieve this robust and reliable process.

The first sub-goal was to identify a suitable parameter range for the reliable joining of thermoplastic components and aluminum alloys. Based on this fundamental knowledge, the laser-based surface modification of the metallic joining partner was investigated. It was demonstrated that a quasi-stochastic nanostructure, produced using pulsed laser radiation, enhanced van der Waals force formation and increased the bond strength.

For the second and third sub-goal, an MPC approach to regulate the process temperature and force during FPJ was analyzed. This holistic approach

enabled the reliable joining of various thermoplastic-aluminum bonds without the need for an experimental reconfiguration of the controller. Furthermore, it was proven that effects, such as variations in the tool, irregularities in the material, or heat accumulation, can be compensated for by using this control algorithm, regardless of the material combination.

In conclusion, it was shown that the direct bonds produced had higher strength than adhesive bonds when the process was well controlled. Furthermore, the technological maturity of FPJ was quantified according to the method of Schindler (2014) to be 61(6) %, and future courses of action for industrialization were identified.

7.2 Economic evaluation

For the industrial application of FPJ, it is essential to evaluate the technological advantages (Section 6.2.5) and the economic benefits compared to already established joining processes. In this section, the economic aspects of FPJ are compared with those of adhesive bonding, using the example of a stringer-reinforced aircraft side shell (made of CFRP) of the twin-jet wide-body aircraft Airbus A350 XWB (Figure 1.2). Today, these CFRP side shells are fabricated using thermosets. However, research is currently focusing on replacing these with thermoplastics, which can be processed faster (Barile et al. 2020). In this context, the joining technology introduced in this dissertation, including the process control, was compared with the current state of the art – namely, the adhesive bonding of CFRP made of thermosets.

The outer skin of A350 XWB airplanes is made of CFRP side shells with reinforcing metallic stringers bonded onto the inside (Premium AEROTEC GmbH 2014). The size of a single panel is approximately 13 m × 5 m. The stringers are adhesively bonded to the inside of the outer skin; an adhesive is dispersed onto the stringer surfaces, the stringers are placed onto the inner side of the panel by robots, before they are pressed onto the skin. To accelerate the curing process, the panels are hardened in a customized autoclave at 180 °C for

2 h[14]. Robot-based handling systems are used to apply the adhesive and align and press the stringers onto the panel. These systems include at least two robots. To guarantee the placement's accuracy, an external, highly sensitive measuring system is the current state of the art.

The long, two-dimensional bond between the stringers and the shell is a compelling example of adhesive bonding that could be replaced by FPJ. It is assumed that the FPJ process, which was initially developed using machine tools, can be performed on heavy-duty industrial robots. This hypothesis is based on the circumstance that FSW, which is more demanding in terms of forces, is also performed using heavy-duty industrial robots (Völlner 2010; Bachmann 2020; Sigl et al. 2020). The additional costs that arise due to the implementation of the closed-loop control, developed in the context of this thesis, are limited to those of the measurement equipment, the software, and the use of heavy-duty industrial robots. As shown in Publication 3 (Meyer et al. 2020), a real-time PLC system is required to implement a closed-loop control. Using the add-on SIMATIC Target 1500S (*Siemens AG*, Munich, Germany), the control approach, designed in MATLAB Simulink, can be transformed into a CPU-executable object. This conversion allows a simple commercial implementation of the developed holistic process control. In addition, the real-time PLC system, the robots, the software licenses, the measuring instruments (temperature and force measuring unit), and the tools (placing of the thermoelements) have to be considered. This increased investment is offset by eliminating the curing time in the autoclave (with an out-of-autoclave (OOA) process). In terms of an economic evaluation, only modules that differ when switching from adhesive bonding to FPJ are considered in the following.

The fixed costs for the adhesive bonding process are calculated using the investment for the handling robots (€90,000[14]), the measuring technology (€10,000[14]), and an autoclave (€6.5 million[14]), resulting in a total of €6.60 million. In contrast, an FPJ-driven process would incur costs for two heavy-duty industrial robots (€200,000[14]), including the measurement hardware

[14] These estimations are based on data provided by experts from *iwb*, Airbus Materials XRX, and Premium AEROTEC.

(€50,000[15]) and the software licenses (€20,000[15]). These costs result in an overall investment of €270,000.

For the economic feasibility study, the following assumptions are made:

- For implementing an FPJ-based manufacturing, the initial investment cost (C_F) of €270,000 has to be considered, as outlined in the previous paragraph. In contrast, the initial investment cost (C_B) to realize the adhesive bonding using an autoclave is €6.60 million.

- The running costs (M_F and M_B) for the maintenance and the service of the whole plant and machinery (FPJ-plant and adhesive bonding including the autoclave) were assumed to be 10 % of the investment costs per year (Huber 2017, p. 145). This assumption leads to €27,000 per year for the FPJ-based process and €660,000 per year for the adhesive bonding process using the autoclave.

- According to the German Federal Ministry of Finance (2001), the depreciation period for the whole equipment is six years. Assuming a linear depreciation and no liquidation value, the imputed depreciation (D_F and D_B) for the FPJ system is €45,000 per year (based on C_F of €270,000), and for the adhesive bonding process using the autoclave €1.10 million per year (based on C_B of €6.60 million).

- The imputed interest rate (R) is considered with 2 % (Stopka & Urban 2017, p. 388). Then, taking into account the capital commitment development with a linear depreciation according to Stopka & Urban (2017, p. 94), the imputed interests (I_F) for the FPJ-system can be calculated:

$$I_F = \frac{C_F}{2} \cdot R = \frac{270{,}000\,€}{2} \cdot 0.02 = 2{,}700\,€/\text{a}. \tag{7.1}$$

  For the adhesive bonding process using the autoclave, with the initial investment cost of €6.61 million, results in an imputed interest (I_B) of

[15] These estimations are based on data provided by experts from *iwb*, Airbus Materials XRX, and Premium AEROTEC.

$$I_B = \frac{C_B}{2} \cdot R = \frac{6{,}600{,}000\,€}{2} \cdot 0.02 = 66{,}000\,€/\text{a}. \tag{7.2}$$

Considering these assumptions, the total annual cost (A_F) for an FPJ-based manufacturing results in

$$\begin{aligned} A_F &= M_F + D_F + I_F \\ &= 27{,}000\,€/\text{a} + 45{,}000\,€/\text{a} + 2{,}700\,€/\text{a} \\ &= 74{,}700\,€/\text{a}. \end{aligned} \tag{7.3}$$

In contrast, the total annual costs (A_B) for the adhesive bonding process using the autoclave sum up to

$$\begin{aligned} A_B &= M_B + D_B + I_B \\ &= 661{,}000\,€/\text{a} + 1{,}100{,}000\,€/\text{a} + 66{,}100\,€/\text{a} \\ &= 1{,}826{,}100\,€/\text{a}. \end{aligned} \tag{7.4}$$

The comparison of the two manufacturing methods demonstrates that FPJ-based manufacturing can yield cost advantages. This benefit is mainly achieved by the elimination of the autoclave. In addition to the cost advantages of the process, the production time has to be considered in detail. In the following, the production time of the two joining processes will be compared using the example of a side shell panel (Figure 1.2).

One side shell panel requires 20 stringers with a length of 12 m each[15]. For FPJ of the high-strength EN AW-2024-T3 and PPS-CF combination, the maximum strength, according to Meyer et al. (2021b), is obtained at an average feed velocity of 300 mm/min. Consequently, a joining time of 13.3 h per panel is required. In contrast, the adhesive is applied at approximately 5000 mm/min[15]. In addition to the application of the adhesive, a period of 30 min is assumed for the transport of the panels from the joining facility to the autoclave and back[15]. Including the curing time in the autoclave, a throughput time per panel of 3.8 h is necessary.

When considering the increased cycle time for the FPJ process, the number of units produced is crucial. A two-shift system of eight working hours each, with 250 working days per year, and an average availability of 90 % for the plants (i.e., 10 % of the time is used for maintenance and service) would result in 3600 $^{h}/_{a}$ in which production could occur. Assuming that a single section of an aircraft consists of four panels, and a supplier produces up to two sections per aircraft, the capacity utilization limit for an FPJ facility would be 33.8 aircraft per year, and for a bonding process using the autoclave 118.4 aircraft per year. To produce more than 33.8 aircraft per year with an FPJ facility, either the shift system has to be expanded (to a three-shift system) or a second FPJ facility has to be installed (in which case the personnel costs would increase, which has not been considered thus far[16]). For this reason, the FPJ-based manufacturing of airplanes appears reasonable, especially for small quantities or where significant variations in the number of units being manufactured can be expected. For high order volumes, the increased throughput time of the FPJ-based production can have disadvantages. Therefore, a company-specific evaluation of the autoclave system versus the FPJ-based plant is suggested.

During the coronavirus crisis (coronavirus disease 2019, also known as COVID-19) in 2020, and with the subsequent travel restrictions, border closures, and economic consequences, the tourism and aviation industries have suffered a considerable economic downturn. This slump has resulted in a decline in passengers, and a drop in the worldwide export volume and the demand for new aircraft. While 93 aircraft of the A350 family were produced in 2018, Airbus reduced the number by 40 % for 2020 (Airbus SE 2020). To compensate for such fluctuations, including those unique in history, flexible production systems with low investment needs are of particular relevance. Therefore, it is expected that the FPJ technology will prevail for smaller or volatile volumes in the long run due to its lower investment and running costs and enhanced technological benefits.

[16] The costs for staff have not been considered, as they strongly depend on the number of aircraft to be manufactured, and thus also on the degree of utilization of the facilities and the time in which these are not in use.

7.3 Discussion

In this section, the scientific relevance of this Ph.D. thesis is reflected on, based on the five publications and the state of the art.

Based on FSW, FPJ was developed for bonding plastic components and metal sheets. For the corresponding processes, Bachmann (2020) and Wirth et al. (2014a) showed that the forces and temperatures occurring during the joining process considerably influence the resulting strength. For this reason, scientists were focusing on the closed-loop control of these parameters. Gebhard & Zaeh (2008) demonstrated that changing from a position- to a force-controlled process could lead to an uncontrolled plunging of the tool when heat accumulation occurs. This plunging could damage the workpiece. Therefore, for FSW, Fehrenbacher et al. (2014a) investigated a combined force and temperature control. Although possible cross-effects were not considered, the advantage of this approach was demonstrated. To effectively control even larger deviations around the operating point, Taysom et al. (2016) deployed an MPC approach to demonstrate the benefits, using the example of a temperature control. The last two aspects were considered and elaborated on in this Ph.D. thesis. The following stages of scientific progress (SP) were achieved in the framework of this thesis:

SP 1 In Publication 1, a parameter range was described, enabling a reliable direct bonding of non-polar PE-HD with aluminum alloys by FPJ (Section 3.2). By using this technology, rivets and screws can be substituted, resulting in a reduction in the total mass of the joint.

SP 2 In Publication 2, it was shown that a quasi-chaotic nanostructuring, generated by pulsed laser radiation, is superior to other surface processing strategies concerning the resulting bond strength. Furthermore, it was demonstrated that the recrystallized layer of the plastic on the metallic joining partner is the decisive boundary layer (F 1, p. 60).

SP 3 In Publication 3, it was proven that the model-predictive force control approach has advantages over conventional control strategies. Furthermore, this MPC approach is robust in terms of model uncertainties and disturbances. The method developed to design an MPC is generally

valid, and eliminates the need for a complex reparametrization of the controller when changing the material combination (F 2, p. 60).

SP 4 Within Publication 4, a differential equation to describe the thermal balance for FPJ was presented. A torque-dependent system model could be derived based on this differential equation, which considers interactions between the friction temperature and the axial force. This system model served as the basis for a holistic, adaptive multivariable MPC, capable of producing reliable results under model uncertainties. Also, a 1D FDM multilayer system for the in-situ calculation of the joining zone temperature was implemented. This 1D model simplifies the 3D process considerably. Nevertheless, due to the dimensions of the tool (diameter of 25 mm) and the relatively small dimensions of the joining partners (3 mm and 5 mm), this simplification can be accepted to describe the heat balance during the process and calculate the temperature in the plastic component (F 2, p. 60).

SP 5 In Publication 5, it was demonstrated that direct bonds produced by FPJ have a similar, or higher, bond strength than adhesively bonded joints. Thus, when switching from adhesive bonding to FPJ, the curing time can be avoided, manufacturing costs are reduced, and the bond strength is increased (F 3, p. 60).

7.4 Outlook

The holistic, model-predictive force and temperature control for plastic-metal direct joining presented in this thesis offers the opportunity for further improvement.

Starting with the findings on the pretreatment of the surface of the aluminum alloys, the following new baselines become apparent: The maximum lap shear strength for plastic-metal direct bonds, joined by FPJ, was achieved by a quasi-stochastic nanostructure, based on the research of Heckert (2019). This pattern was fabricated on the aluminum surface by pulsed laser radiation. However, this pretreatment method is time-consuming, and this aspect should be studied in future research activities.

A decisive factor in FPJ and FSW is the contact force. This parameter significantly influences the weld seam quality (Hartl et al. 2020). The method presented for designing a model-predictive force control is generally valid and can be transferred to FSW or other pressure welding processes. Nevertheless, proof of this still needs to be provided.

In industry, not only plastic-metal bonds are of relevance, but also combinations of different metals. One challenge in this context is the joining process. In this respect, FSW is a method for joining dissimilar metals, like aluminum and copper. During this joining process, a temperature-dependent diffusion layer occurs at the boundary between the two materials. The maximum temperature and the time at which this occurs influence the chemical composition of the intermetallic phases in this layer, and thus the bond strength (Grabmann et al. 2019; Krutzlinger et al. 2014; Marstatt et al. 2018). This temperature cannot be measured or controlled directly. For this purpose, the developed model-based temperature control, combined with the developed heat conduction model, provides a basis for improving the seam quality of dissimilar metal-metal bonds.

Bibliography

In the following bibliography, non-English titles have been translated into English and placed in parentheses after the original title. Wherever a number is not mentioned, it does not exist or is not known to the author of this thesis.

Achereiner 2009
Achereiner, F.: Improvement of adhesion properties for different polymer materials using gas-phase fluorination. Ph.D. thesis. Friedrich–Alexander University Erlangen–Nürnberg (FAU). 2009.

Airbus SE 2019
Airbus SE: *Press release: Airbus achieves new commercial aircraft delivery record in 2018*. Toulouse, France. 2019.

Airbus SE 2020
Airbus SE: *Press release: Airbus plans to further adapt to COVID-19 environment*. Blagnac, France. 2020.

Akkerman 2005
Akkerman, R.: Laminate mechanics for balanced woven fabrics. *Composites Part B: Engineering* 37 (2005) 2–3, pp. 108–116. ISSN: 1359-8368.

Albrecht et al. 2018
Albrecht, K.; Osswald, T.; Baur, E.; Meier, T.; Wartzack, S.; Müssig, J.: Fibre Length Reduction in Natural Fibre-Reinforced Polymers during Compounding and Injection Moulding – Experiments Versus Numerical Prediction of Fibre Breakage. *Journal of Composites Science* 2 (2018) 2, pp. 20–37.

Alessio et al. 2020
Alessio, R. P.; Andre, N. M.; Goushegir, S. M.; dos Santos, J. F.; Mazzaferro, J. A. E.; Amancio-Filho, S. T.: Prediction of the mechanical and failure behavior of metal-composite hybrid joints using cohesive surfaces. *Materials Today Communications* 24 (2020) n. No., pp. 101205-1–101205-9. ISSN: 2352-4928.

Altmaier et al. 2019
Altmaier, P.; Scheuer, A.; Kretschmer, M.; Vogt, K.; Al-Wazir, T.; Scheurle, K.-D.; Richter, K.; Hofman, J.; Behle, C.: *Leipzig Statement for the Future of Aviation*. Leipzig, Germany. 2019.

André et al. 2018
André, N. M.; Goushegir, S. M.; dos Santos, J. F.; Canto, L. B.; Amancio-Filho, S. T.: Influence of the interlayer film thickness on the mechanical performance of AA2024-T3/CF-PPS hybrid joints produced by friction spot joining. *Welding International* 32 (2018) 1, pp. 1–10. ISSN: 0950-7116.

Arbegast et al. 1999
Arbegast, W. J.; Hartley, P. J.; ASM International: Friction Stir Weld Technology Development at Lockheed Martin Michoud Space System - An Overview. In: Materials Park, Ohio, USA: ASM International. 1999, pp. 541–546. ISBN: 0-871-70627-X.

Bachmann et al. 2017
Bachmann, A.; Gamper, J.; Krutzlinger, M.; Zens, A.; Zaeh, M. F.: Adaptive model-based temperature control in friction stir welding. *The International Journal of Advanced Manufacturing Technology* 93 (2017) 1–4, pp. 1157–1171. ISSN: 0268-3768.

Bachmann et al. 2018
Bachmann, A.; Roehler, M.; Pieczona, S. J.; Kessler, M.; Zaeh, M. F.: Torque-based adaptive temperature control in friction stir welding: a feasibility study. *Production Engineering* 12 (2018) 3–4, pp. 391–403. ISSN: 0944-6524.

Bachmann 2020
Bachmann, A.: Regelung der Temperatur beim Rührreibschweißen [engl. Temperature control in friction stir welding]. Ph.D. thesis. Technical University of Munich (TUM). 2020.

Bachmann & Zaeh 2016
Bachmann, A.; Zaeh, M. F.: Pyrometer-Assisted Temperature Control in Friction Stir Welding. In: *Proceedings of the 11th International Friction Stir Welding Symposium*. Cambridge, UK: TWI Ltd. 2016.

de Backer & Bolmsjö 2013
de Backer, J.; Bolmsjö, G.: Thermoelectric method for temperature measurement in friction stir welding. *Science and Technology of Welding and Joining* 18 (2013) 7, pp. 558–565. ISSN: 1362-1718.

de Backer et al. 2014
de Backer, J.; Bolmsjö, G.; Christiansson, A.-K.: Temperature control of robotic friction stir welding using the thermoelectric effect. *The International Journal of Advanced Manufacturing Technology* 70 (2014) 1–4, pp. 375–383. ISSN: 0268-3768.

Bargel et al. 2000
Bargel, H.-J.; Cardinal, P.; Hilbrans, H.; Hübner, K.-H.; Schulze, G.; Wurzel, G.: *Werkstoffkunde [engl. Materials Science]*. 7. Springer Textbooks. Berlin/Heidelberg, Germany: Springer. 2000. ISBN: 3-540-66855-1.

Barile et al. 2020
Barile, M.; Lecce, L.; Iannone, M.; Pappadà, S.; Roberti, P.: Thermoplastic Composites for Aerospace Applications. In: *Revolutionizing Aircraft Materials and Processes*. Ed. by Pantelakis, S.; Tserpes, K. Cham, Germany: Springer. 2020, pp. 87–114. ISBN: 978-3-030-35346-9.

Baskharone 2013
Baskharone, E. A., ed. (2013): *The Finite Element Method with Heat Transfer and Fluid Mechanics Applications*. Cambridge, Great Britain: Cambridge University Press. 2013. ISBN: 978-1-139-62666-8.

Batz + Burgel GmbH & Co. KG 2021
Batz + Burgel GmbH & Co. KG: Data Sheet: EN AW-2024 (2021). Ed. by Batz + Burgel GmbH & Co. KG.

Baur et al. 2013
Baur, E.; Brinkmann, S.; Osswald, T. A.; Rudolph, N.; Schmachtenberg, E.: *Saechtling Kunststoff Taschenbuch [engl. Saechtling Plastic Paperback]*. Munich, Germany: Carl Hanser Verlag GmbH & Co. KG. 2013. ISBN: 978-3-446-43442-4.

Bergweiler 2013
Bergweiler, G.: Local heat treatment with laser radiation to improve forming and functional properties of high stength steels. Ph.D. thesis. RWTH Aachen University. 2013. ISBN: 978-3-86359-162-5.

Bikerman 1961
Bikerman, J. J.: *The Science of Adhesive Joints*. New York, USA: Academic Press. 1961. ISBN: 978-1-4832-6773-9.

Bodily et al. 2012
Bodily, B.; Heinimann, M.; Bray, G.; Colvin, E.; Witters, J.: Advanced Aluminum and Aluminum-Lithium Solutions for Derivative and Next Generation Aerospace Structures. In: *SAE Technical Paper Series*. SAE Technical Paper Series. Warrendale, Pennsylvania, USA: SAE International. 2012.

Bohn & Unbehauen 2016
Bohn, C.; Unbehauen, H.: *Identifikation dynamischer Systeme [engl. Identification of dynamic systems]*. Wiesbaden, Germany: Springer. 2016. ISBN: 978-3-8348-1755-6.

de Bruyne 1939
de Bruyne, N. A.: The nature of adhesion. *Aircraft Engineer* 18 (1939) 12, pp. 52–54.

Buffa et al. 2006
Buffa, G.; Hua, J.; Shivpuri, R.; Fratini, L.: A continuum based FEM model for friction stir welding—model development. *Materials Science and Engineering: A* 419 (2006) 1-2, pp. 389–396. ISSN: 0921-5093.

Buffa et al. 2016
Buffa, G.; Baffari, D.; Campanella, D.; Fratini, L.: An Innovative Friction Stir Welding Based Technique to Produce Dissimilar Light Alloys to Thermoplastic Matrix Composite Joints. *Procedia Manufacturing* 5 (2016) n. No., pp. 319–331. ISSN: 2351-9789.

Carr & Turner 2016
Carr, E. J.; Turner, I. W.: A semi-analytical solution for multilayer diffusion in a composite medium consisting of a large number of layers. *Applied Mathematical Modelling* 40 (2016) 15-16, pp. 7034–7050. ISSN: 0307-904X.

Costanzi et al. 2017
Costanzi, G.; Bachmann, A.; Zäh, M. F.: Entwicklung eines FSW-Spezialwerkzeugs zur Messung der Schweißtemperatur [engl.: Development of a special FSW tool to measure the welding temperature]. In: *DVS-Congress 2017*. Ed. by DVS. DVS-Berichte. Dusseldorf, Germany: DVS Media GmbH. 2017. ISBN: 978-3-96144-008-5.

Dance & Kellar 2004
Patent: WO 2004 028731 A1 (08.04.2004). Dance, B. G. I. D.; Kellar, E. J. C. K.: Workpiece structure modification.

Davis et al. 2010
Davis, T. A.; Shin, Y. C.; Yao, B.: Observer-based adaptive robust control of friction stir welding axial force. In: *2010 IEEE/ASME International Conference on Advanced Intelligent Mechatronics*. Montreal, Canada: IEEE. 2010, pp. 1162–1167. ISBN: 978-1-4244-8031-9.

Diaz et al. 2017
Diaz, I. C.; Jin, Y.; Ares, E.: Cycle time study of wing spar assembly on aircraft factory. *Procedia Manufacturing* 13 (2017) n. No., pp. 1019–1025. ISSN: 2351-9789.

DIN 8580
DIN 8580:2003-09: Manufacturing processes – Terms and definitions, division (2003). Berlin, Germany: Beuth.

DIN EN 515
DIN EN 515: Aluminium and aluminium alloys – Wrought products – Temper designations (2017). Berlin, Germany: Beuth.

DIN EN 573-1
DIN EN 573-1: Aluminium and aluminium alloys – Chemical composition and form of wrought products – Part 1: Numerical designation system (2005). Berlin, Germany: Beuth.

DIN EN 573-3
DIN EN 573-3: Aluminium and aluminium alloys – Chemical composition and form of wrought products – Part 3: Chemical composition and form of products (2018). Berlin, Germany: Beuth.

DIN EN 60027-6
DIN EN 60027-6: Letter symbols to be used in electrical technology – Part 6: Control technology (2007). Berlin, Germany: Beuth.

DIN EN ISO 25239-1
DIN EN ISO 25239-1:2019-06: Friction stir welding – Aluminium – Part 1: Vocabulary (2019). Berlin, Germany: Beuth.

Dittmar & Pfeiffer 2009
Dittmar, R.; Pfeiffer, B.-M.: *Modellbasierte prädiktive Regelung: Eine Einführung für Ingenieure [engl. Model-based predictive control: An introduction for engineers]*. Munich, Germany: Oldenbourg. 2009. ISBN: 978-3-48627-523-0.

Domininghaus et al. 2008
Domininghaus, H.; Elsner, P.; Eyerer, P.; Hirth, T.: *Kunststoffe: Eigenschaften und Anwendungen [engl. Plastics: Properties and Applications]*. 7. VDI-Buch. Berlin/Heidelberg, Germany: Springer. 2008. ISBN: 978-3-540-72400-1.

Earl et al. 2012
Earl, C.; Hilton, P.; O'Neill, B.: Parameter Influence on Surfi-Sculpt Processing Efficiency. *Physics Procedia* 39 (2012) n. No., pp. 327–335. ISSN: 1875-3892.

Edelmann 2012
Edelmann, K.: CFK-Thermoplast-Fertigung für den A350 XWB [engl.: CFRP thermoplastic production for the A350 XWB]. *Lightweight Design* 5 (2012) 2, pp. 42–47. ISSN: 1865-4819.

Ehrenstein 2006
Ehrenstein, G. W.: *Faserverbund-Kunststoffe: Werkstoffe – Verarbeitung – Eigenschaften [engl. Fiber-reinforced plastics: Materials – Processing – Properties]*. 2. Munich, Germany: Hanser. 2006. ISBN: 3-446-22716-4.

Enami et al. 2020
Enami, K.; Kimura, F.; Yokoyama, K.; Murakami, T.; Kajihara, Y.: Experimental and simulative investigation of the effects of laser-structured metal surface on metal-polymer direct joining. *Precision Engineering* 62 (2020) n. No., pp. 273–281. ISSN: 0141-6359.

Ensinger Ltd 2021
Ensinger Ltd: Data Sheet: TECAMID 6 GF30 black – Stock Shapes (2021). Ed. by Ensinger Ltd.

European Commission 2019
European Commission: *The European Green Deal*. n. No., 2019, pp. 1–24.

Fahrenwaldt 2009
Fahrenwaldt, H. J.: *Praxiswissen Schweißtechnik [engl. Welding technology practical knowledge]*. Wiesbaden, Germany: Springer. 2009. ISBN: 978-3-83480-382-5.

Fehrenbacher et al. 2008
Fehrenbacher, A.; Pfefferkorn, F. E.; Zinn, M. R.; Ferrier, N. J.; Duffie, N. A.: Closed-loop control of temperature in friction stir welding. In: *Proceedings of the 7th International Symposium on Friction Stir Welding*. Cambridge, UK: TWI Ltd. 2008. ISBN: 978-1-90376-106-9.

Fehrenbacher et al. 2011a
Fehrenbacher, A.; Duffie, N. A.; Ferrier, N. J.; Pfefferkorn, F. E.; Zinn, M. R.: Toward Automation of Friction Stir Welding Through Temperature Measurement and Closed-Loop Control. *Journal of Manufacturing Science and Engineering* 133 (2011) 5. ISSN: 1087-1357.

Fehrenbacher et al. 2011b
Fehrenbacher, A.; Cole, E. G.; Zinn, M. R.; Ferrier, N. J.; Duffie, N. A.; Pfefferkorn, F. E.: Towards Process Control of Friction Stir Welding for Different Aluminum Alloys. In: *Friction stir welding and processing VI*. Ed. by Mishra, R. S. Vol. 51. Hoboken, Netherlands: Wiley. 2011, pp. 381–388. ISBN: 978-1-11806-230-2.

Fehrenbacher et al. 2014a
Fehrenbacher, A.; Smith, C. B.; Duffie, N. A.; Ferrier, N. J.; Pfefferkorn, F. E.; Zinn, M. R.: Combined Temperature and Force Control for Robotic Friction Stir Welding. *Journal of Manufacturing Science and Engineering* 136 (2014) 2, pp. 021007-1–021007-15. ISSN: 1087-1357.

Fehrenbacher et al. 2014b
Fehrenbacher, A.; Duffie, N. A.; Ferrier, N. J.; Pfefferkorn, F. E.; Zinn, M. R.: Effects of tool–workpiece interface temperature on weld quality and quality improvements through temperature control in friction stir welding. *The International Journal of Advanced Manufacturing Technology* 71 (2014) 1–4, pp. 165–179. ISSN: 0268-3768.

Flock 2012
Flock, D.: Heat conduction bonding of plastic-metal hybrid parts. Ph.D. thesis. RWTH Aachen University. 2012.

Fuchs et al. 2014
Fuchs, A. N.; Wirth, F. X.; Rinck, P.; Zaeh, M. F.: Laser-generated Macroscopic and Microscopic Surface Structures for the Joining of Aluminum and Thermoplastics using Friction Press Joining. *Physics Procedia* 56 (2014) n. No., pp. 801–810. ISSN: 1875-3892.

Ganeev 2014
Ganeev, R. A.: *Laser – Surface Interactions*. Dordrecht, Netherlands: Springer. 2014. ISBN: 978-94-007-7340-0.

Gebhard & Zaeh 2008
Gebhard, P.; Zaeh, M. F.: Force Control Design for CNC Milling Machines for Friction Stir Welding. In: *Proceedings of the 7th International Symposium on Friction Stir Welding*. Cambridge, UK: TWI Ltd. 2008. ISBN: 978-1-90376-106-9.

Gebhard 2011
Gebhard, P.: Dynamisches Verhalten von Werkzeugmaschinen bei Anwendung für das Rührreibschweißen [engl.: Dynamic performance of machine tools used for friction stir welding]. Ph.D. thesis. Technical University of Munich (TUM). 2011. ISBN: 978-3-8316-4129-1.

Gemmel Metalle & Co. GmbH 2021
Gemmel Metalle & Co. GmbH: Data Sheet: AlMgSi1 F30 (2021). Ed. by Gemmel Metalle & Co. GmbH.

German Federal Ministry of Finance 2001
German Federal Ministry of Finance: *AfA-Tabelle für den Wirtschaftszweig Maschinenbau [engl. Depreciation table for the mechanical engineering sector]*. Berlin, Germany: German Federal Ministry of Finance. 2001.

Goushegir et al. 2014
Goushegir, S. M.; dos Santos, J. F.; Amancio-Filho, S. T.: Friction Spot Joining of aluminum AA2024/carbon-fiber reinforced poly(phenylene sulfide) composite single lap joints: Microstructure and mechanical performance. *Materials & Design* 54 (2014) n. No., pp. 196–206. ISSN: 0261-3069.

Grabmann et al. 2019
Grabmann, S.; Zens, A.; Marstatt, R.; Haider, F.; Zaeh, M. F.: Temperature-controlled friction stir welding process of Al-Cu joints with complex geometries. In: *Proceedings of the 22nd International ESAFORM Conference on Material Forming: ESAFORM 2019*. AIP Conference Proceedings. Vitoria-Gasteiz, Spain: AIP Publishing. 2019, pp. 050004-1–050004-7.

Habenicht 2009
Habenicht, G.: *Kleben: Grundlagen, Technologien, Anwendungen [engl. Bonding: Basics, Technologies, Applications]*. 6. VDI-Book. Berlin/Heidelberg, Germany: Springer. 2009. ISBN: 978-3-540-85264-3.

Habenicht 2016
Habenicht, G.: *Kleben – erfolgreich und fehlerfrei [engl. Bonding – Successful and defect free]*. Wiesbaden, Germany: Springer. 2016. ISBN: 978-3-658-14695-5.

Han et al. 2020
Han, S. C.; Wu, L. H.; Jiang, C. Y.; Li, N.; Jia, C. L.; Xue, P.; Zhang, H.; Zhao, H. B.; Ni, D. R.; Xiao, B. L.; Ma, Z. Y.: Achieving a strong polypropylene/aluminum alloy friction spot joint via a surface laser processing pretreatment. *Journal of Materials Science & Technology* 50 (2020) n. No., pp. 103–114. ISSN: 1005-0302.

Hartl et al. 2020
Hartl, R.; Praehofer, B.; Zaeh, M. F.: Prediction of the surface quality of friction stir welds by the analysis of process data using Artificial Neural Networks. *Proceedings of the Institution of Mechanical Engineers, Part L: Journal of Materials: Design and Applications* 234 (2020) 5, pp. 732–751. ISSN: 1464-4207.

Heckert 2019
Heckert, A.: Oberflächenstrukturierung von Aluminium mittels gepulster Laserstrahlung für das thermische Fügen an endlosfaserverstärkte Thermoplaste [engl. Pulsed Laser Surface Pre-Treatment of Aluminium for Thermal Joining with Thermoplastics]. Ph.D. thesis. Technical University of Munich (TUM). 2019.

Heckert & Zaeh 2014a
Heckert, A.; Zaeh, M. F.: Laser Surface Pre-treatment of Aluminium for Hybrid Joints with Glass Fibre Reinforced Thermoplastics. *Physics Procedia* 56 (2014) n. No., pp. 1171–1181. ISSN: 1875-3892.

Heckert & Zaeh 2014b
Heckert, A.; Zaeh, M. F.: Laser Surface Pre-treatment of Aluminium for Hybrid Joints with Glass Fibre Reinforced Thermoplastics. In: *Proceedings of the 33rd International Congress on Applications of Lasers & Electro-Optics*. Ed. by Laser Institute of America. Vol. 56. San Diego, California, USA: Laser Institute of America (LIA pub). 2014, pp. 1171–1181.

Hickson et al. 2011
Hickson, R. I.; Barry, S. I.; Mercer, G. N.; Sidhu, H. S.: Finite difference schemes for multilayer diffusion. *Mathematical and Computer Modelling* 54 (2011) 1-2, pp. 210–220. ISSN: 0895-7177.

Huber 2017
Huber, J.: Verfahren zur Klassifikation von Ungänzen bei der optischen Prüfung von Batterieseparatoren [engl. Procedure for the classification of discontinuities at the optical inspection of battery separators]. Ph.D. thesis. Technical University of Munich (TUM). 2017. ISBN: 978-3-8316-4593-0.

Huda et al. 2009
Huda, Z.; Taib, N. I.; Zaharinie, T.: Characterization of 2024-T3: An aerospace aluminum alloy. *Materials Chemistry and Physics* 113 (2009) 2–3, pp. 515–517. ISSN: 0254-0584.

ICAO 2016
ICAO – International Civil Aviation Organization: *Consolidated statement of continuing ICAO policies and practices related to environmental protection – Global Market-based Measure (MBM) scheme: Resolution A39-3*. 2016.

Illing et al. 2017
Illing, T.; Schoßig, M.; Bierögel, C.; Langer, B.; Grellmann, W.: Hygrothermal Ageing of Injection-Moulded PA6/GF Materials Considering Automotive Requirements. In: *Deformation and Fracture Behaviour of Polymer Materials*. Ed. by Grellmann, W.; Langer, B. Vol. 247. Springer Series in Materials Science. Cham, Germany: Springer. 2017, pp. 405–419. ISBN: 978-3-319-41877-3.

Kaiser 2016
Kaiser, W.: *Kunststoffchemie für Ingenieure: Von der Synthese bis zur Anwendung [engl. Polymer chemistry for engineers: From synthesis to application]*. 4. Munich, Germany: Hanser. 2016. ISBN: 978-3-446-44638-0.

Karwa 2020
Karwa, R.: *Heat and Mass Transfer*. Singapore: Springer. 2020. ISBN: 978-981-15-3987-9.

Krutzlinger et al. 2015
Krutzlinger, M.; Bachmann, A.; Wirth, F. X.; Roth, A.; Suenger, S.; Pieczona, S. J.; Zaeh, M. F.: Implementierung einer Messsensorik in ein Fräsbearbeitungszentrum zur Ermittlung der Prozesskräfte und des Prozessmoments beim Rührreibschweißen [engl.: Implementation of a measuring sensor system in a milling machining center to determine the process forces and the process torque during friction stir welding]. In: *Tagungsband [engl.: proceedings] DVS Congress 2015*. Ed. by DVS – Deutscher Verband für Schweißen und verwandte Verfahren e. V. DVS-Berichte. Dusseldorf, Germany: DVS Media GmbH. 2015, pp. 209–214. ISBN: 978-3-945023-46-4.

Krutzlinger et al. 2014
Krutzlinger, M.; Marstatt, R.; Suenger, S.; Luderschmid, J.; Zaeh, M. F.; Haider, F.: Formation of Joining Mechanisms in Friction Stir Welded Dissimilar Al-Ti Lap Joints. *Advanced Materials Research* 966-967 (2014) n. No., pp. 510–520.

Küll 2002
Küll, H.: Plastic Composites Replacing Aluminium in the Wings: Airbus to Fly with PPS. *Kunststoffe International* 92 (2002) 1, pp. 74–76.

Kumar et al. 2005
Kumar, B.; Widener, C.; Jahn, A.; Tweedy, B.; Cope, D.; Lee, R.: Review of the Applicability of FSW Processing to Aircraft Applications. In: *46^{th} AIAA/ASME/ASCE/AHS/ASC Structures, Structural Dynamics and Materials Conference*. Reston, Virigina, USA: American Institute of Aeronautics and Astronautics. 2005, pp. 423–441. ISBN: 978-1-62410-065-9.

Lapidus & Pinder 1982
Lapidus, L.; Pinder, G. F.: *Numerical solution of partial differential equations in science and engineering*. A Wiley-Interscience publication. New York, New York, USA: Wiley. 1982. ISBN: 0-471-09866-3.

Liu et al. 2014
Liu, F. C.; Liao, J.; Nakata, K.: Joining of metal to plastic using friction lap welding. *Materials & Design* 54 (2014) n. No., pp. 236–244. ISSN: 0261-3069.

Liu et al. 2015
Liu, F. C.; Liao, J.; Gao, Y.; Nakata, K.: Effect of plasma electrolytic oxidation coating on joining metal to plastic. *Science and Technology of Welding and Joining* 20 (2015) 4, pp. 291–296. ISSN: 1362-1718.

Lohwasser & Chen 2010
Lohwasser, D.; Chen, Z.: *Friction stir welding: From basics to applications*. Woodhead Publishing in materials. Cambridge, UK: Woodhead Publishing. 2010. ISBN: 978-1-84569-450-0.

Lomov & Verpoest 2005
Lomov, S.; Verpoest, I.: Manufacturing and internal geometry of textiles. In: *Design and Manufacture of Textile Composites*. Woodhead: Elsevier. 2005, pp. 1–61. ISBN: 978-1-855-73744-0.

Longhurst et al. 2010
Longhurst, W. R.; Strauss, A. M.; Cook, G. E.; Cox, C. D.; Hendricks, C. E.; Gibson, B. T.; Dawant, Y. S.: Investigation of force-controlled friction stir welding for manufacturing and automation. *Proceedings of the Institution of Mechanical Engineers, Part B: Journal of Engineering Manufacture* 224 (2010) 6, pp. 937–949. ISSN: 0954-4054.

Lu & Viljanen 2006
Lu, X.; Viljanen, M.: An analytical method to solve heat conduction in layered spheres with time-dependent boundary conditions. *Physics Letters A* 351 (2006) 4-5, pp. 274–282. ISSN: 0375-9601.

Lunze 2016
Lunze, J.: *Regelungstechnik 1: Systemtheoretische Grundlagen, Analyse und Entwurf einschleifiger Regelungen [engl. Control engineering 1: System theoretical basics, analysis, and design of single-loop controls]*. 11. Berlin, Germany: Springer. 2016. ISBN: 978-3-662-52677-4.

Magalhães 2016
Magalhães, A.: Thermo-electric temperature measurements in friction stir welding – Towards feedback control of temperature. Ph.D. thesis. University West. 2016.

Mahoney & Mishra 2007
Mahoney, M. W.; Mishra, R. S.: *Friction stir welding and processing*. Materials Park, Ohio, USA: ASM International. 2007. ISBN: 978-0-87170-840-3.

March 2021
March, N.: Analytical, numerical and macroscopic modelling approaches for diffusive transport processes in heterogenous media. Ph.D. thesis. Queensland University of Technology (QUT). 2021.

March & Carr 2019
March, N.; Carr, E. J.: Finite volume schemes for multilayer diffusion. *Journal of Computational and Applied Mathematics* 345 (2019), pp. 206–223. ISSN: 0377-0427.

Marsh 2010
Marsh, G.: Airbus A350 XWB update. *Reinforced Plastics* 54 (2010) 6, pp. 20–24. ISSN: 0034-3617.

Marstatt et al. 2018
Marstatt, R.; Krutzlinger, M.; Luderschmid, J.; Constanzi, G.; Mueller, J. F. J.; Haider, F.; Zaeh, M. F.: Intermetallic layers in temperature controlled Friction Stir Welding of dissimilar Al-Cu-joints. *IOP Conference Series: Materials Science and Engineering* 373 (2018) n. No., pp. 012017-1–012017-7.

Merklein 2001
Merklein, M.: Laserstrahlumformen von Aluminiumwerkstoffen – Beeinflussung der Mikrostruktur und der mechanischen Eigenschaften [engl.: Laser beam forming of aluminum materials – influencing the microstructure and mechanical properties]. Ph.D. thesis. Friedrich–Alexander University Erlangen–Nürnberg (FAU). 2001. ISBN: 3-8752-5156-3.

Meyer et al. 2019a
Meyer, S. P.; Wunderling, C.; Zaeh, M. F.: Friction press joining of dissimilar materials: A novel concept to improve the joint strength. In: *Proceedings of the 22nd International ESAFORM Conference on Material Forming: ESAFORM 2019*. AIP Conference Proceedings. Vitoria-Gasteiz, Spain: AIP Publishing. 2019, pp. 050031-1–050031-6.

Meyer et al. 2019b
Meyer, S. P.; Wunderling, C.; Zaeh, M. F.: Influence of the laser-based surface modification on the bond strength for friction press joining of aluminum and polyethylene. *Production Engineering* 13 (2019) 6, pp. 721–730. ISSN: 0944-6524.

Meyer et al. 2020
Meyer, S. P.; Bernauer, C. J.; Grabmann, S.; Zaeh, M. F.: Design, evaluation, and implementation of a model-predictive control approach for a force control in friction stir welding processes. *Production Engineering* 14 (2020) 4, pp. 473–489. ISSN: 0944-6524.

Meyer et al. 2021a
Meyer, S. P.; Fuderer, S.; Zaeh, M. F.: A Holistic, Model-Predictive Process Control for Friction Stir Welding Processes Including a 1D FDM Multi-Layer Temperature Distribution Model. *Metals* 11 (2021) 3, pp. 502-1–502-22.

Meyer et al. 2021b
Meyer, S. P.; Herold, M. T.; Habedank, J. B.; Zaeh, M. F.: A Study on the Bond Strength of Plastic-Metal Direct Bonds Using Friction Press Joining. *Metals* 11 (2021) 4, pp. 660-1–660-18.

Mishra & Ma 2005
Mishra, R. S.; Ma, Z. Y.: Friction stir welding and processing. *Materials Science and Engineering: R: Reports* 50 (2005) 1–2, pp. 1–78. ISSN: 0927-796X.

Mittal & Pizzi 1999
Mittal, K. L.; Pizzi, A.: *Adhesion Promotion Techniques: Technological Applications*. Vol. 14. Materials Engineering Ser. Boca Raton, Florida, USA: Chapman and Hall/CRC. 1999. ISBN: 0-8247-0239-5.

de Monte 2002
de Monte, F.: An analytic approach to the unsteady heat conduction processes in one-dimensional composite media. *International Journal of Heat and Mass Transfer* 45 (2002) 6, pp. 1333–1343. ISSN: 0017-9310.

Musiol et al. 2011
Musiol, J.; Zaeh, M. F.; Guertler, M. R.: Contribution on modelling the remote ablation cutting. In: *International Congress on Applications of Lasers & Electro-Optics*. Orlando, Florida, USA: Laser Institute of America. 2011, pp. 369–377. ISBN: 978-0-912035-94-9.

Nandan et al. 2006
Nandan, R.; Roy, G. G.; Debroy, T.: Numerical simulation of three-dimensional heat transfer and plastic flow during friction stir welding. *Metallurgical and Materials Transactions A* 37 (2006) 4, pp. 1247–1259. ISSN: 1073-5623.

Oakes & Landers 2009
Oakes, T.; Landers, R. G.: Design and implementation of a general tracking controller for Friction Stir Welding processes. In: *2009 American Control Conference*. St. Louis, Missouri, USA: IEEE. 2009, pp. 5576–5581. ISBN: 978-1-4244-4523-3.

Osswald & Menges 2012
Osswald, T. A.; Menges, G.: *Materials Science of Polymers for Engineers*. 3. Cincinnati, Ohio, USA: Hanser Publications. 2012. ISBN: 978-1-56990-514-2.

Ostermann 2014
Ostermann, F.: *Anwendungstechnologie Aluminium [engl. Application Technology Aluminum]*. Berlin/Heidelberg, Germany: Springer. 2014. ISBN: 978-3-66243-806-0.

Premium AEROTEC GmbH 2011
Premium AEROTEC GmbH: *Press release: Airbus A350 XWB – work packages Premium AEROTEC*. Augsburg, Germany. 2011.

Premium AEROTEC GmbH 2014
Premium AEROTEC GmbH: *Press release: Premium AEROTEC starts its production for the largest Airbus A350 XWB version in Nordenham.* Augsburg/Nordenham, Germany. 2014.

Quilter 2001
Quilter, A.: *White Paper: Composites in Aerospace Applications.* Englewood, Colorado, USA: IHS Corporate Headquarters. 2001.

Reddy & Gartling 2010
Reddy, J. N.; Gartling, D. K.: *The Finite Element Method in Heat Transfer and Fluid Dynamics, Third Edition.* 3rd ed. Computational Mechanics and Applied Analysis. Hoboken, New Jersey, USA: CRC Press. 2010. ISBN: 978-1-43988-257-3.

Rodrigo & Worthy 2016
Rodrigo, M. R.; Worthy, A. L.: Solution of multilayer diffusion problems via the Laplace transform. *Journal of Mathematical Analysis and Applications* 444 (2016) 1, pp. 475–502. ISSN: 0022-247X.

Rodríguez-Vidal et al. 2016
Rodríguez-Vidal, E.; Sanz, C.; Soriano, C.; Leunda, J.; Verhaeghe, G.: Effect of metal micro-structuring on the mechanical behavior of polymer–metal laser T-joints. *Journal of Materials Processing Technology* 229 (2016) n. No., pp. 668–677. ISSN: 0924-0136.

Rofin-Sinar Laser GmbH 2020
Rofin-Sinar Laser GmbH: Fiber Lasers – PoweLine F Series for Marking and Micro Processing. Ed. by Rofin-Sinar Laser GmbH. Bergkirchen, Germany: Rofin-Sinar Laser GmbH.

Roth 2016
Roth, A.: Modellierung des Rührreibschweißens unter besonderer Berücksichtigung der Spalttoleranz [engl. Modelling the friction stir welding process with particular regard to the gap tolerance]. Ph.D. thesis. Technical University of Munich (TUM). 2016. ISBN: 978-3-8316-4639-5.

Ruhstorfer 2012
Ruhstorfer, M.: Rührreibschweißen von Rohren [engl. Friction Stir Welding of Tubes]. Ph.D. thesis. Technical University of Munich (TUM). 2012. ISBN: 978-3-8316-4197-0.

S-POLYTEC GmbH 2021
S-POLYTEC GmbH: Data Sheet: PE-HD (2021). Ed. by S-POLYTEC GmbH.

Schindler 2014
Schindler, S.: Strategische Planung von Technologieketten für die Produktion [engl. Strategic Technology Chain Planning for Production]. Ph.D. thesis. Technical University of Munich (TUM). 2014. ISBN: 978-3-8316-4434-6.

Schonhorn 1985
Schonhorn, H.: Adhesion and Adhesives: Interactions at Interfaces. *Journal of Plastic Film & Sheeting* 1 (1985) 2, pp. 163–179. ISSN: 8756-0879.

Schröer 1994
Schröer, D.: Chemie der Phasengrenze Metall-Polymer: Untersuchungen zur Vorbehandlung und Plasmaunterstützten Metallisierung von Hochleistungspolymeren [engl.: Chemistry of the Metal-Polymer Phase Interface: Investigations on the pretreatment and plasma-assisted metallization of high-performance polymers]. Ph.D. thesis. University of Münster. 1994.

Schuck 2009
Schuck, M.: Principles of compatibility for assembly injection moulding. Ph.D. thesis. Friedrich–Alexander University Erlangen–Nürnberg (FAU). 2009. ISBN: 978-3-931864-44-6.

Schürmann 2007
Schürmann, H.: *Konstruieren mit Faser-Kunststoff-Verbunden [engl. Designing with fiber-plastic composites]*. 2. VDI-Buch. Berlin/Heidelberg, Germany: Springer. 2007. ISBN: 978-3-540-72189-5.

Schwab et al. 2018
Schwab, D.; Schäfer, E.; Wunderling, C.; Meyer, S.: High-speed nested scanner for large-area material processing. In: *10th CIRP Conference on Photonic Technologies LANE 2018*. Fürth, Germany. 2018.

Sharpe & Schonhorn 1964
Sharpe, L. H.; Schonhorn, H.: Surface Energetics, Adhesion, and Adhesive Joints. In: *Contact Angle, Wettability, and Adhesion*. Ed. by Fowkes, F. M. Vol. 43. Advances in Chemistry. Washington, D.C., USA: American Chemical Society. 1964, pp. 189–201. ISBN: 0-8412-0044-0.

Shaw 1963
Shaw, M. C.: The role of friction in deformation processing. *Wear* 6 (1963) 2, pp. 140–158. ISSN: 0043-1648.

Sigl et al. 2020
Sigl, M. E.; Bachmann, A.; Mair, T.; Zaeh, M. F.: Torque-Based Temperature Control in Friction Stir Welding by Using a Digital Twin. *Metals* 10 (2020) 7, pp. 914-1–914-17.

Silva et al. 2017
Silva, A. C. F.; Backer, J. de; Bolmsjö, G.: Temperature measurements during friction stir welding. *The International Journal of Advanced Manufacturing Technology* 88 (2017) 9–12, pp. 2899–2908. ISSN: 0268-3768.

Song & Kovacevic 2003
Song, M.; Kovacevic, R.: Numerical and experimental study of the heat transfer process in friction stir welding. *Proceedings of the Institution of Mechanical Engineers, Part B: Journal of Engineering Manufacture* 217 (2003) 1, pp. 73–85. ISSN: 0954-4054.

Soron & Kalaykov 2006
Soron, M.; Kalaykov, I.: A Robot Prototype for Friction Stir Welding. In: *2006 IEEE Conference on Robotics, Automation and Mechatronics*. Luoyang, Henan, China: IEEE. 2006, pp. 1–5. ISBN: 1-4244-0024-4.

Steffenhagen 2011
Steffenhagen, B.: *Kleine Formelsammlung Regelungstechnik [engl. Brief collection of Control Engineering Equations]*. Munich, Germany: Carl Hanser Verlag GmbH & Co. KG. 2011. ISBN: 978-3-446-41467-9.

Stopka & Urban 2017
Stopka, U.; Urban, T.: *Investition und Finanzierung [engl. Investment and financing]*. Berlin, Germany: Springer. 2017. ISBN: 978-3-642-01691-2.

Taysom et al. 2016
Taysom, B. S.; Sorensen, C. D.; Hedengren, J. D.: Dynamic modeling of friction stir welding for model predictive control. *Journal of Manufacturing Processes* 23 (2016) n. No., pp. 165–174. ISSN: 1526-6125.

Taysom et al. 2017
Taysom, B. S.; Sorensen, C. D.; Hedengren, J. D.: A comparison of model predictive control and PID temperature control in friction stir welding. *Journal of Manufacturing Processes* 29 (2017) n. No., pp. 232–241. ISSN: 1526-6125.

Taysom & Sorensen 2019
Taysom, B. S.; Sorensen, C. D.: Advances in Signal Processing for Friction Stir Welding Temperature Control. In: *Friction Stir Welding and Processing X*. Ed. by Hovanski, Y.; Mishra, R.; Sato, Y.; Upadhyay, P.; Yan, D. Vol. 40. The Minerals, Metals & Materials Series. Cham, Germany: Springer. 2019, pp. 135–147. ISBN: 978-3-030-05751-0.

TenCate Advanced Composites BV 2021
TenCate Advanced Composites BV: Data Sheet: Cetex TC1100 PPS (2021). Ed. by TenCate Advanced Composites BV.

Thyagarajan & Ghatak 2011
Thyagarajan, K.; Ghatak, A.: *Lasers*. Boston, MA, USA: Springer. 2011. ISBN: 978-1-4419-6441-0.

Tittle 1965
Tittle, C. W.: Boundary Value Problems in Composite Media: Quasi-Orthogonal Functions. *Journal of Applied Physics* 36 (1965) 4, pp. 1486–1488. ISSN: 0021-8979.

Turkovich & Erwin 1983
Turkovich, R. von; Erwin, L.: Fiber fracture in reinforced thermoplastic processing. *Polymer Engineering & Science* 23 (1983) 13, pp. 743–749. ISSN: 0032-3888.

United Nations 2015
United Nations: *Transforming our world: the 2030 Agenda for Sustainable Development: A/RES/70/1*. n. No., 2015, pp. 1–38.

Völlner 2010
Völlner, G.: Rührreibschweißen mit Schwerlast-Industrierobotern [engl. Friction Stir Welding with heavy duty industrial robots]. Ph.D. thesis. Technical University of Munich (TUM). 2010. ISBN: 3-8316-0955-1.

Völz 2016
Völz, A.: *Modellprädiktive Regelung nichtlinearer Systeme mit Unsicherheiten [engl. Model predictive control of nonlinear systems with uncertainties]*. Ed. by Völz, A. Wiesbaden, Germany: Springer. 2016. ISBN: 978-3-658-16278-8.

Voyutskii & Vakula 1963
Voyutskii, S. S.; Vakula, V. L.: The role of diffusion phenomena in polymer-to-polymer adhesion. *Journal of Applied Polymer Science* 7 (1963) 2, pp. 475–491. ISSN: 0021-8995.

Weddeling et al. 2011
Weddeling, C.; Kronthaler, M.; Wirth, F. X.; Tekkaya, A. E.; Zaeh, M. F.: Innovative joining methods for the manufacturing of lightweight frame structures. In: *Materials Forum Intelligent Lightweight Construction*. Hannover, Germany: Hannover Messe. 2011.

Wirth et al. 2011
Wirth, F. X.; Ruhstorfer, M.; Zaeh, M. F.: Mischverbindungen durch Reibpressfügen: Fügen von Aluminiumprofilen mit Kunststoff ohne Klebstoff [engl. Dissimilar joints using friction press joining: Joining aluminum profiles with plastic elements without adhesive]. *wt Werkstattstechnik online* 101 (2011) 9, pp. 564–569.

Wirth et al. 2014a
Wirth, F. X.; Zaeh, M. F.; Krutzlinger, M.; Silvanus, J.: Analysis of the Bonding Behavior and Joining Mechanism during Friction Press Joining of Aluminum Alloys with Thermoplastics. *Procedia CIRP* 18 (2014) n. No., pp. 215–220. ISSN: 2212-8271.

Wirth et al. 2014b
Wirth, F. X.; Fuchs, A. N.; Rinck, P.; Zaeh, M. F.: Friction Press Joining of Laser-Texturized Aluminum with Fiber Reinforced Thermoplastics. *Advanced Materials Research* (2014) 966–977, pp. 536–545.

Wu et al. 2018
Wu, L. H.; Nagatsuka, K.; Nakata, K.: Direct joining of oxygen-free copper and carbon-fiber-reinforced plastic by friction lap joining. *Journal of Materials Science & Technology* 34 (2018) 1, pp. 192–197. ISSN: 1005-0302.

Wunderling et al. 2020
Wunderling, C.; Mayr, L.; Meyer, S. P.; Zaeh, M. F.: Laser-based surface pre-treatment for metal-plastic hybrids using a new process strategy. *Journal of Materials Processing Technology* 282 (2020) n. No., pp. 116675-1–116675-8. ISSN: 0924-0136.

Wunderling et al. 2019
Wunderling, C.; Scherm, M.; Meyer, S.; Zaeh, M. F.: Thermal distortion in surface pretreatment of metal-polymer hybrids using continuous wave laser radiation. In: *High-Power Laser Materials Processing: Applications, Diagnostics, and Systems VIII*. Ed. by Kaierle, S.; Heinemann, S. W. San Francisco, California, USA: SPIE. 2019, 109110A-1–109110A-11. ISBN: 978-1-510-62464-1.

Xiao et al. 2017
Xiao, Y.; Zhan, H.; Gu, Y.; Li, Q.: Modeling heat transfer during friction stir welding using a meshless particle method. *International Journal of Heat and Mass Transfer* 104 (2017), pp. 288–300. ISSN: 0017-9310.

S. Zhao et al. 2016
Zhao, S.; Bi, Q.; Wang, Y.: An axial force controller with delay compensation for the friction stir welding process. *The International Journal of Advanced Manufacturing Technology* 85 (2016) 9–12, pp. 2623–2638. ISSN: 0268-3768.

X. Zhao et al. 2007
Zhao, X.; Kalya, P.; Landers, R. G.; Krishnamurthy, K.: Design and Implementation of a Nonlinear Axial Force Controller for Friction Stir Welding Processes. In: *2007 American Control Conference*. New York City, USA: IEEE. 2007, pp. 5553–5558. ISBN: 1-4244-0988-8.

X. Zhao et al. 2009
Zhao, X.; Kalya, P.; Landers, R. G.; Krishnamurthy, K.: Empirical Dynamic Modeling of Friction Stir Welding Processes. *Journal of Materials Processing Technology* 131 (2009) 2, pp. 021001-1–021001-9. ISSN: 09240136.

Ziegler & Nichols 1942
Ziegler, J. G.; Nichols, N. B.: Optimum Settings for Automatic Controllers. *Transactions of the ASME* 64 (1942) n. No., pp. 759–768.

Publications of the author

Emrich et al. 2021
Emrich, N.; Meyer, S. P.; Daub, R.; Schiffers, R.: Evaluation of Polyamide Copper Hybrids for Automotive Battery Systems. In: *Annual Technical Conference (ANTEC) of the Society of Plastics Engineers (SPE)*. Denver, Colorado, USA. 2021.

Meyer 2021
Meyer, S. P.: Reibpressfügen als innovative Fügetechnik für Kunststoff-Metall-Verbunde [engl.: Friction press joining as an innovative joining method for plastic-metal composites]. *iwb-Newsletter* (2021) 1, pp. 37–38.

Meyer et al. 2021a
Meyer, S. P.; Fuderer, S.; Zaeh, M. F.: A Holistic, Model-Predictive Process Control for Friction Stir Welding Processes Including a 1D FDM Multi-Layer Temperature Distribution Model. *Metals* 11 (2021) 3, pp. 502-1–502-22.

Meyer et al. 2021b
Meyer, S. P.; Herold, M. T.; Habedank, J. B.; Zaeh, M. F.: A Study on the Bond Strength of Plastic-Metal Direct Bonds Using Friction Press Joining. *Metals* 11 (2021) 4, pp. 660-1–660-18.

Wunderling & Meyer 2021
Wunderling, C.; Meyer, S. P.: Forschungsprojekt PROLEI auf dem FOREL-Kolloquium 2019 erfolgreich abgeschlossen [engl.: PROLEI research project successfully concluded at the FOREL Colloquium 2019]. *iwb-Newsletter* (2021) 1, p. 34.

Emrich et al. 2020
Emrich, N.; Meyer, S. P.; Daub, R.: Ageing behavior of thermally joined hybrids of laser pre-treated metal and thermoplastic polymers. In: *Proceedings of the 35th International Conference of the Polymer Processing Society (PPS-35)*. AIP Conference Proceedings. Izmir, Turky: AIP Publishing. 2020, pp. 020001-1–020001-5.

Meyer et al. 2020
Meyer, S. P.; Bernauer, C. J.; Grabmann, S.; Zaeh, M. F.: Design, evaluation, and implementation of a model-predictive control approach for a force control in friction stir welding processes. *Production Engineering* 14 (2020) 4, pp. 473–489. ISSN: 0944-6524.

Wunderling et al. 2020
Wunderling, C.; Mayr, L.; Meyer, S. P.; Zaeh, M. F.: Laser-based surface pre-treatment for metal-plastic hybrids using a new process strategy. *Journal of Materials Processing Technology* 282 (2020) n. No., pp. 116675-1–116675-8. ISSN: 0924-0136.

Habedank & Meyer 2019
Habedank, J. B.; Meyer, S. P.: Lernfabrik Fügetechnik (LFT): Von den Grundlagen zu aktuellen Forschungsthemen [engl.: Learning Factory Joining Technology (LFT): From the basics to current research topics]. *iwb-Newsletter* (2019) 4, p. 10.

Lugauer et al. 2019
Lugauer, F. P.; Kandler, A.; Meyer, S. P.; Wunderling, C.; Zaeh, M. F.: Induction-based joining of titanium with thermoplastics. *Production Engineering* 13 (2019) 3, pp. 409–424. ISSN: 0944-6524.

Meyer & Wunderling 2019
Meyer, S. P.; Wunderling, C.: Prozesskette für das Fügen endlosfaser-verstärkter Kunststoffe mit Metallen [engl.: Process chain for joining continuous fiber-reinforced plastics with metals]. *iwb-Newsletter* (2019) 2, pp. 4–5.

MEYER et al. 2019a
Meyer, S. P.; Wunderling, C.; Zaeh, M. F.: Friction press joining of dissimilar materials: A novel concept to improve the joint strength. In: *Proceedings of the 22nd International ESAFORM Conference on Material Forming: ESAFORM 2019*. AIP Conference Proceedings. Vitoria-Gasteiz, Spain: AIP Publishing. 2019, pp. 050031-1–050031-6.

MEYER et al. 2019b
Meyer, S. P.; Wunderling, C.; Zaeh, M. F.: Influence of the laser-based surface modification on the bond strength for friction press joining of aluminum and polyethylene. *Production Engineering* 13 (2019) 6, pp. 721–730. ISSN: 0944-6524.

MEYER et al. 2019c
Meyer, S. P.; Jaeger, B.; Wunderling, C.; Zaeh, M. F.: Friction stir welding of glass fiber-reinforced polyamide 6: Analysis of the tensile strength and fiber length distribution of friction stir welded PA6-GF30. *IOP Conference Series: Materials Science and Engineering* 480 (2019), pp. 012013-1–012013-12.

WUNDERLING et al. 2019
Wunderling, C.; Scherm, M.; Meyer, S.; Zaeh, M. F.: Thermal distortion in surface pretreatment of metal-polymer hybrids using continuous wave laser radiation. In: *High-Power Laser Materials Processing: Applications, Diagnostics, and Systems VIII*. Ed. by Kaierle, S.; Heinemann, S. W. San Francisco, California, USA: SPIE. 2019, 109110A-1–109110A-11. ISBN: 978-1-510-62464-1.

SCHÄFER et al. 2018
Schäfer, C.; Meyer, S. P.; Osswald, T. A.: A novel extrusion process for the production of polymer micropellets. *Polymer Engineering & Science* 44 (2018) n. No., pp. 2264–2275. ISSN: 0032-3888.

SCHWAB et al. 2018
Schwab, D.; Schäfer, E.; Wunderling, C.; Meyer, S.: High-speed nested scanner for large-area material processing. In: *10th CIRP Conference on Photonic Technologies LANE 2018*. Fürth, Germany. 2018.

Wunderling et al. 2018
Wunderling, C.; Meyer, S. P.; Zaeh, M. F.: Thermisches Fügen von Metall-Kunststoff-Hybridverbindungen: Potenzialanalyse der Oberflächenvorbehandlung mittels Dauerstrich-Laserstrahlung [engl.: Thermal joining of metal-plastic hybrid joints: Potential analysis of the surface pretreatment by means of continuous wave laser radiation]. *wt-online* 108 (2018) 10, pp. 708–715.

Schäfer et al. 2017
Schäfer, C.; Bryant, J. S.; Osswald, T. A.; Meyer, S. P.: Micropelletization of Virgin and Reycled Thermoplasitc Materials. In: *Annual Technical Conference (ANTEC) of the Society of Plastics Engineers (SPE)*. Anaheim, California, USA. 2017.

Meyer et al. 2013a
Patent application: DE 10 2011 081 703 A1 (28.02.2013). BSH Hausgeräte GmbH. Meyer, S. P.; Nagl, M.; Speckbacher, S.; Stadler, G.: Method for operating household appliance with flow-type heater, involves determining harness value of water upstream flow-type heater and determining hardness value of water downstream flow-type heater.

Meyer et al. 2013b
Patent: DE 10 2011 081 703 B4 (24.05.2017). BSH Hausgeräte GmbH. Meyer, S. P.; Nagl, M.; Speckbacher, S.; Stadler, G.: Method for operating household appliance with flow-type heater, involves determining harness value of water upstream flow-type heater and determining hardness value of water downstream flow-type heater.

A List of supervised students

In the context of this work, the author supervised, with substantial scientific, technical, and content-related input the following student research projects at the Institute for Machine Tools and Industrial Management (*iwb*), Technical University of Munich (TUM), between 2017 and 2021. Various aspects of FPJ, laser-based surface treatment, and process control were investigated, and some of the results have been incorporated in this thesis. The author thanks all of these students for their efforts in supporting this scientific work.

Table A.1: List of the research projects supervised by the author, including submission dates and *iwb*-reference numbers

Surname, First name	**Title of thesis**
Martineau, Florian Marc	*Development of a heat source model for friction press joining based on process parameters* Bachelor's thesis (November 23rd, 2018; *iwb*-No.: 2018/43156)
Wagner, Sara Katherina	*Process-characterization for friction press joining of laser-structured aluminum with thermoplastics* Master's thesis (February 5th, 2019; *iwb*-No.: 2019/43729)
Bernauer, Christian Josef	*Development and validation of a force control system for friction press joining of plastic-metal hybrid composites* Master's thesis (September 30th, 2019; *iwb*-No.: 2019/47333)

continued on next page

Surname, First name	**Title of the thesis**
Herold, Maren Tabea	*Experimental study of joining methods and technology assessment using the example of plastic-aluminum composites* Bachelor's thesis (June 19th, 2020; *iwb*-No.: 2020/52757)
Fuderer, Sebastian	*Model-based multi-variable control for friction press joining* Semester's thesis (December 2nd, 2020; *iwb*-No.: 2020/54390)
Sun, Chenyi	*Modelling of heat conduction in multi-layer systems* Semester's thesis (May 2nd, 2021; *iwb*-No.: 2021/56748)

B Embedded publications

B.1 Overview

In this chapter, all of the publications (P1 – P5) relevant to this work are listed. For each publication, the authors' detailed contributions – including conception, elaboration, and final editing – are listed. An overview of all the authors and their contributions to the publications that contributed to this work are shown in Table B.1. All publications were evaluated through a peer-review process.

The author would like to thank all of these scientists for their excellent cooperation that resulted in this thesis.

Table B.1: List of the individual contributions of each author, in terms of content and formal elaboration of each publication

	P1	P2	P3	P4	P5
S. P. Meyer	85 %	85 %	75 %	85 %	80 %
C. J. Bernauer	0 %	0 %	15 %	0 %	0 %
S. Fuderer	0 %	0 %	0 %	10 %	0 %
S. Grabmann	0 %	0 %	5 %	0 %	0 %
J. B. Habedank	0 %	0 %	0 %	0 %	5 %
M. T. Herold	0 %	0 %	0 %	0 %	10 %
C. Wunderling	10 %	10 %	0 %	0 %	0 %
M. F. Zaeh	5 %	5 %	5 %	5 %	5 %

B.2 Publication 1 – "Friction press joining of dissimilar materials: A novel concept to improve the joint strength"

Publication 1 (*Friction press joining of dissimilar materials: A novel concept to improve the joint strength*) was officially presented at the *22nd International Conference on Material Forming (ESAFORM 2019)* in Vitoria-Gasteiz (Spain) on May 9th, 2019, and published in the AIP Conference Proceedings on July 2nd, 2019. The individual contributions of the authors in the preparation of the publication are shown in Table B.2.

Table B.2: Overview of the individual contributions of the authors to the conceptual, elaboration, and writing activities for Publication 1 – MEYER et al. (2019a)

Author	Conceptualization	Elaboration	Writing	Total
S. P. Meyer	85 %	90 %	85 %	85 %
C. Wunderling	10 %	10 %	5 %	10 %
M. F. Zaeh	5 %	0 %	10 %	5 %

B.3 Publication 2 – "Influence of the laser-based surface modification on the bond strength for friction press joining of aluminum and polyethylene"

Publication 2 (*Influence of the laser-based surface modification on the bond strength for friction press joining of aluminum and polyethylene*) was submitted to the journal *Production Engineering*, published by Springer, on October 14th, 2019, and was accepted on October 23rd, 2019. It was published online on November 3rd, 2019. The individual contributions of the authors to the preparation of the publication are shown in Table B.3.

Table B.3: Overview of the individual contributions of the authors to the conceptual, elaboration, and writing activities for Publication 2 – MEYER et al. (2019b)

Author	Conceptualization	Elaboration	Writing	Total
S. P. Meyer	85 %	90 %	85 %	85 %
C. Wunderling	10 %	10 %	5 %	10 %
M. F. Zaeh	5 %	0 %	10 %	5 %

B.4 Publication 3 – "Design, evaluation, and implementation of a model-predictive control approach for a force control in friction stir welding processes"

Publication 3 (*Design, evaluation, and implementation of a model-predictive control approach for a force control in friction stir welding processes*) was submitted to the journal *Production Engineering*, published by Springer, on May 11^{th}, 2020, and was accepted on June 9^{th}, 2020. It was published online on June 30^{th}, 2020. The individual contributions of the authors to the preparation of the publication are shown in Table B.4.

Table B.4: Overview of the individual contributions of the authors to the conceptual, elaboration, and writing activities for Publication 3 – MEYER et al. (2020)

Author	Conceptualization	Elaboration	Writing	Total
S. P. Meyer	85 %	40 %	80 %	75 %
C. J. Bernauer	10 %	50 %	5 %	15 %
S. Grabmann	0 %	10 %	5 %	5 %
M. F. Zaeh	5 %	0 %	10 %	5 %

B.5 Publication 4 – "A Holistic, Model-Predictive Process Control for Friction Stir Welding Processes Including a 1D FDM Multi-Layer Temperature Distribution Model"

Publication 4 (*A Holistic, Model-Predictive Process Control for Friction Stir Welding Processes Including a 1D FDM Multi-Layer Temperature Distribution Model*) was submitted to the journal *Metals*, published by MDPI, on February 23$^{\text{rd}}$, 2021, and was accepted on March 13$^{\text{th}}$, 2021. It was published online on March 18$^{\text{th}}$, 2021. The individual contributions of the authors to the preparation of the publication are shown in Table B.5.

Table B.5: Overview of the individual contributions of the authors to the conceptual, elaboration, and writing activities for Publication 4 – MEYER et al. (2021a)

Author	Conceptualization	Elaboration	Writing	Total
S. P. Meyer	90 %	80 %	90 %	85 %
S. Fuderer	5 %	20 %	0 %	10 %
M. F. Zaeh	5 %	0 %	10 %	5 %

B.6 Publication 5 – "A Study on the Bond Strength of Plastic-Metal Direct Bonds Using Friction Press Joining"

Publication 5 (*A study on the bond strength of plastic-metal direct bonds using friction press joining*) was submitted to the journal *Metals*, published by MDPI, on March 14$^{\text{th}}$, 2021, and was accepted on April 15$^{\text{th}}$, 2021. It was published online on April 18$^{\text{th}}$, 2021. The individual contributions of the authors to the preparation of the publication are shown in Table B.6.

Table B.6: Overview of the individual contributions of the authors to the conceptual, elaboration, and writing activities for Publication 5 – MEYER et al. (2021b)

Author	**Conceptualization**	**Elaboration**	**Writing**	**Total**
S. P. Meyer	85 %	90 %	75 %	80 %
M. T. Herold	5 %	10 %	5 %	10 %
J. B. Habedank	5 %	0 %	10 %	5 %
M. F. Zaeh	5 %	0 %	10 %	5 %

C Engineering drawings

C.1 Clamping

The attached technical drawings supplement Chapter 5 and show the clamping system used for the experimental tests conducted on the Heller MCH 250 machining center. The author alone conceived and designed the clamping system. The manufacturing was carried out by the in-house mechanical workshop of the Institute for Machine Tools and Industrial Management (*iwb*), Technical University of Munich (TUM).

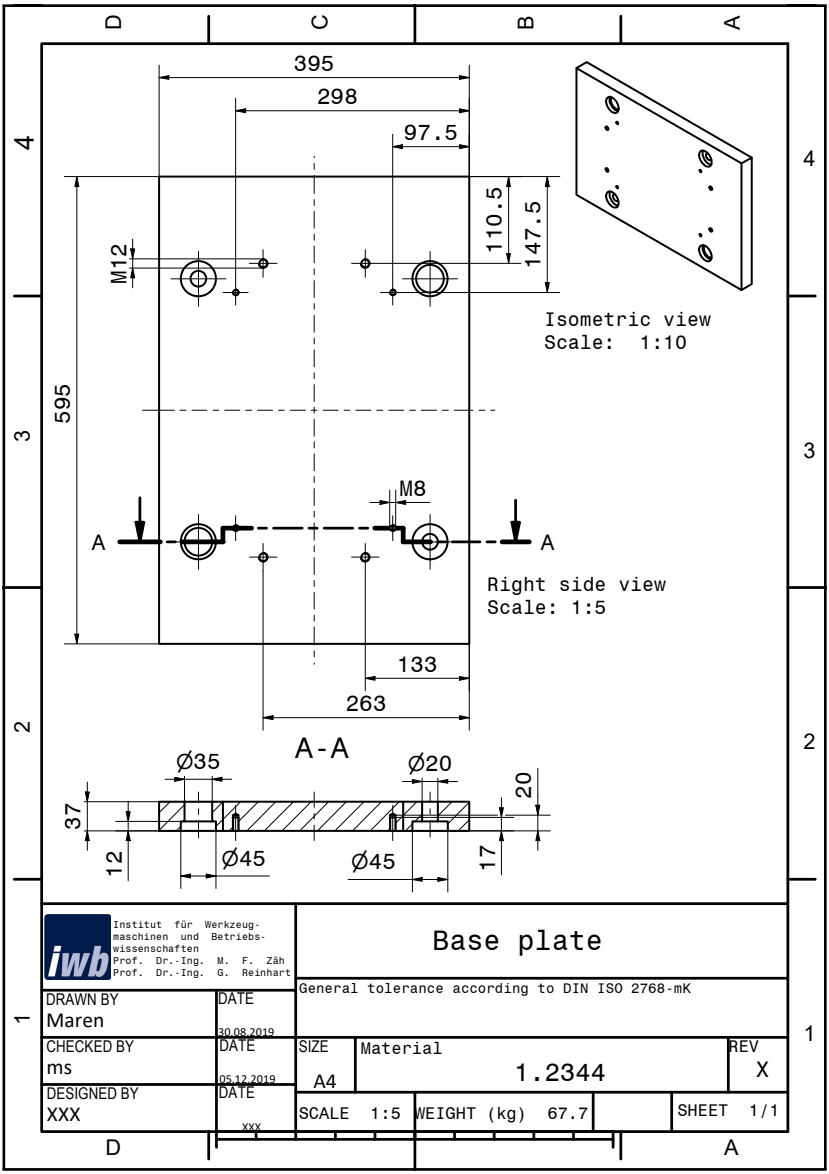

Figure C.1: Engineering drawing of the base plate for the mounting of the clamping system for the Heller MCH 250

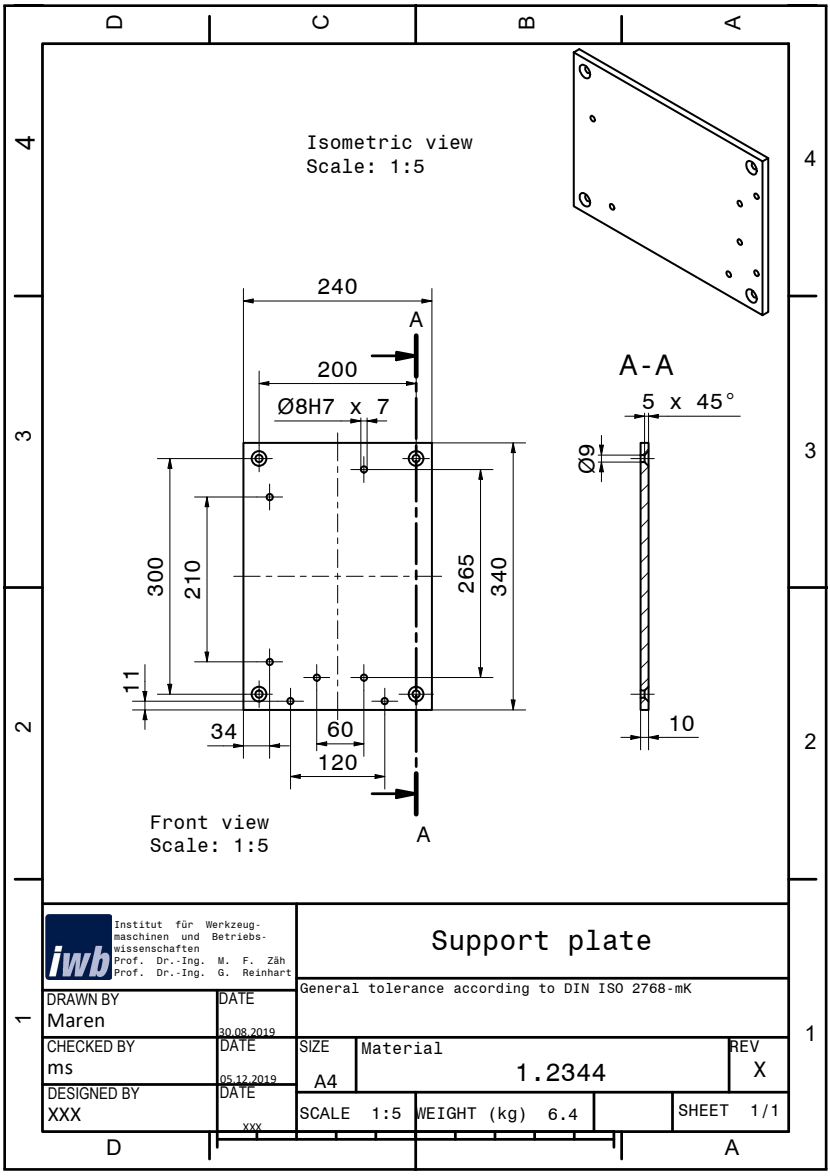

Figure C.2: Engineering drawing of the support plate for the mounting of the specimens on the base plate

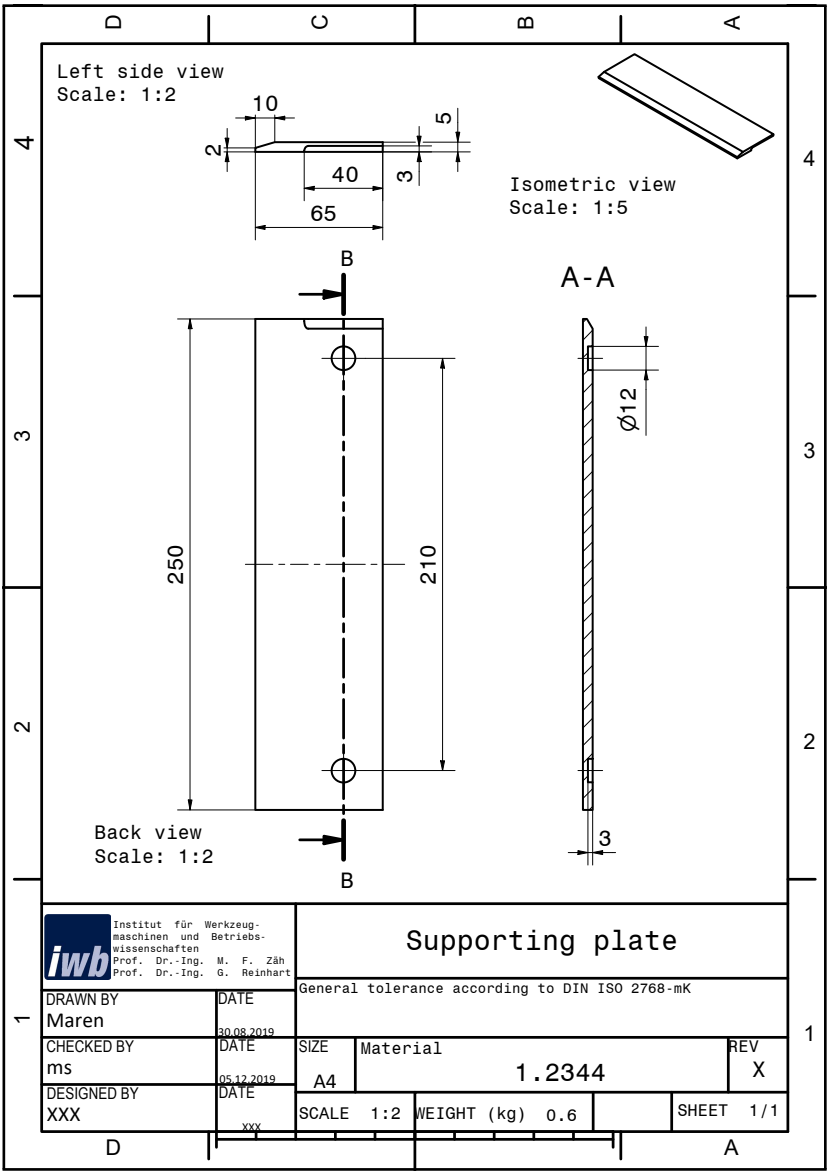

Figure C.3: Engineering drawing of the supporting plate to stabilize the metallic joining partner on the support plate

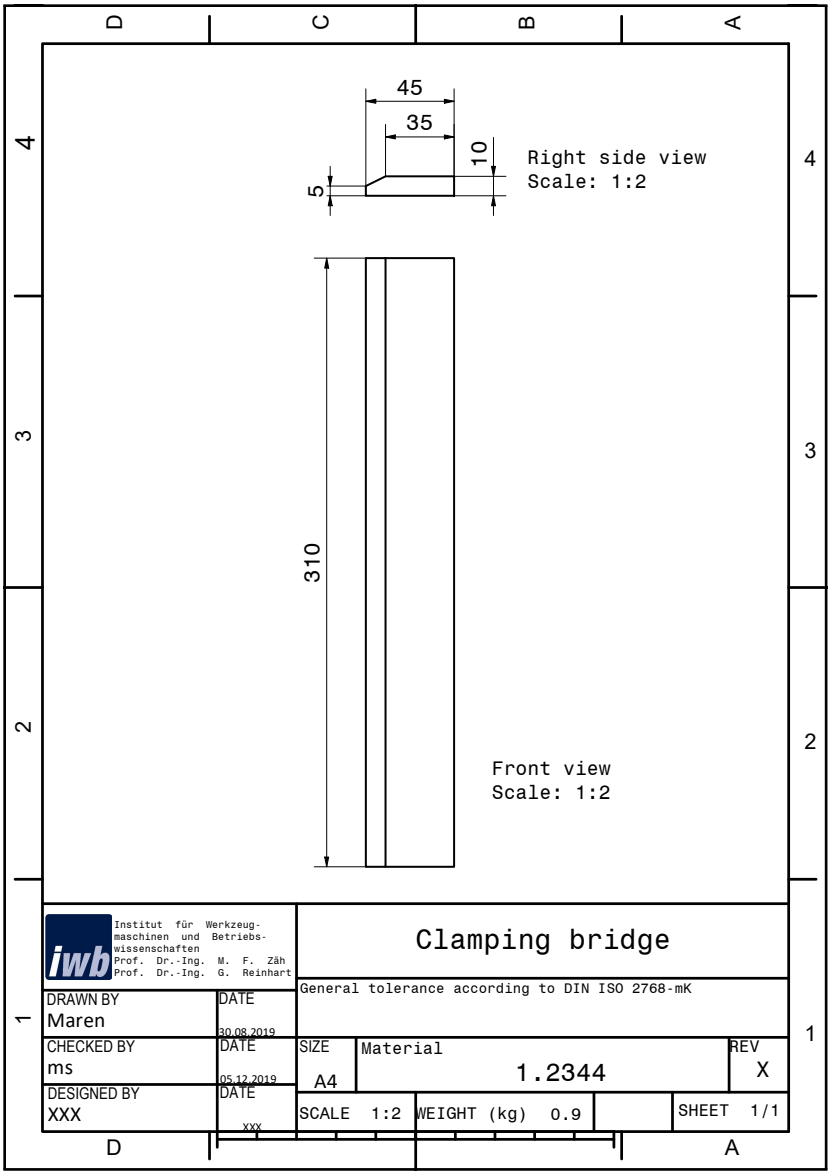

Figure C.4: Engineering drawing of the clamping bridge for the mounting of the two joining partners on the support plate

C.2 Tools

The following technical drawings supplement Chapter 5 and represent the tools used for the experiments. The author alone conceived and designed the tools. The manufacturing was done by the in-house mechanical workshop of the Institute for Machine Tools and Industrial Management (*iwb*), Technical University of Munich (TUM). The tools were vacuum hardened to increase their abrasion resistance, and eroded to allow insertion of the thermocouples into the tools. The vacuum hardening process was conducted by *Härterei Weber und Wallner GmbH & Co. KG*, Starnberg, Germany. The subsequent eroding for the TC hole was executed by *HPN Erodierzentrum Werkzeugbau GmbH*, Hohenlinden, Germany.

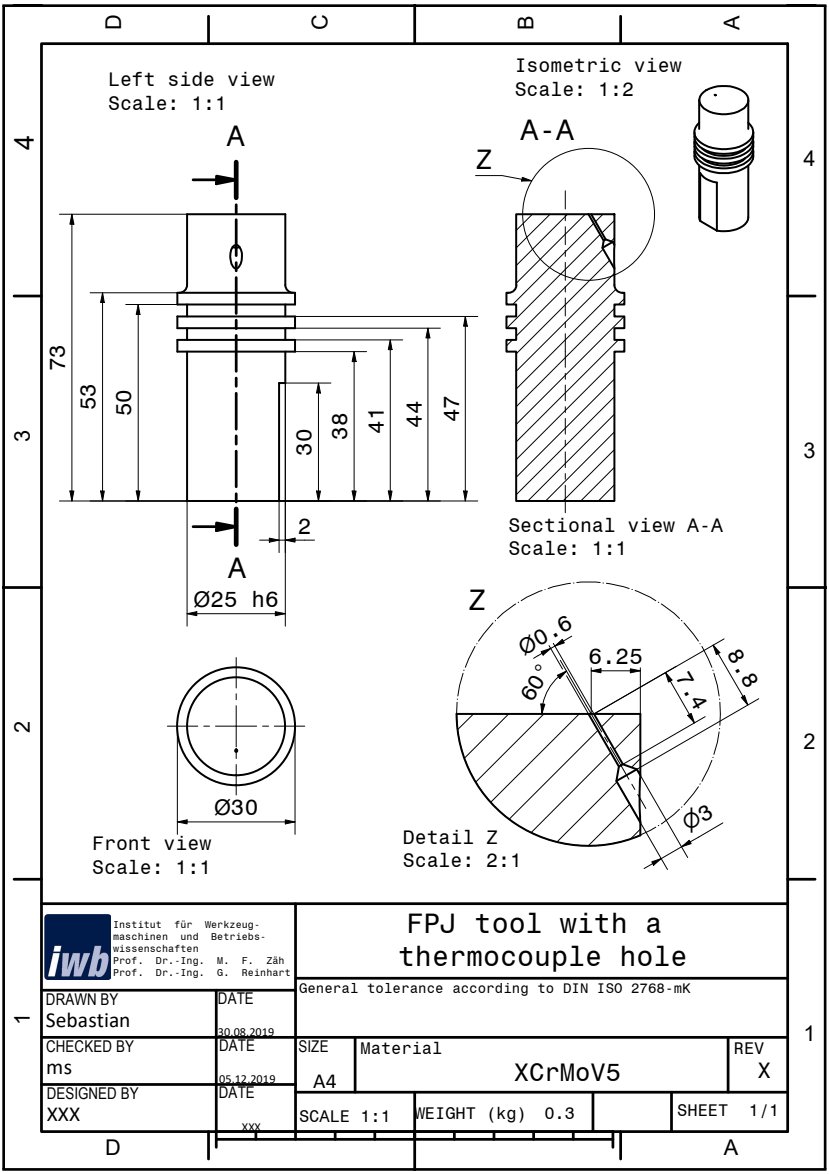

Figure C.5: Engineering drawing of the FPJ tool used, with a TC hole for measuring the temperature

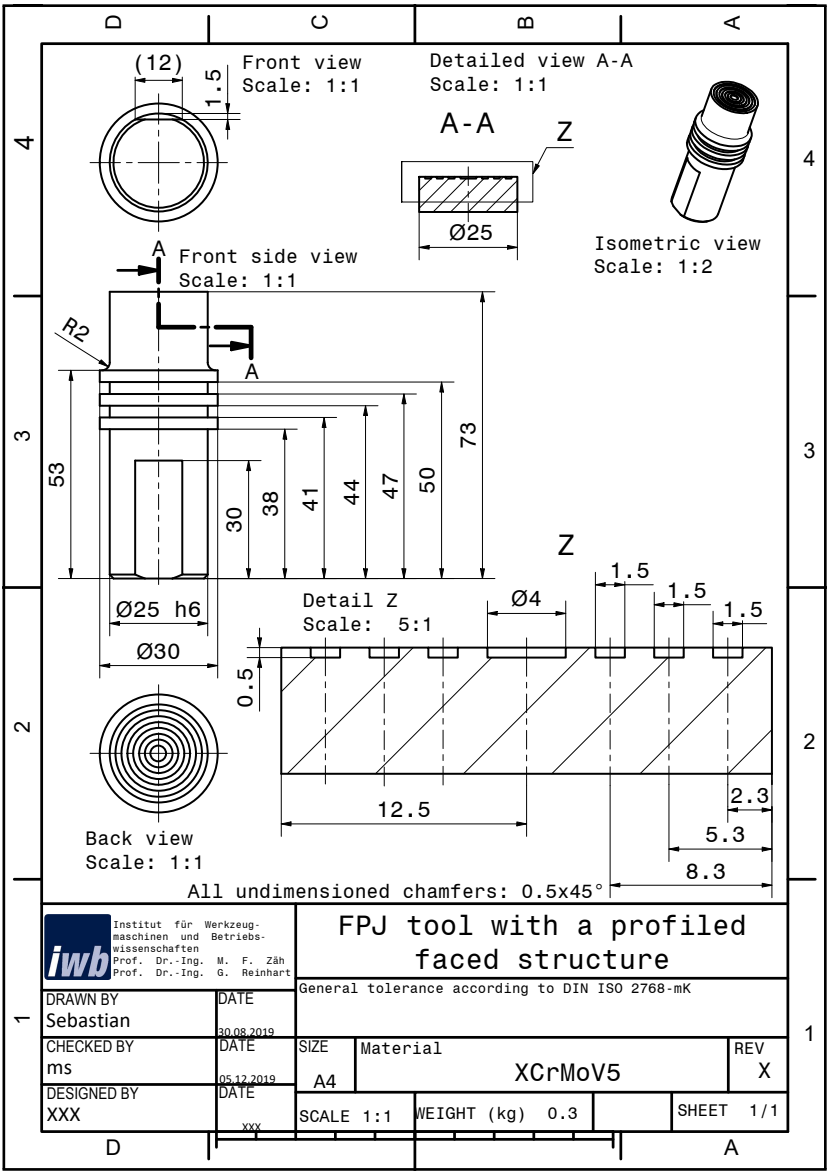

Figure C.6: Engineering drawing of the FPJ tool with a profiled friction surface (grooves)